

COMPARISON OF POST-TENSIONED CAST IN PLACE  
CONCRETE AND STEEL-CONCRETE  
COMPOSITE BENT CAPS

by

FRANCISCO DAVID BERROCAL RUIZ

Presented to the Faculty of the Graduate School of  
The University of Texas at Arlington in Partial Fulfillment  
of the Requirements  
for the Degree of

MASTER OF SCIENCE IN CIVIL ENGINEERING

THE UNIVERSITY OF TEXAS AT ARLINGTON

December 2015

Copyright © by Francisco David Berrocal Ruiz 2015

All Rights Reserved



### Acknowledgements

I would like to sincerely thank Dr. Nur Yazdani for his continuous support and guidance during the completion of my M.S. program at The University of Texas at Arlington, for his patience, motivation, and immense knowledge. Attending his extraordinary courses has been an honor, and his motivation helped me to succeed in the completion of my degree.

My most sincere and deepest gratitude are extended to Dr. Seyedali Abolmaali and Dr. Seyed Mohammad Razavi for willingly accepting my invitation to be part of my thesis committee, as well as for the outstanding courses I had the honor to attend.

I would like also to extend my gratitude to the Civil Engineering staff. Although dealing with international students is not always easy, I have always been received with a smile.

I am deeply grateful to my Company, Ferrovial-Agroman, for giving me the opportunity to work in an exciting project, for their support during the completion of my M.S. program, and for their commitment with the training and education of their employees. My special gratitude to Carlos Fernandez Lillo for giving me the opportunity of taking my M.S degree, and to Leonardo Le for his help and support in the development of this research work.

Thanks to my parents, for their constant support and motivation to become a better person, for their understanding and guidance, for their unwavering love and encouragement to overcome the life challenges. My gratitude is extended to my brothers, for their unconditional love and support.

Finally, the last but not the least. I extend my deepest gratitude to my loving wife, Maria Angeles, for her unconditional love and motivation, for her patience and endless support during long hours of study with her by my side, for her confidence and encouragement.

August 12, 2015



## Abstract

# COMPARISON OF POST-TENSIONED CAST IN PLACE CONCRETE AND STEEL-CONCRETE COMPOSITE BENT CAPS

FRANCISCO DAVID BERROCAL RUIZ

The University of Texas at Arlington, 2015

Supervising Professor: Nur Yazdani

Civil engineering projects are conditioned not only by the technology available but also by resources availability as well as budget and construction time. Special conditions applicable to particular projects can also control their development.

The correct selection from the different feasible alternatives can determine the final output of a project. In that sense, the importance of bridge structures on both the overall budget and schedule of civil engineering projects makes the selection of the proper structural typology decisive for their success or failure. In some cases, special characteristics can establish the need of innovative solutions to guarantee a successful development of the project.

The evolution of the urban areas and consequently the increase in their population, translates into increasing traffic volumes that, eventually, may overcome the existing transportation infrastructures capacity. The construction of new projects to increase the capacity of the transportation system in consolidated urban areas generates conflicts with existing infrastructures that may require the development of new construction processes, techniques and structural typologies to limit the impact on the traffic.

The complexity of the IH-635 Managed Lanes Project located in Dallas County has posed several technical and constructive challenges, leading to the adoption of solutions different from the traditionally adopted. The particular solution given to the substructure of Bridge 4 crossing over IH-35E on the IH-635 project has been analyzed on this study. Two alternatives will be analyzed in terms of structural behavior, cost-efficiency and schedule: the original cast in place post-tensioned concrete structure and the finally built steel-concrete composite prefabricated bent cap solution.

## Table of Contents

Acknowledgements .....	iii
Abstract .....	v
List of Illustrations .....	x
List of Tables .....	xiv
Chapter 1 INTRODUCTION.....	1
1.1 Introduction .....	1
1.2 Project Background .....	1
1.3 Need Statement.....	5
1.4 Research Objectives .....	6
1.5 Thesis Organization.....	7
Chapter 2 BACKGROUND AND LITERATURE REVIEW .....	9
2.1 Historical Introduction .....	9
2.2 Structural Background .....	11
2.2.1 Introduction .....	11
2.2.2 Hammerhead Pier .....	13
2.2.3 Bent Pier .....	15
2.2.4 Solid Wall Pier .....	16
2.2.5 Integral Pier .....	17
2.2.6 Proposed Pier Typologies .....	18
2.3 Cost Estimation Background .....	20
2.4 Scheduling Background.....	22
2.5 Case of Study Background.....	24
Chapter 3 FINITE ELEMENT MODELLING.....	33
3.1 Materials .....	33

3.1.1 Concrete .....	33
3.1.2 Reinforcing Steel .....	46
3.1.3 Prestressing Steel .....	48
3.1.4 Structural Steel .....	51
3.2 Loads .....	53
3.3 Boundary Conditions .....	54
3.4 Post-Tensioned Concrete Cap Model .....	55
3.4.1 Introduction .....	55
3.4.2 Prestressing Force .....	61
3.4.2.1 Prestress Loss .....	61
3.4.2.2 Load-Balancing Force .....	69
3.3.3 Element Types.....	71
3.3.4 Mesh Generation .....	73
3.3.5 FEM validation .....	75
3.4 Steel-Concrete Composite Cap Model .....	78
3.4.1 Introduction .....	78
3.4.2 Element Types.....	83
3.4.3 Mesh Generation .....	84
3.4.4 FEM Validation .....	86
Chapter 4 COST ESTIMATE AND SCHEDULE .....	90
4.1. Materials and Activities Identified .....	90
4.1.1 Post-Tensioned Bent Cap .....	90
4.2.2 Composite Bent Cap .....	92
4.2. Unit Costs and Cost Estimate.....	95
4.3 Activities Duration .....	97

Chapter 5 SUMMARY AND RESULTS DISCUSSION .....	101
5.1 Summary .....	101
5.2 FEM Modelling and Results.....	104
5.3 Cost and Schedule Comparison.....	108
Chapter 6 CONCLUSIONS AND RECOMMENDATIONS FOR FUTURE RESEARCH .....	111
6.1 Conclusions .....	111
6.2 Recommendations for Future Research .....	112
Appendix A Bridge 4 Drawings .....	117
Appendix B Load Calculations .....	134
Appendix C Prestress Loss Calculations .....	149
Appendix D Post-Tensioned Concrete Cap Model. Validation Calculations .....	154
Appendix E Steel-Concrete Composite Cap Model. Validation Calculations .....	159
Appendix F Cost Estimation.....	164
References.....	167
Biographical Information .....	173

## List of Illustrations

Figure 1-1 Project Location .....	2
Figure 1-2 Bridge 4 Location.....	3
Figure 1-3 Bridge 4 Crossing over IH-35E.....	4
Figure 1-4 Bridge 4 Typical Section.....	5
Figure 2-1 The Alcantara Bridge (Spain) .....	10
Figure 2-2 a) Balanced Hammerhead Pier b) Unbalanced Hammerhead Pier .....	14
Figure 2-3 a) Rectangular Bent Pier b) Inverted T Bent Pier.....	15
Figure 2-4 Solid Wall Pier .....	17
Figure 2-5 Integral Steel Pier Cap .....	18
Figure 2-6 Gantt Chart Example (Newitt, 2009) .....	23
Figure 2-7 Network Schedule (Hutchings, 2004).....	24
Figure 2-8 Bridge 4 Location Before Construction.....	26
Figure 2-9 Bridge 4 Plan View .....	27
Figure 2-10 Composite Bent Cap Lifting Operation.....	28
Figure 2-11 Bent Caps 7, 8 and 9 in Place.....	28
Figure 2-12 Bridge 4 Construction. Girders in Place .....	30
Figure 2-13 Bridge 4 Finished and in Service.....	32
Figure 3-1 Typical Stress-Strain Curves for Concrete in Compression (Wight & MacGregor, 2012).....	36
Figure 3-2 Compressive stress-strain curve adopted for modelling concrete with Abaqus (Wahalathantri, Thambiratnam, Chan, & Fawzia, 2011).....	37
Figure 3-3 Modified Tension Stiffening Model for Abaqus (Wahalathantri, Thambiratnam, Chan, & Fawzia, 2011).....	39

Figure 3-4 Definition of Inelastic Strain, Plastic Strain and Damage Parameter for (Cyclic) Compression Loading (Birtel & Mark, 2006).....	40
Figure 3-5 Definition of Cracking Strain, Plastic Strain and Damage Parameter for (Cyclic) Tensile Loading (Birtel & Mark, 2006) .....	40
Figure 3-6 Stress-Strain Curve. Concrete Under Uniaxial Compression .....	43
Figure 3-7 Damage Parameter. Concrete Under Compression .....	43
Figure 3-8 Stress-Strain Curve. Concrete Under Uniaxial Tension .....	45
Figure 3-9 Damage Parameter. Concrete Under Tension.....	45
Figure 3-10 Typical Stress-Strain Curves for Reinforcing Steel (Nilson, Darwin, & Dolan, 2004) .....	46
Figure 3-11 Grade 60 Reinforcing Steel. Stress-Strain Curve.....	47
Figure 3-12 Typical Stress-Strain Curves for Prestressing Steel (Naaman, 2012) .....	48
Figure 3-13 Typical Determination of Yield Strength for Prestressing Steel (Naaman, 2012) .....	49
Figure 3-14 Grade 270 Low Relaxation Prestressing Steel. Stress-Strain Curve .....	50
Figure 3-15 Typical Stress-Strain Curves Structural Steel .....	51
Figure 3-16 Grade 50 Structural Steel. Stress-Strain Curve .....	52
Figure 3-17 Live Load Model .....	53
Figure 3-18 Boundary Conditions .....	55
Figure 3-19 Plan View Geometry of Post-Tensioned Concrete Cap .....	57
Figure 3-20 Tendons Profiles.....	57
Figure 3-21 Prestressed Concrete Cap Typical Section.....	58
Figure 3-22 Concrete Cap Part in Abaqus Model .....	59
Figure 3-23 Reinforcement Parts in Abaqus Model.....	60
Figure 3-24 Prestress Loss per Tendon. Creep Loss $\Delta f_{ps}(C)$ .....	66

Figure 3-25 Prestress Loss per Tendon. Shrinkage Loss $\Delta f_{ps}(SH)$ .....	68
Figure 3-26 Prestress Loss per Tendon. Steel Relaxation Loss $\Delta f_{ps}(RL)$ .....	69
Figure 3-27 Load Balancing Force. Draped Tendons.....	70
Figure 3-28 Parabolic Tendon Free Body Diagram .....	70
Figure 3-29 Abaqus Naming Convention for Truss Elements .....	72
Figure 3-30 Abaqus 2 Nodes 3D Truss Element T3D2 .....	72
Figure 3-31 Abaqus Naming Convention for Continuum Elements .....	73
Figure 3-32 Abaqus 4 Nodes 3D Tetrahedral Element C3D4 .....	73
Figure 3-33 Post-Tensioned Cap Model. Number of Nodes vs. Mesh Size .....	74
Figure 3-34 Post-Tensioned Cap Model. 5 Inches (127 mm) Mesh Size Detail.....	75
Figure 3-35 Post-Tensioned Cap. Bending Stresses (psi) Distribution. 5 Inches (127 mm) Mesh Model.....	76
Figure 3-36 Plan View Geometry of Steel-Concrete Composite Cap.....	79
Figure 3-37 Composite Cap Typical Section .....	79
Figure 3-38 Concrete Slab Part in Abaqus Model .....	80
Figure 3-39 Reinforcement Parts in Concrete Slab .....	81
Figure 3-40 Steel Cap Part in Abaqus Model .....	82
Figure 3-41 Stiffeners and Diaphragms Parts in Abaqus Model .....	83
Figure 3-42 Abaqus Naming Convention for Conventional Shell Elements .....	84
Figure 3-43 Abaqus 3 Nodes 3D Conventional Shell Element S3 .....	84
Figure 3-44 Composite Cap Model. Number of Nodes vs. Mesh Size .....	85
Figure 3-45 Composite Cap Model. 3 Inches (76.2 mm) Mesh Detail.....	86
Figure 3-46 Bending Stresses (psi) Distribution in Concrete Slab. 3 Inches (76.2 mm) Mesh Model.....	87



Figure 3-47 Bending Stresses (psi) Distribution in Steel Section. 3 Inches (76.2 mm)	
Mesh Model.....	87
Figure 4-1 Composite Bent Cap Ready to be Placed.....	94
Figure 4-2 Lifting of Composite Bent Cap.....	95
Figure 4-3 Post-Tensioned Bent Cap Construction Schedule.....	99
Figure 4-4 Composite Bent Cap Construction Schedule.....	99
Figure 5-1 Post-Tensioned Cap Model. Deflections (inches).....	107
Figure 5-2 Composite Cap Model. Deflections (inches).....	107
Figure 6-1 Post-Tensioned Cap. End and Support Detail.....	114
Figure 6-2 Post-Tensioned Cap. Detail A.....	114
Figure 6-3 Post-Tensioned Cap. Transverse Section at Support.....	115

## List of Tables

Table 2-1 Bridge Classification Based on Slab Position and Structural Form. (Barker & Puckett, 2013) .....	12
Table 3-1 Default Parameters of CDP Model under Compound Stress .....	35
Table 3-2 Concrete Compressive Behavior Model .....	42
Table 3-3 Concrete Tensile Behavior Model.....	44
Table 3-4 Summary of Girder Reactions at Support.....	54
Table 3-5 Tendons Elevations .....	58
Table 3-6 Post-Tensioned Cap Model. Mesh Characteristics .....	74
Table 3-7 Post-tensioned Concrete Cap Model. Validation Analysis. US Units .....	77
Table 3-8 Post-Tensioned Concrete Cap Model. Validation Analysis. SI Units .....	77
Table 3-9 Composite Bent Cap Model. Mesh Characteristics .....	85
Table 3-10 Composite Cap Model. Validation Analysis. US Units .....	88
Table 3-11 Composite Cap Model. Validation Analysis. SI Units .....	89

## Chapter 1

### INTRODUCTION

#### 1.1 Introduction

The construction market has dramatically changed during the last decades. Construction companies from all around the world have internationalized their operations, looking for new growing opportunities abroad in markets with an increasing competitiveness. In that sense, it is extremely important for the projects main contractors and developing agencies to accurately determine, from the set of feasible engineering alternatives, the one that better guarantee the successful development of the projects.

An aspect of large transportation projects stands out from the rest of them for its remarkable influence in the overall result of the project: bridge structures. Bridges construction can determine whether a project is successfully developed or not because of the amount of resources and time needed in their construction. Also, the need of increasing the capacity of existing transportation infrastructures in already consolidated urban areas, where maintaining a minimum service level for the traffic during the construction of the project is key to keep the normal daily activity, has posed other challenges for the structural engineer.

#### 1.2 Project Background

The IH-635 Managed Lanes Project is located in North Dallas (Texas) and comprises works on both IH-35 and IH-635 freeways. Started in early 2011, it is expected to be completed and opened to public on summer 2015. After its completion, it will

dramatically increase the traffic capacity of this important east-west corridor in Dallas. It will consist of four to six general purpose lanes per bound, two managed lanes per bound, and two to three frontage road lanes per bound.

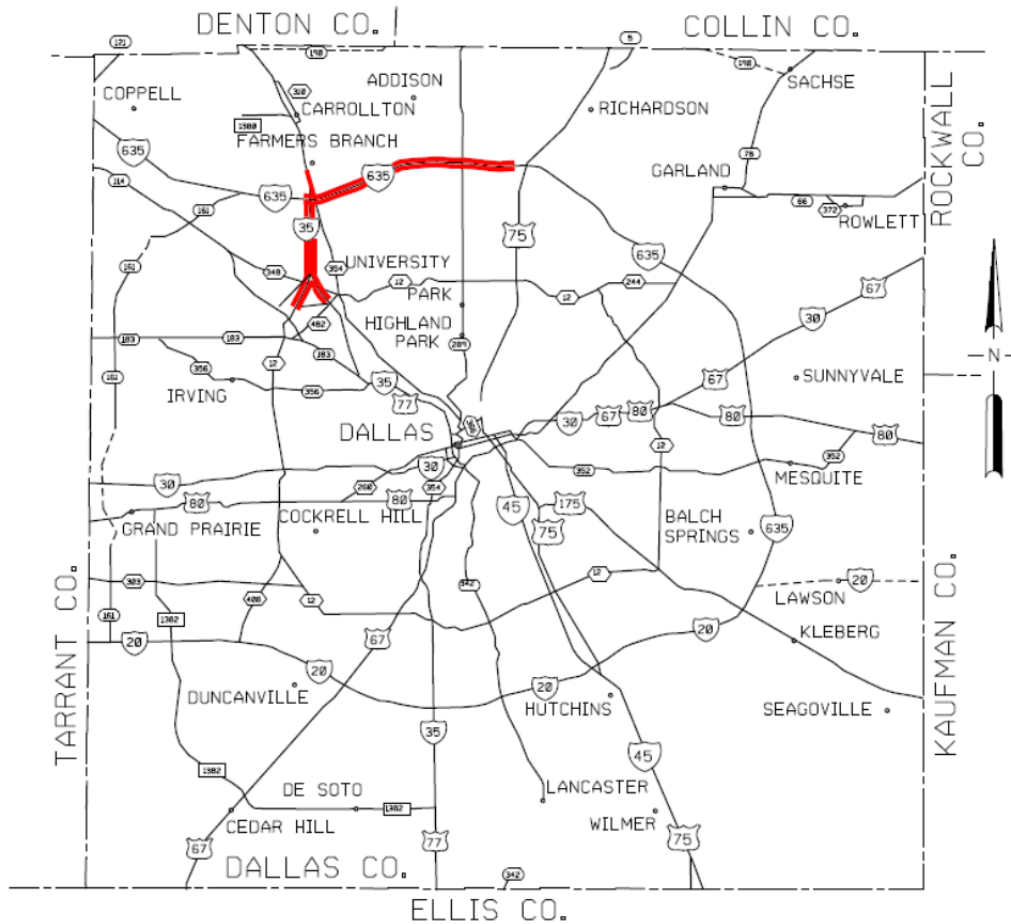


Figure 1-1 Project Location

The IH-35 IH-635 interchange became one of the major landmarks of the project because of its complexity and extensive use of structures. A new Loop 12-IH 635 WB

direct connector has been built, implying the construction of a new bridge (Bridge 4) to solve its crossing over IH-35 highway northbound direction.

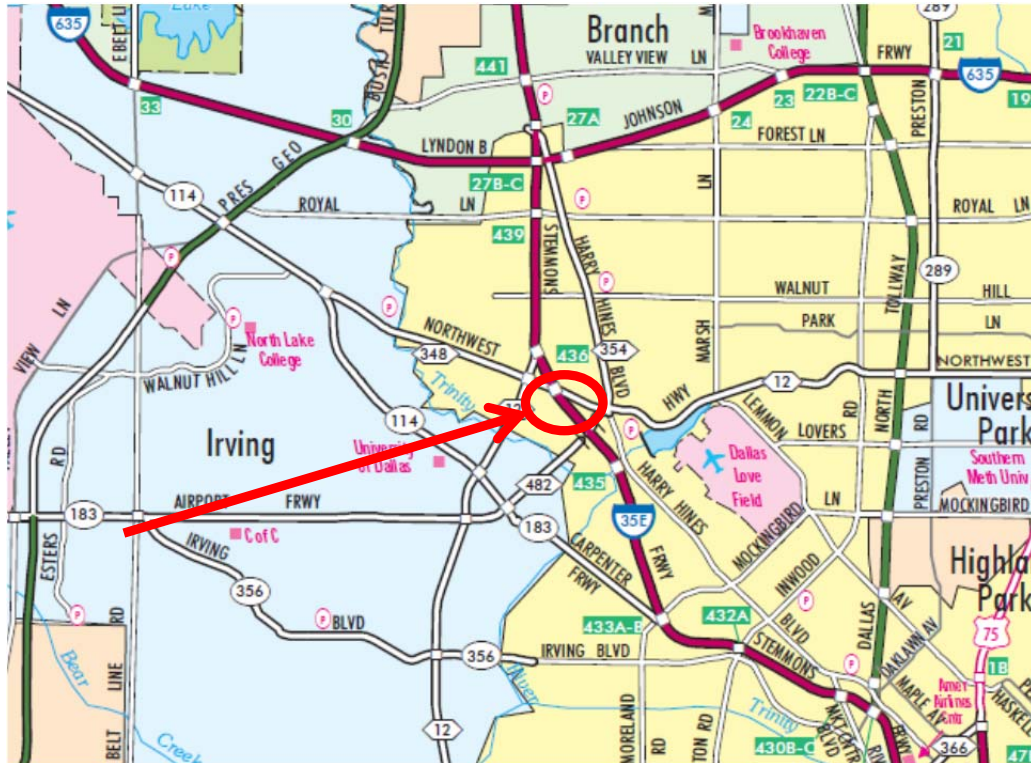


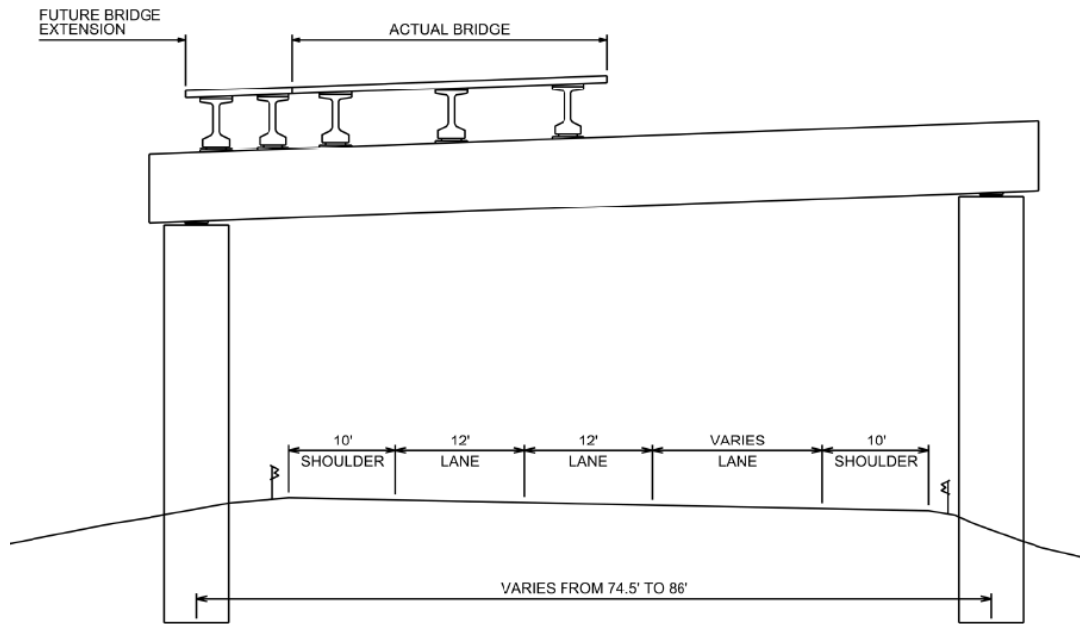
Figure 1-2 Bridge 4 Location

The LBJ Project design and construction teams faced there one of the many challenges they needed to overcome for the successful development of the project. The IH-35 and its existing interchange with IH-635 is a major traffic corridor in Dallas area, supporting high traffic volumes, particularly during peak hours. The construction of a new bridge using conventional design and construction methodologies over this important corridor may imply closing the highway to the traffic and, therefore, seriously impacting the traffic and overall economic activity in this important area of the Metroplex.



Figure 1-3 Bridge 4 Crossing over IH-35E

The singularity of the problem faced needed of an innovative solution. The originally designed post-tensioned cast in place concrete bent cap solution could not be built without a long term closure of the IH-35E highway for the required form work and concrete curing times. The solution to be adopted may have to be prefabricated and simply supported on the columns to limit to the minimum the impact to the traffic. With spans varying from 74.5 ft. to 86 ft. (22.71 to 26.21 m.) between supports, a precast prestressed concrete bent cap would have been too heavy to be safely lifted. A composite steel-concrete bent cap, consisting of a rectangular shaped section of steel with a top compression concrete slab, was designed and built as a lighter alternative complying with the previously mentioned requirements.



NOTE : 1 ft = 0.3 m

Figure 1-4 Bridge 4 Typical Section

This study will consist of the performance of a comparison between both solutions in terms of structural behavior, cost-efficiency and construction time.

### 1.3 Need Statement

Selecting the most appropriate solution for the design of a bridge structure is a difficult task that involves the contribution of professionals with different backgrounds. The particular conditions of the project in hand have to be deeply analyzed to obtain the expected outcome in terms of quality, safety, cost and schedule.

The continuous development of our cities translates in increasing traffic volumes that will eventually overcome the existing transportation infrastructures capacity. Therefore, the construction of new projects to increase traffic capacity of our highways and toll ways in consolidated urban areas and conflicting with other existing infrastructures may lead to the development of new construction processes, techniques and structural typologies.

The current construction market conditions, with an increasing competitiveness for the construction companies, have made the design optimization key for the structural engineer success. In that sense, the availability of comprehensive and detailed guidance documents describing the new processes, techniques and structural typologies is extremely important to ensure that engineers properly comply with their commitment with the society.

In the opinion of this research's author, engineers like himself with a privileged position in a major construction company and therefore, with a unique opportunity of participating in large construction projects have the responsibility of showing to the engineering community those innovative methods, solutions or techniques used in such projects. This research is the result of that commitment

#### 1.4 Research Objectives

The objective of this research is to establish adequate modeling techniques to be used in the analysis and design of both structural typologies in future researches, and conduct a comparison between the two previously discussed structural solutions in terms of structural behavior at service, cost-efficiency and construction schedule. The tasks to be completed are:



- Literature Review. Currently available literature about bridge design, cost estimation and construction scheduling methodologies will be analyzed, identifying their applicability to the case in study
- Structural analysis. Both the posttensioned concrete bent cap original design and the steel-concrete composite bent cap alternative will be modeled using the commercial software ABAQUS to accurately simulate their structural behavior.
- Cost estimation. The total direct cost of both structural alternatives has been determined for their use in preliminary studies.
- Construction scheduling. The construction time required for both solutions have been determined to be used as guidance for preliminary studies.
- Conclusions. The results obtained are compared to determine the advantages and disadvantages of each of the solutions analyzed.

### 1.5 Thesis Organization

Chapter 1 introduces the problem in hand and its controlling parameters. The justification of its need, objectives of the research and the document organization are also presented in this chapter.

Chapter 2 presents the current situation of bridge substructure design in the available literature and related researches. Cost estimation and construction planning literature references are also researched to better establish methodologies to be used in subsequent chapter's analyses.

Chapter 3 describes the finite element model analysis performed for the two bent cap typologies studied, establishing the required parameters for the development of accurate models and methods for their validations.

Chapter 4 provides the cost analysis and construction schedule of the two solutions studied in this Thesis.

Chapter 5 summarizes the results obtained, allowing for their comparison and discussion.

Chapter 6 includes the conclusions drawn from the work performed in this thesis. Proposals for future researches are also provided.

Appendix A includes the drawings in which the general geometry of Bridge 4 and the particular details of the two different structural alternatives studied are shown.

Appendix B presents a summary of the load calculations performed by modeling the bridge using the software PGSuper.

Appendix C provides the prestress losses calculations performed to determine the effective prestress force to be applied in the development of the first finite element model.

Appendix D shows the hand calculations performed to validate the results obtained from the post-tensioned bent cap model developed in Abaqus.

Appendix E presents the calculations performed to validate the composite bent cap model developed using Abaqus.

Appendix F includes the detailed estimates obtained for the two structural solutions studied.

Finally, a list of the references used in the development of this thesis is included.

## Chapter 2

### BACKGROUND AND LITERATURE REVIEW

This chapter presents the information gathered about the topic under analysis. After a brief historical introduction, substructure typologies available in the literature researched are presented and their main characteristics are outlined. Once the two typologies proposed have been described, cost estimation and construction planning methodologies are investigated to determine the techniques that will better serve for the purposes of this study. Finally, the case under analysis is described.

#### 2.1 Historical Introduction

Bridge building is inherent to human society development. The first bridge in human history was probably built in prehistoric times when the need of crossing a river made a man cut a tree and use it for that purpose.

For a long time, the bridge building technology did not experience a noticeable advance, and bridges were built from locally and naturally available materials. It is not until the rise of the Roman Empire when this technology sees a revolution. The need of an extensive net of transportation infrastructures to allow quick and safe communication and transportation of people and goods led to the discovery of the stone arc. Some of those bridges have become major landmarks, like the Alcantara Bridge in Spain, which is still opened to traffic after 2,000 years in service.



Figure 2-1 The Alcantara Bridge (Spain)

The fall of the Roman Empire changed drastically the way bridges were seen. They were no longer an essential infrastructure and they had the disadvantage of being hard to defend from invaders. As a consequence, many of them were demolished during the Middle Ages.

Bridge construction did not experience an increase until the Renaissance, but the lack of new materials prevented engineers from developing new bridge typologies. That situation changed during the 19<sup>th</sup> century with the availability of new construction materials. Improvements in the fabrication processes of gray iron first and steel later cut the prices of those materials. Later, the discovery and development of reinforced and prestressed concrete meant a new revolution for the structural engineering. The appearance of those new construction materials, joined to the development of the modern Mechanics of Materials theory, led to the development of the modern bridge concept.

## 2.2 Structural Background

### *2.2.1 Introduction*

The terms pier and bent are used to refer to any type of substructure used to transfer the bridge superstructure loads to the bridge foundation in intermediate supports between abutments.

The evolution of pier typologies is a consequence of the intensive use of bridges caused by the changes in our transportation infrastructures (Zhao & Tonia, 2012). While bridges were originally used to cross over natural features, the development of the modern transportation networks and their interactions and conflicts have introduced new design constraints for bridges.

The literature available about bridge design usually establishes bridge classifications based mainly, when not exclusively, in the superstructure typology –this is, beams and deck- the materials used and, in some cases, other criteria. For example, (Lebet & Hirt, 2013) establish the following as main criteria for bridge classification:

- Type of use.
- Geometry.
- Structural form.
- Type of slab.
- Cross section.
- Slab position.
- Erection method.
- Slab construction.

Most of the bridge classifications are based in a single criterion. For example, the classifications proposed by (Lee & Sternberg, 2015) and (Zhao & Tonias, 2012) are based only in the structural form of the bridge superstructure. Other authors base their classifications in more than one criterion.

Table 2-1 Bridge Classification Based on Slab Position and Structural Form.

(Barker & Puckett, 2013)

<b>BRIDGE CLASIFICATION</b>	
Main structure below the deck line	Arched and truss-arched bridges
Main structure above the deck line	Suspension, cable-stayed and through-truss bridges
Main structure coincident with the deck line	Girder and slab bridges

This widespread consideration of a bridge being only its superstructure has led to a general lack of information about the possible alternatives that the structural engineer has when facing the design of a bridge substructure.

In general, abutment design is deeply analyzed (Zhao & Tonias, 2012), particularly when referring to integral abutments. For example, (Barr, Halling, Huffaker, & Boyle, 2013) investigated the reasons behind abutment spalling on an integral abutment bridge in Salt Lake City by first instrumenting and monitoring the bridge and second by developing and calibrating a finite element model of the bridge. (Nikravan, 2013) studied the structural behavior of integral bridges when subjected to temperature variations using 3D finite element models, and determined the key parameters that impact the behavior of such bridges.

However, pier typologies are generally omitted or, in the best of the scenarios, limited to the standard solutions made of cast in place reinforced concrete supported either by one –hammerhead bent cap- or more than one –column and pile bent cap (Chen & Duan, 2014). Some special typologies like the straddle bent caps are briefly described in other documents (Colleti & Sheahan, 2012), but their main characteristics and design processes are not covered in depth.

Some public agencies have also published several documents detailing the design process of the most common bent cap typologies. Design examples of rectangular column bent caps (TxDOT, Rectangular Bent Cap Design Example, 2010), inverted T column bent caps (TxDOT, Inverted Tee Bent Cap Design Example, 2010) and hammerhead bent caps (AZDOT, ND) have been developed to help the structural engineer. However, it is difficult for the engineer to find guidance in the design of the two special substructure typologies analyzed in this report.

### *2.2.2 Hammerhead Pier*

This solution consists of the use of one or more columns and a hammer shaped pier cap. Conventionally made of reinforced concrete, this typology is mainly used in urban areas where the space available for the column placement is limited by underpass traffic or existing utilities. In those cases, hammerhead piers with a single column are widely used.

Structurally, this typology works as a rigid-frame structure with one or two cantilevered ends. The characteristic hammerhead shape of this pier type is the result of the cantilevered section optimization. The design is more efficient if the cantilevered portions are balanced in both ends of the cap, resulting in a smaller column section.

Design wise, hammerhead caps are usually considered deep members, what implies that shear deformations are not negligible and, therefore, the Bernoulli hypothesis is not applicable. Under those conditions, the applicable codes establish the strut-and-tie method as the preferred simplified design methodology to be applied in the design of hammerhead piers. (Nicholas, Barth, & Boyajian, 2011) compared the reinforcing requirements of the strength design approach for flexure and shear and the strut-and-tie model method in their application to hammerhead piers design.

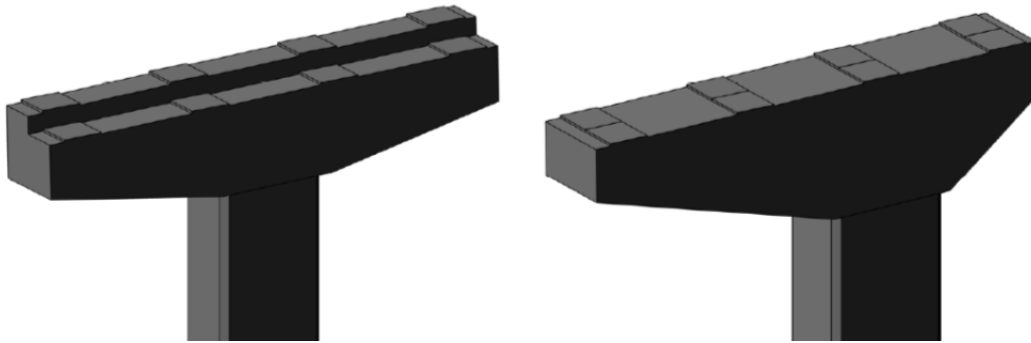


Figure 2-2 a) Balanced Hammerhead Pier b) Unbalanced Hammerhead Pier

As a variation of this type of substructure element, prestress can be introduced. (Pereira, 1994) conducted a research to analyze the behavior of hammerhead piers reinforced with T-headed bars and different levels of prestressing in the cantilever ends by testing under static loading six pier models.



### 2.2.3 Bent Pier

The bent pier consists of a bent beam supported by two or more columns and constituting a rigid frame structure. Usually made of reinforced concrete, this is the most common type of pier in highway bridges (Zhao & Tonia, 2012).

Different variations of this type of pier can be found depending on the section used for the bent beam. The most common sections are the rectangular; and the inverted T section, that is used when a higher modulus of inertia is needed to resist the loads applied.

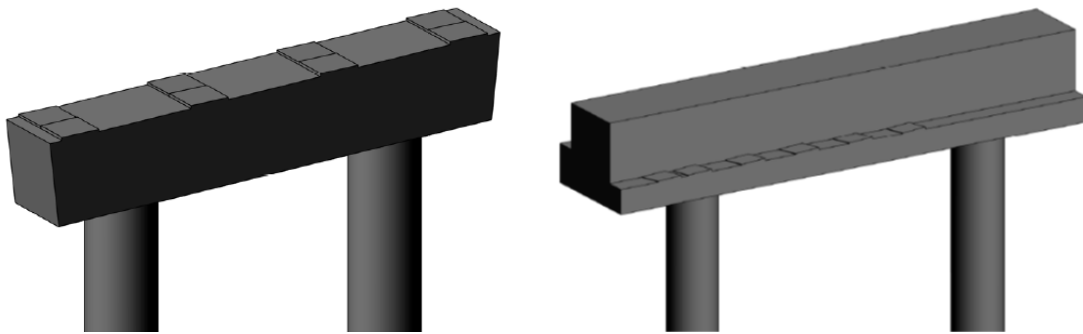


Figure 2-3 a) Rectangular Bent Pier b) Inverted T Bent Pier

Although columns are usually made of reinforced concrete, other alternatives like cast-in shell steel piles are available. (Ferley, 2013) developed finite element models to analyze the behavior of the connections between reinforced concrete bent caps and cast-in-shell piles under lateral loads.

(Bracci, Keating, & Hueste, 2000) studied the cause of unexpected cracks in the cantilevered regions of reinforced concrete bent caps when subjected to service loads. The research consisted of testing 16 full-scale specimens until failure, and concluded that

the flexural cracking was related to the stress levels in longitudinal reinforcement below the service stress limits in the applicable codes.

As a variation of this typology, prestress can be introduced while keeping the rigid frame configuration. (Billington S. L., 1994) studied the structural behavior of two-span continuous bent caps with different levels of prestress by constructing and loading to failure 4 models.

A singularity of the inverted T section is that the girders are usually supported by the bottom flange. (Furlong, Ferguson, & Ma, 1971) studied the behavior of the structural section under that particular loading case by performing 24 load tests over 6 different specimens. As a result of the study, reinforcement details and design procedures for the bottom flange as well as the web shear strength for inverted T bent caps were provided.

#### *2.2.4 Solid Wall Pier*

A solid wall pier is constituted by a reinforced concrete solid wall. Because of the slenderness of the solution and the possibility of being built streamlined, this typology of pier is mainly used in water crossings.

Its use in highway bridges is limited to not excessively wide bridges. The use of wide solid wall piers can create a tunnel effect and may need of the placement of illumination systems.



Figure 2-4 Solid Wall Pier

#### *2.2.5 Integral Pier*

This type of pier implies a rigid connection to the bridge superstructure. Integral connections between bridge superstructure and substructure, for bridges either made of concrete or made of steel, are used to reduce the structure depth and increase the vertical clearance (Colleti & Sheahan, 2012), and improve the structural seismic performance (Wassef & Davis, 2004).

Several studies have been performed to analyze some particular aspects of integral piers. For example, (Ales, 1994) developed a new connection detail between an integral steel cap girder and concrete piers, while (Wassef & Davis, 2004) included the development of recommended methodologies, specifications and design examples about integral steel box-beam pier caps. Also, (Denio, Yura, & Kreger, 1995) studied the shear

strength and reinforcing details to be provided in the connection between steel bent caps and concrete piers by performing eleven static load tests over six pier cap specimens.

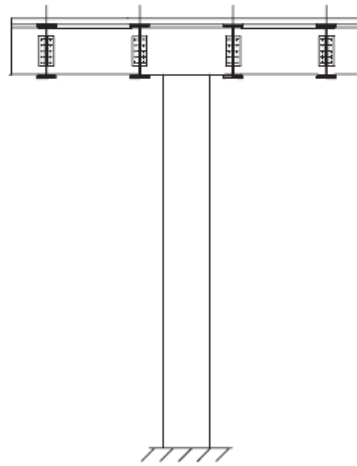


Figure 2-5 Integral Steel Pier Cap

#### *2.2.6 Proposed Pier Typologies*

As stated before, the construction of new transportation infrastructures and the improvement of the existing ones in urban areas may imply impacting traffic flows in existing roadways. These impacts not only affect the traffic, but also the general activity of the area, by limiting the regular development of the economic activity and generating discomfort to the public in general.

The pier caps typologies described before imply a cast in place construction when made of concrete, or a considerable amount of work to be performed in the crossing area when made of steel. However, limiting the impact of new project construction over existing traffic in situations like the one studied in this research can only be achieved by the use of prefabricated solutions.

Structural prefabricated systems have been successfully used in different structure typologies with the well-known advantages:

- Reduction of the construction time and the number of operations to be performed in situ.
- Improved in plant quality control.
- Work zone safety improvement.
- Lower environmental impact.

The development of bridge substructure prefabricated structural systems will add to the previously exposed advantages a reduction in the number and time of traffic detours and closures. In that sense, different researches have been performed to study the applicability of such systems to bridge substructure construction. For example, (Unly, 2010) proposed different precast reinforced concrete systems applicable to the construction of abutments and bent caps.

(Billington, Barnes, & Breen, 1998) proposed reinforced concrete precast systems applicable to the construction of single and double column inverted T hammerhead pier caps and developed connection details between the different elements forming the pier caps.

(Matsumoto, et al., 2001) developed a precast reinforced concrete system for the construction of pile bent caps to be used in nonseismic regions and three different connection details to cast in place or precast trestle piles. The study includes testing of the systems described and proposes design methodologies for the elements proposed.

Other systems have been applied successfully. For example, precast post-tensioned simply supported bent caps with an inverted T section and with spans up to 58 ft. (17.68 m.) have been successfully used for the u-section bridges along the managed lanes in the LBJ project.

However, there is a practical limit for the span length of these precast elements due to their self-weight to allow for their safely lifting and placement.

Two pier cap typologies are presented in this dissertation. The first one consist of the use of cast in place posttensioned concrete pier cap with a rectangular section, and simply supported on concrete columns built at both sides of the affected roadway. In this case, the pier cap will work as a prestressed concrete girder simply supported at both ends. The original design of Bridge 4 used this typology in the crossing over IH-35E in the LBJ project.

The second proposed typology tries to solve the weight problem that limits the application of the previously described precast concrete systems by using different materials applied to the same structural concept: the use of a composite steel-concrete section, constituted by a rectangular steel section topped by a cast in place concrete slab to resist the top compression, and again simply supported at both ends. This solution has also the advantage of simplifying the construction process by changing the time consuming process of post-tensioning the tendons on an elevated position by simply lifting and placing the steel-concrete section once the concrete slab has reached enough strength to support its self-weight.

### 2.3 Cost Estimation Background

Accurately determining the cost of a construction project is a difficult task that implies the use of experience, engineering judgment and scientific principles (Bhargava, 2009). Guidance and databases including unit cost for different construction activities and materials are very useful for the cost estimator, but he usually needs to face the problem of the opacity of the companies and their reticence to make public such data.

Different methods are available for the estimator depending on the project stage and information available, and accuracy needed (Pratt, 2011):

- Preliminary estimating techniques. Estimates prepared in early stages of the project are usually prepared using these techniques because of the lack of detailed information about the project.
- Detailed estimating techniques. These methods are intended to be used at advanced stages of the project, when the information available about the project is more detailed and none or few design decisions are left to be made.

The importance of precisely estimating construction cost in all the phases of a project is essential for its successful development. Design wise, it is crucial to properly determine construction cost at early stages of the project as an aid for the decision makers (Samphaongoen, 2009) to ensure the appropriate structural typology selection.

Independently from the level of development of the project, the following two different types of cost can be defined (Pratt, 2011):

- Direct cost. It can be defined as the cost of material, labor and equipment directly used for the construction of a unit measurement of the construction activities identified for the project. This cost, provided that the construction processes are optimized, should not significantly vary depending on the company performing the work.
- Indirect cost or general expenses. It is included in this category the cost of all the auxiliary items that the contractor needs to properly develop his activity but that are not specifically related to any of the construction activities identified for the project. This cost may greatly vary depending on the construction company policies and internal methods of operation.

The cost of the pier cap typologies proposed in this research will be evaluated in terms of direct cost to provide designers with accurate information for alternative selection processes.

## 2.4 Scheduling Background

(Mubarak, 2010) defined scheduling as

'The determination of the timing and sequence of operations in the project and their assembly to give the overall completion time'.

Construction scheduling has evolved as the construction market conditions changed in the past (Hutchings, 2004). Nowadays, the competitiveness in the construction market leaves no room for the companies to misestimate the time needed for the project completion.

Therefore, if the proper estimation of a project cost is important, precisely knowing the time needed for the project completion is crucial to meet the deadlines and vital for the project success. In the same way that it was previously discussed when referring to cost estimation, schedules are developed during the different phases a project consists of. Depending on the particular case, correct conclusions obtained from an alternative selection process may condition the project development.

Different methods are available for the project scheduler depending on the grade of accuracy and the additional information required. The two most common methodologies are:

- Bar (Gantt) charts. Originally developed by Henry L. Gantt, this method is by far the most extended one for scheduling construction projects (Newitt,



2009). The chart consists of a graphical representation of the activities to be completed for the project completion, their duration and order of precedence. Bar charts are the simplest method used nowadays in project scheduling, and have the advantage of being easy to develop, read and update. But that simplicity becomes also its major disadvantage because of its incapacity of showing activities relationships in large and complex projects (Hutchings, 2004)

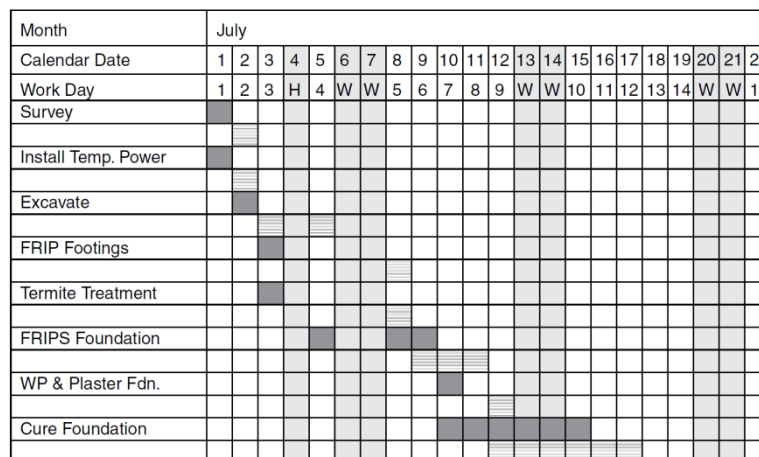


Figure 2-6 Gantt Chart Example (Newitt, 2009)

- Critical Path Method (CPM). This methodology is usually used in conjunction with Gantt Charts in project scheduling applied to complex projects. The method consist of determining those activities that will condition the construction process, and then establishing and showing graphically the construction paths through them and determining the duration of those paths. This method has the advantage of properly showing the activities precedence relationships in large projects. Between its disadvantages, the

CPM is complex to implement and understand, requiring a better qualified staff (Newitt, 2009).

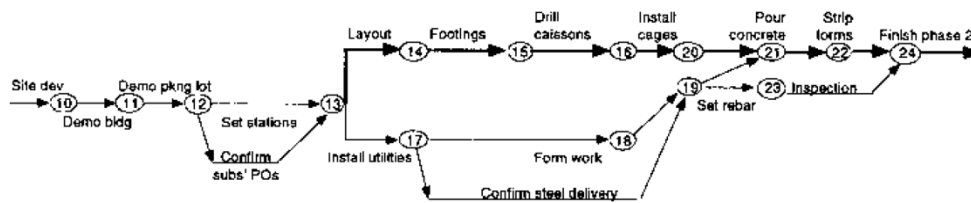


Figure 2-7 Network Schedule (Hutchings, 2004)

- Program evaluation and Review Technique (PERT). This method is a variation of the CPM in which different times (optimistic time, most likely time, pessimistic time) to account for the fact that actual activities duration may vary from those assigned. Therefore, it is considered a probabilistic method.
- Linear scheduling method (LSM). This method consists of the graphical representation of the activities, precedence relationships and duration times in a flowchart like diagram. It can be considered a simplification of the CPM method for use in construction projects with a low number of activities with large associated quantities (Mubarak, 2010).

## 2.5 Case of Study Background

Approximately 13 miles long, the LBJ Express includes improvements along IH-635 corridor from Luna Road to Greenville Avenue, as well as between Loop 12 and Valwood Parkway on IH-35E. The works that are being performed includes the

reconstruction of the IH-635 highway and its frontage roads, and the construction of 4 new managed lanes (two per bound).

Because of its complexity and the extensive use of bridges, the IH-35 IH-635 interchange became one of the major landmarks of the project. To provide direct access from both Loop 12 to the new managed lanes, a new Loop 12-IH 635 WB direct connector has been built. Its crossing over IH-35E has been solved with the construction of Bridge 4.

With a total length of 1,016 ft. (304.8 m), the bridge is divided into 9 spans with 3 TX54 girders per span, with the exception of span 3 that is constituted by 3 steel plate girders. The future extension of the bridge with two new girders per span was also considered in the design.

Spans 6 to 9 and the bent caps 7 to 9 were in conflict with the corridor IH-35E. The typology originally designed for these bent caps consisted of a cast in place post-tensioned rectangular section simply supported on two cast in place columns, with span lengths varying from 74.5 ft. (22.71 m) for bent 7 to 86 ft. (26.21 m) for bent 9.

The construction of that solution, implying a long term closure of IH-35E, will have seriously affected the overall traffic flow in the area. To limit the conflicts with IH35E traffic, an alternative prefabricated solution formed by a rectangular steel section topped with a concrete slab simply supported by cast in placed column was proposed and built.

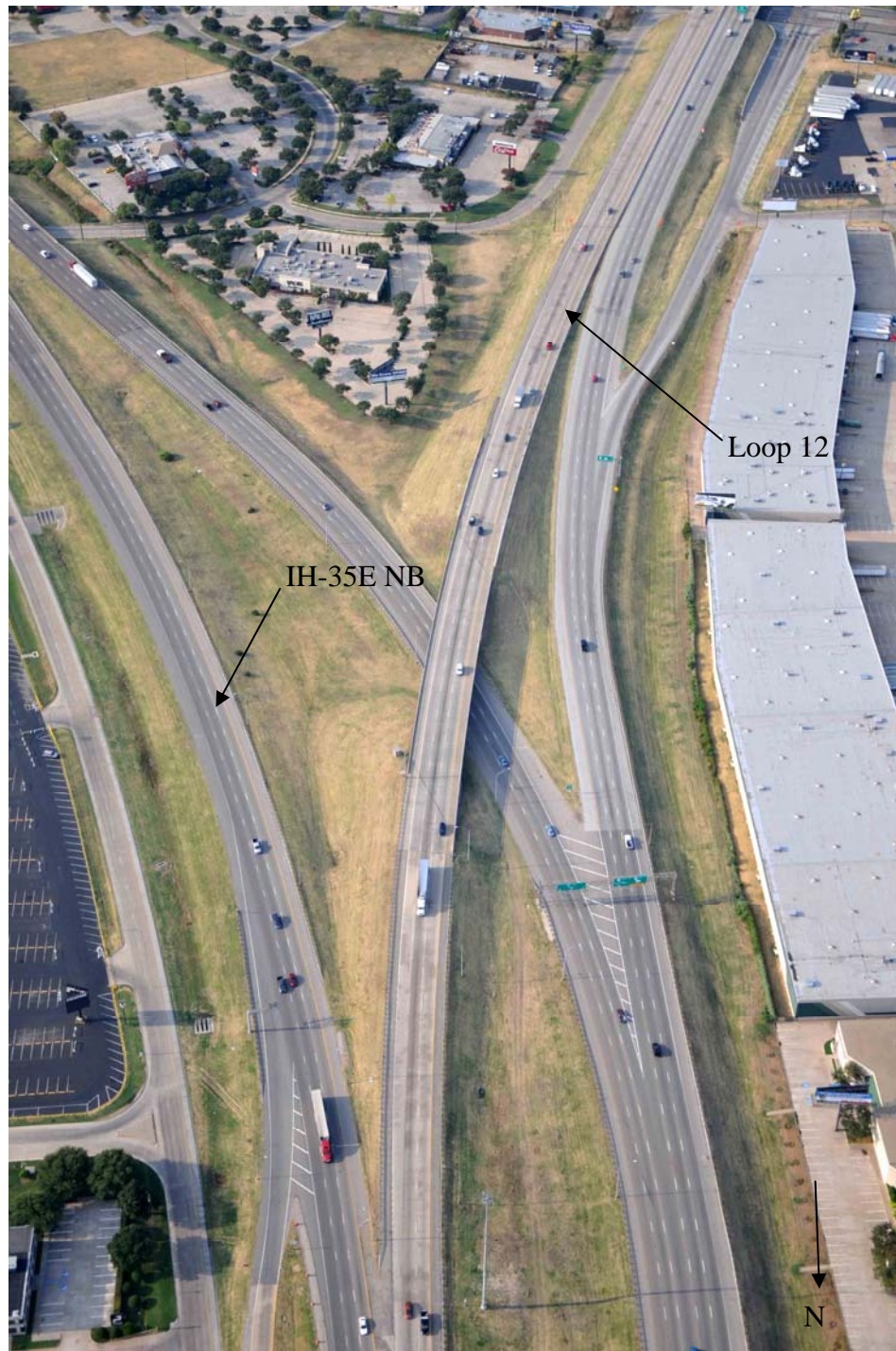


Figure 2-8 Bridge 4 Location Before Construction

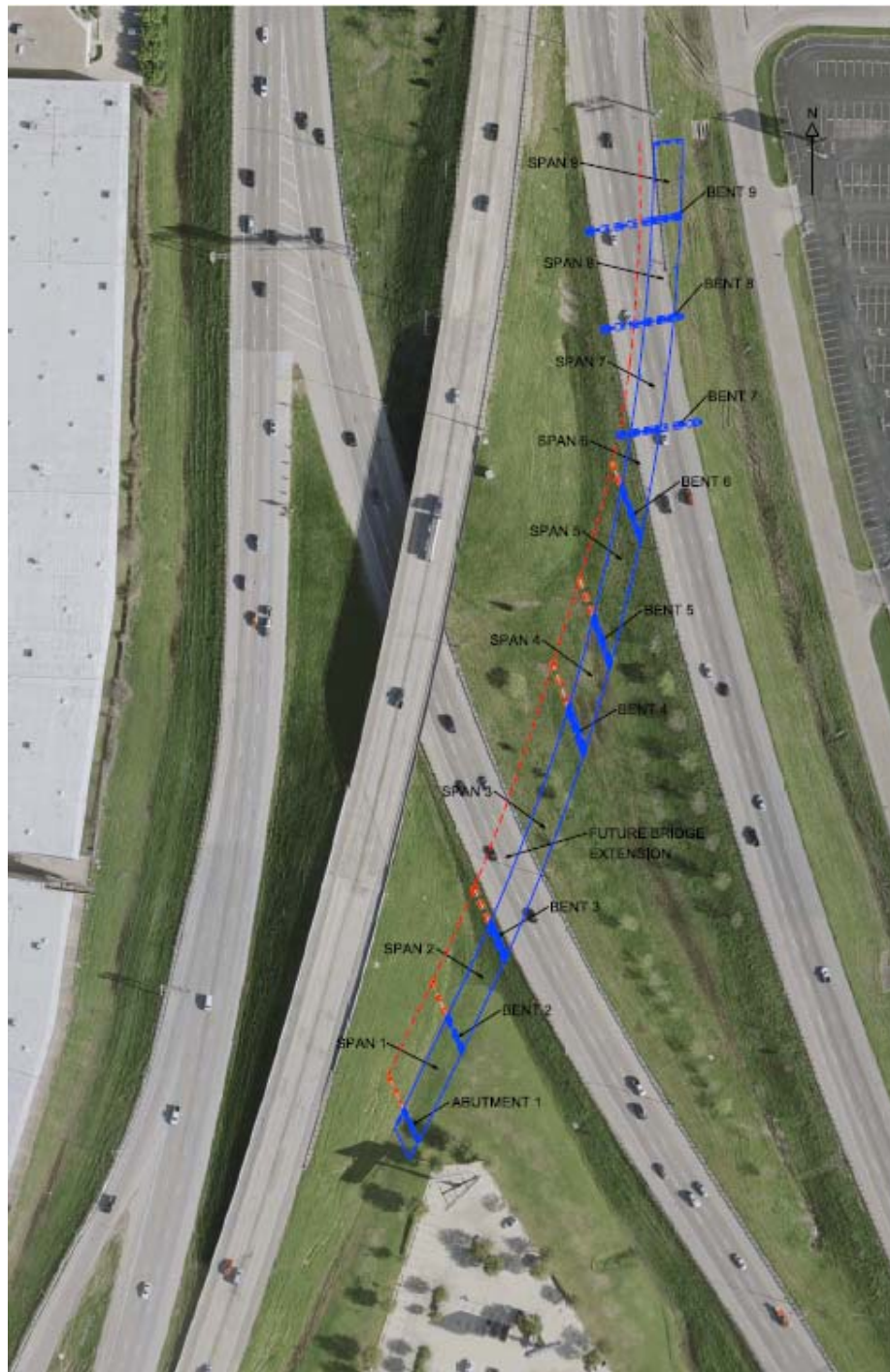


Figure 2-9 Bridge 4 Plan View





Figure 2-10 Composite Bent Cap Lifting Operation



Figure 2-11 Bent Caps 7, 8 and 9 in Place

Both alternatives applied to the particular geometry of bent 7 in Bridge 4 have been analyzed in terms of structural behavior, cost and construction schedule. The main characteristics of the post-tensioned solution are:

- The bent cap section is 6.33 ft. (1.93 m) wide and 8.5 ft. (2.59 m) high.
- It is simply supported on two cast in place 6 ft. (1.83 m) diameter concrete columns. The pin connection is achieved by using elastomeric pads and a shear key to ensure the transmission of the prestressing force.
- The span length is 74.5 ft. (22.71 m).
- It carries the loads from spans 6 and 7. Although the current bridge has only 3 TX54 girders per span, two additional girders have been considered to account for the future extension of the bridge.
- 6 parabolic tendons with 31 0.6 in. (15.24 mm) diameter grade 270 low relaxation prestressing steel strands are to be installed. The nominal area of each tendon is 6.727 in<sup>2</sup> (4,340 mm<sup>2</sup>). The jacking force per tendon is 1,362 kips (6,058.48 kN).
- The concrete nominal strength is 6,000 psi (41.37 MPa), and the strength required at jacking is 5,000 psi (34.47 MPa).





Figure 2-12 Bridge 4 Construction. Girders in Place



The main characteristics of the composite solution are:

- The bent cap steel section is 6.00 ft. (1.83 m) wide and 5.67 ft. (1.73 m) high, topped by a concrete slab 10 in. (254 mm) thick.
- Two diaphragms are placed at each support, as well as girder stiffeners at each girder location. Also, interior stiffeners are placed spaced as required by design.
- The concrete slab is connected to the steel section by the use of shear studs with heads.
- Grade 50 structural steel is used in the steel section.
- The top slab concrete nominal strength is 6,000 psi (41.37 MPa).
- It is simply supported on two cast in place 6 ft. (1.83 m) diameter concrete columns. The pin connection is achieved by using elastomeric pads placed on top of the columns.
- The span length is 74.5 ft. (22.71 m).
- It carries the loads from spans 6 and 7. Although the current bridge has only 3 TX54 girders per span, two additional girders have been considered to account for the future extension of the bridge.

Additional information about the two proposed solutions can be found in Appendix A.



Figure 2-13 Bridge 4 Finished and in Service

## Chapter 3

### FINITE ELEMENT MODELLING

The main objective of this chapter is establish modelling techniques to be used in the application of the finite element method using the commercial software Abaqus to model the structural typologies presented minimizing the computational cost of running the models. First, the materials models to be used are presented. The second part describes the live loads to be used in the models based on the applicable structural codes. Then, after describing the boundary conditions assumed, the models developed are presented. Finally, the validation of the two models developed is performed to investigate the accuracy of the results obtained.

#### 3.1 Materials

Properly modelling material properties is essential for developing accurate finite element models (FEM) since the material models will determine how the structure behaves when subjected to the design loading case.

The commercial software Abaqus includes several material models to help the user in FEM development. The material properties used in the development of the FEM models included in this research are described below.

##### *3.1.1 Concrete*

Abaqus software includes the following three models applicable to concrete as a brittle material:

Brittle cracking model. This model is intended to be used for materials with brittle behavior dominated by tensile cracking, allowing the removal of elements in the model based on a failure criterion. It assumes a simplified linear elastic response for the material in compression, and a linear elastic-plastic behavior in tension. However, the behavior of concrete when subjected to compressive stresses is known to be plastic. Therefore, the use of this model is not adequate for models like the ones developed in this dissertation, in which concrete is going to be subjected mainly to compression.

Concrete smeared cracking model. Also thought to be used for modelling brittle materials dominated by tensile cracking, it allows for the use of a plastic behavior for the material under compression and it uses a linear elastic-plastic model under tension. It only accounts for tensile cracking (that means it does not model properly compression failure, and therefore, is considered not adequate for the cases of study). It models the postfailure behavior and the reinforcement interaction by the use of the tension stiffening concept: after reaching the tensile stress limit for the concrete, the tensional stresses are gradually transferred from the concrete element to the reinforcement element.

Concrete damage plasticity (CDP) model. This model is intended to be used for materials with brittle behavior with the possibility of establishing failure criteria in compression and tension by the use of damage parameters. It models both the behaviors of the material in tension and compression as linear elastic-plastic, and it considers tension stiffening to model the tension postfailure behavior and reinforcement interaction. This is the material model that better approximates the behavior of concrete in the two FEM to be analyzed and, therefore, have been used in this study.

Different parameters have to be determined to properly define the concrete damage plasticity model in Abaqus. The first five parameters to be defined are related to the performance of concrete under compound stress and determine the shape and

orientation of the failure surface. In the absence of more accurate empirical data, (Kmieciak & Kaminski, 2011) propose the following values to be used:

Table 3-1 Default Parameters of CDP Model under Compound Stress

(Kmieciak & Kaminski, 2011)

Parameter name	Value
Dilatation angle	36
Eccentricity	0.1
$f_{bo}/f_{co}$	1.16
$\kappa$	0.667
Viscosity parameter	0

The stress-strain curve for the concrete in compression is obtained using the following model applicable to concrete strengths from 2,175.57 to 18,129.71 psi (15 to 125 MPa) (Wight & MacGregor, 2012):

$$\frac{\sigma_c}{f'_c} = \frac{n(\varepsilon_c/\varepsilon_0)}{n-1+(\varepsilon_c/\varepsilon_0)^{nk}} \quad (1)$$

where

$f'_c$ =peak stress.

$\varepsilon_0$ =strain when  $f_c$  reaches  $f'_c$ . (See Eq. (2))

$n$ =a curve-fitting factor. (See Eq. (3))

$E_c$ = initial tangent modulus (when  $\varepsilon_c=0$ ). (See Eq. (6))

$k$ =factor that calibrates the slope of the ascending and descending branches of the curve. (See Eqs. (4) and (5)).

$$\varepsilon_0 = \frac{f'_c}{E_c} \left( \frac{n}{n-1} \right) \quad (2)$$

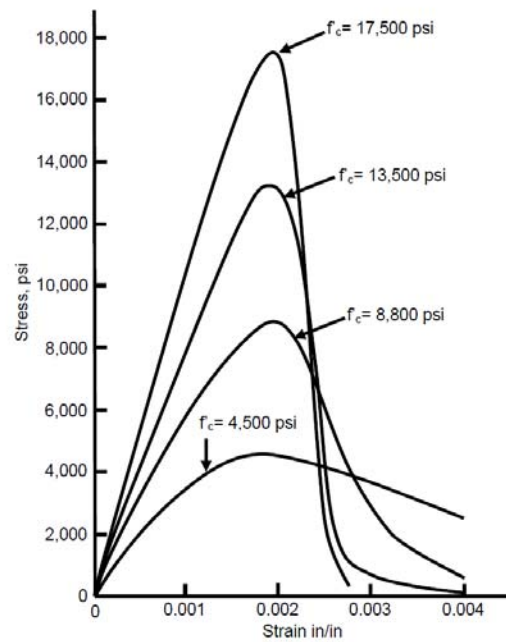
$$n = 0.8 + \left( \frac{f'_c}{2500} \right) \quad (3)$$

$$k = 1 \text{ if } \varepsilon_c / \varepsilon_0 \leq 1 \quad (4)$$

$$k = 0.67 + \left( \frac{f'_c}{9000} \right) \geq 1 \text{ if } \varepsilon_c / \varepsilon_0 > 1 \quad (5)$$

The initial tangent modulus is taken for normal weight concrete as (AASHTO, 2012):

$$E_c = 1,820 \sqrt{f'_c} \text{ (ksi)} \quad (6)$$



NOTE: 1 psi = 6,894.76 Pa

Figure 3-1 Typical Stress-Strain Curves for Concrete in Compression  
(Wight & MacGregor, 2012)

The previous figure shows the stress-strain curves for different concrete strengths obtained by the application of the described model. As can be observed, the behavior of concrete subjected to compressive uniaxial loading is plastic, although the first portion of the curve can be approximated by a straight line with a slope of  $E_c$ . Also, a maximum value of stress and its corresponding strain must be defined as a limit for total compression crushing failure of the concrete. Those two limiting values in the compressive behavior of concrete have been taken as  $0.5f'_c$  and  $0.3f'_c$  (Wahalathantri, Thambiratnam, Chan, & Fawzia, 2011).

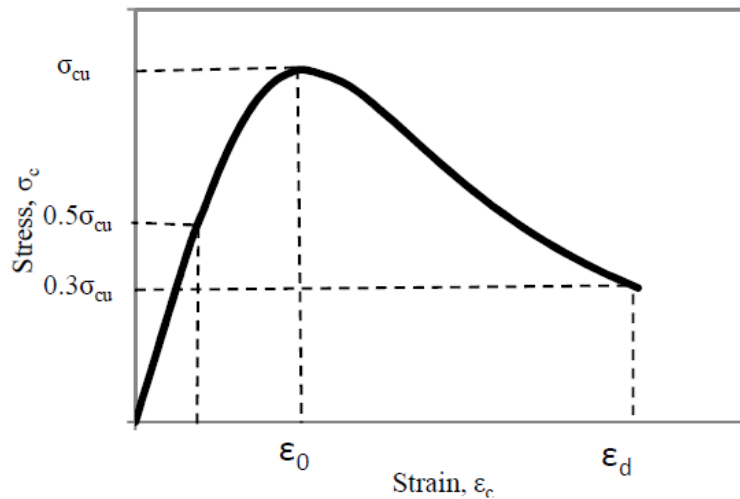


Figure 3-2 Compressive stress-strain curve adopted for modelling concrete with Abaqus  
(Wahalathantri, Thambiratnam, Chan, & Fawzia, 2011)

The following stress-strain relationship for the behavior of concrete when subjected to uniaxial tension has been initially followed (Kmieciak & Kaminski, 2011):

$$\sigma_t = E_c \varepsilon_t \text{ if } \varepsilon_t \leq \varepsilon_r \quad (7)$$

$$\sigma_t = f_r (\varepsilon_r / \varepsilon_t)^n \quad (8)$$

where

$E_c$ = initial tangent modulus (when  $\varepsilon_c=0$ ). (See Eq. (6))

$f_r$ =tensile strength of the concrete. (See Eq. (9))

$\varepsilon_r$ =strain when  $f_t$  reaches  $f_r$ .

$n$ =weakening rate. Assumed a value of 0.4 (Kmieciak & Kaminski, 2011).

The tensile strength of the concrete is taken as its modulus of rupture (AASHTO, 2012):

$$f_r = 0.24 \sqrt{f'_c} \quad (9)$$

However, this type of curves is known to cause run time errors in Abaqus material models. Therefore, the simplified stress-strain relationship shown in Figure 3-3 (Wahalathantri, Thambiratnam, Chan, & Fawzia, 2011) have been used in the development of the finite element models. The material model used implies an elastic behavior up to the modulus of rupture of the material. The subsequent discharge branch, that defines the plastic behavior of the material, is approximated by using three line segments.



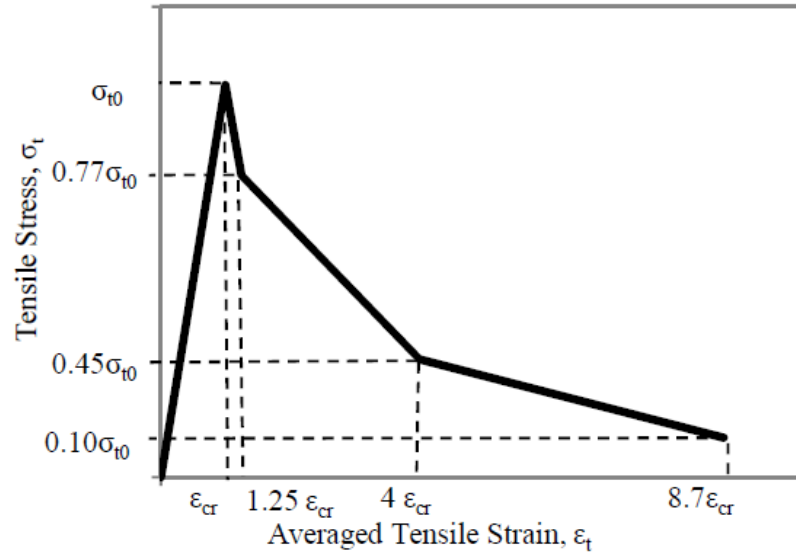


Figure 3-3 Modified Tension Stiffening Model for Abaqus (Wahalathantri, Thambiratnam, Chan, & Fawzia, 2011)

The compressive damage parameter  $d_c$  is related to the plastic strain by the following equation (Birtel & Mark, 2006):

$$d_c = 1 - \frac{\sigma_c E_c^{-1}}{\varepsilon_c^{pl}(1/b_c - 1) + \sigma_c E_c^{-1}} \quad (10)$$

where the compressive plastic strain is proportional to the inelastic strain  $\varepsilon_c^{in} = \varepsilon_c - \sigma_c E_c^{-1}$  using the parameter  $b_c$ . A value of 0.7 for this parameter has been used since it accurately simulates the unloading path of concrete under compression.

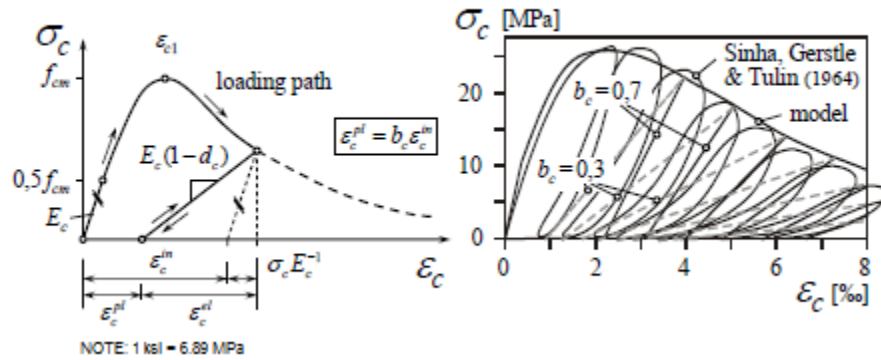


Figure 3-4 Definition of Inelastic Strain, Plastic Strain and Damage Parameter for (Cyclic) Compression Loading (Birtel & Mark, 2006)

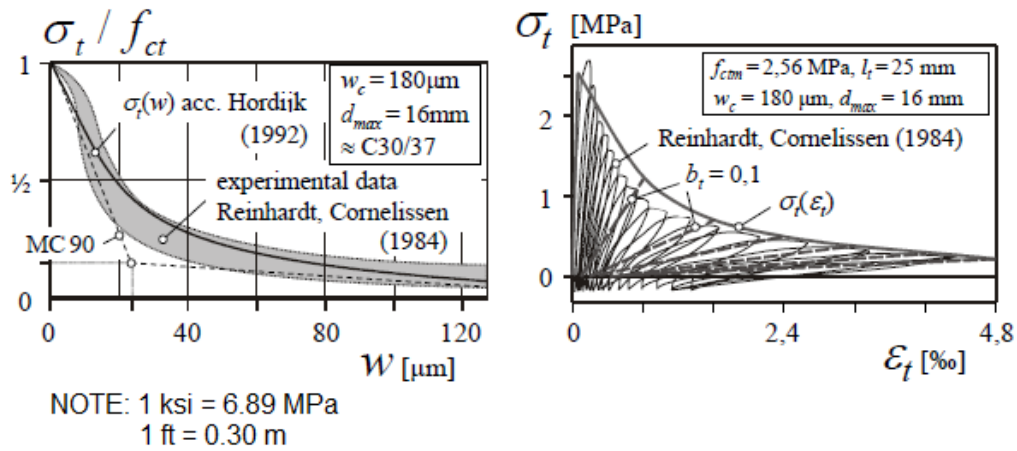


Figure 3-5 Definition of Cracking Strain, Plastic Strain and Damage Parameter for (Cyclic) Tensile Loading (Birtel & Mark, 2006)

Following the same concept, the tension damage parameter  $d_t$  can be defined as follows (Birtel & Mark, 2006):

$$d_t = 1 - \frac{\sigma_t E_c^{-1}}{\varepsilon_t^{pl}(1/b_t - 1) + \sigma_t E_c^{-1}} \quad (11)$$

where the tensile plastic strain is proportional to the cracking strain  $\varepsilon_t^{ck} = \varepsilon_t - \sigma_t E_c^{-1}$  using the experimentally determined parameter  $b_t$  equal to 0.1.

The following tables and figures summarize the values obtained for the compressive behavior for a concrete strength of 6,000 psi (41.37 MPa), as well as its damage parameter.

As discussed above, compressive concrete behavior have been assumed to be linear elastic up to half its peak strength (3,000 psi or 20.68 MPa), followed by a strain hardening branch till the point the material reaches its maximum strength. Finally, a strain softening branch extends up to a limiting stress of 1,800 psi (12.41 MPa) or  $0.3f'_c$ .

Table 3-2 Concrete Compressive Behavior Model

$f'_c$	6,000.000	psi	41.369	MPa
$E_c$	4,458,071.332	psi	30,737.327	MPa
$\nu$	0.200			
$n$	3.2			
$\epsilon_0$	1.958E-03			
$K$	1	if $\epsilon_c/\epsilon_0 \leq 1$		
	1.337	if $\epsilon_c/\epsilon_0 > 1$		
$b_c$	0.7			

$\epsilon_c^{pl}$	$d_c$	$\epsilon_c^{in}$	$\epsilon_c$	$\sigma_c$ (psi)	$\sigma_c$ (MPa)
-	-	-	0.000E+00	0.00	0.00
-	-	-	2.500E-04	1,113.82	7.68
-	-	-	5.000E-04	2,216.26	15.28
0.000E+00	0.000	0.000E+00	6.835E-04	3,000.00	20.68
2.664E-05	0.013	3.805E-05	9.335E-04	3,991.89	27.52
6.897E-05	0.027	9.853E-05	1.183E-03	4,836.80	33.35
1.441E-04	0.048	2.059E-04	1.433E-03	5,472.86	37.73
2.581E-04	0.078	3.688E-04	1.683E-03	5,861.15	40.41
4.282E-04	0.120	6.118E-04	1.958E-03	6,000.00	41.37
6.673E-04	0.186	9.533E-04	2.208E-03	5,591.81	38.55
9.393E-04	0.265	1.342E-03	2.458E-03	4,974.29	34.30
1.223E-03	0.353	1.747E-03	2.708E-03	4,280.41	29.51
1.504E-03	0.443	2.149E-03	2.958E-03	3,607.08	24.87
1.773E-03	0.530	2.533E-03	3.208E-03	3,005.93	20.73
2.029E-03	0.608	2.898E-03	3.458E-03	2,494.47	17.20
2.270E-03	0.677	3.243E-03	3.708E-03	2,070.85	14.28
2.446E-03	0.722	3.495E-03	3.899E-03	1,800.00	12.41

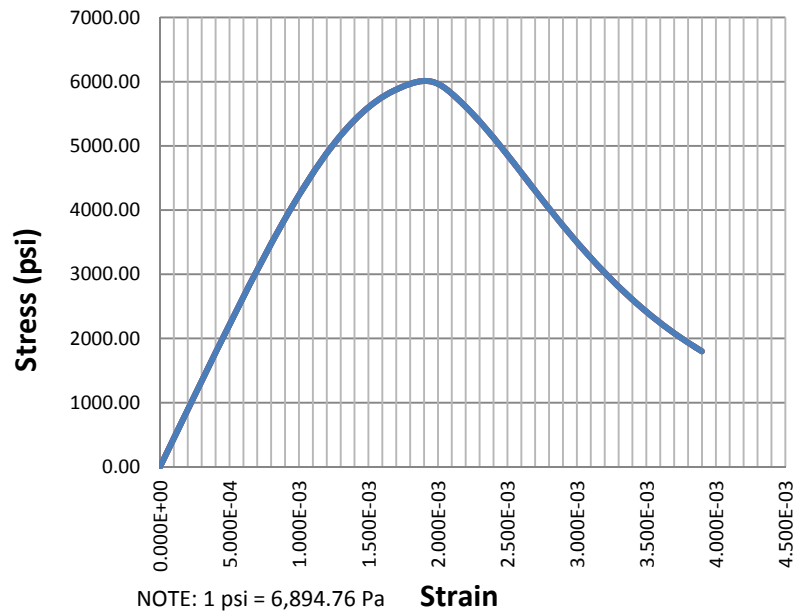


Figure 3-6 Stress-Strain Curve. Concrete Under Uniaxial Compression

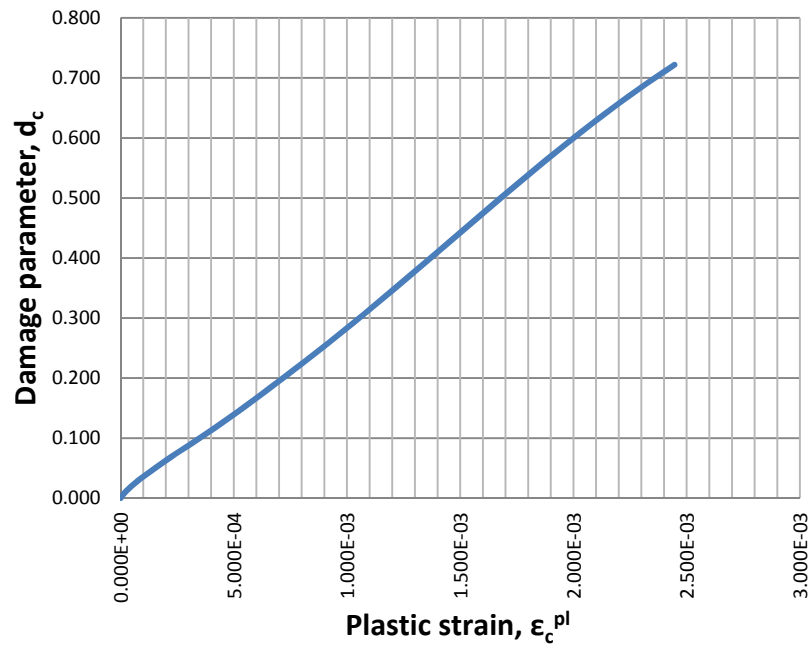


Figure 3-7 Damage Parameter. Concrete Under Compression

In the same way, the tensile performance for a concrete strength of 6,000 psi (41.37 MPa), as well as the tensile damage parameter, are shown in the following tables and figures.

Tensile concrete behavior has been considered linear elastic up to the modulus of rupture of the material, followed by a strain softening branch divided in three different areas as discussed before.

Table 3-3 Concrete Tensile Behavior Model

$f'_c$	6,000.000	psi	41.369	MPa
$n$	0.400			
$\nu$	0.200			
$E_c$	4,458,071.332	psi	30,737.327	MPa
$f_r$	587.878	psi	4.053	MPa
$\varepsilon_r$	1.319E-04			
$b_t$	0.1			

$\varepsilon_t^{pl}$	$d_t$	$\varepsilon_t^{ck}$	$\varepsilon_t$	$\sigma_t$ (psi)	$\sigma_c$ (MPa)
0.000E+00	0.000	0.000E+00	0.000E+00	0.00	0.00
0.000E+00	0.000	0.000E+00	2.198E-05	97.98	0.68
0.000E+00	0.000	0.000E+00	4.396E-05	195.96	1.35
0.000E+00	0.000	0.000E+00	6.593E-05	293.94	2.03
0.000E+00	0.000	0.000E+00	8.791E-05	391.92	2.70
0.000E+00	0.000	0.000E+00	1.099E-04	489.90	3.38
0.000E+00	0.000	0.000E+00	1.319E-04	587.88	4.05
2.110E-06	0.135	2.110E-05	1.429E-04	542.81	3.74
4.220E-06	0.254	4.220E-05	1.538E-04	497.74	3.43
6.330E-06	0.359	6.330E-05	1.648E-04	452.67	3.12
1.308E-05	0.555	1.308E-04	2.253E-04	421.31	2.90
1.982E-05	0.671	1.982E-04	2.857E-04	389.96	2.69
2.657E-05	0.748	2.657E-04	3.462E-04	358.61	2.47
3.332E-05	0.803	3.332E-04	4.066E-04	327.25	2.26
4.007E-05	0.845	4.007E-04	4.670E-04	295.90	2.04
4.681E-05	0.877	4.681E-04	5.275E-04	264.54	1.82
5.791E-05	0.910	5.791E-04	6.308E-04	230.25	1.59
6.901E-05	0.934	6.901E-04	7.341E-04	195.96	1.35
8.011E-05	0.952	8.011E-04	8.374E-04	161.67	1.11
9.121E-05	0.966	9.121E-04	9.407E-04	127.37	0.88
1.023E-04	0.978	1.023E-03	1.044E-03	93.08	0.64
1.134E-04	0.987	1.134E-03	1.147E-03	58.79	0.41

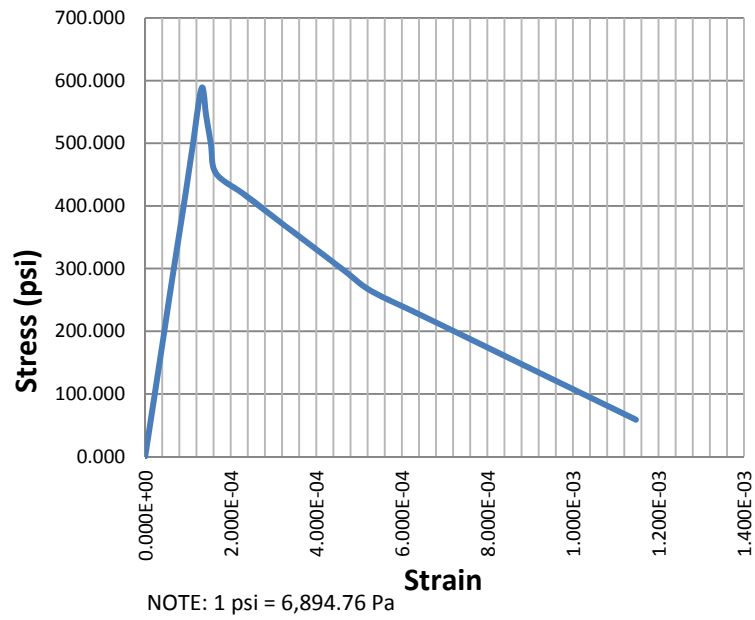


Figure 3-8 Stress-Strain Curve. Concrete Under Uniaxial Tension

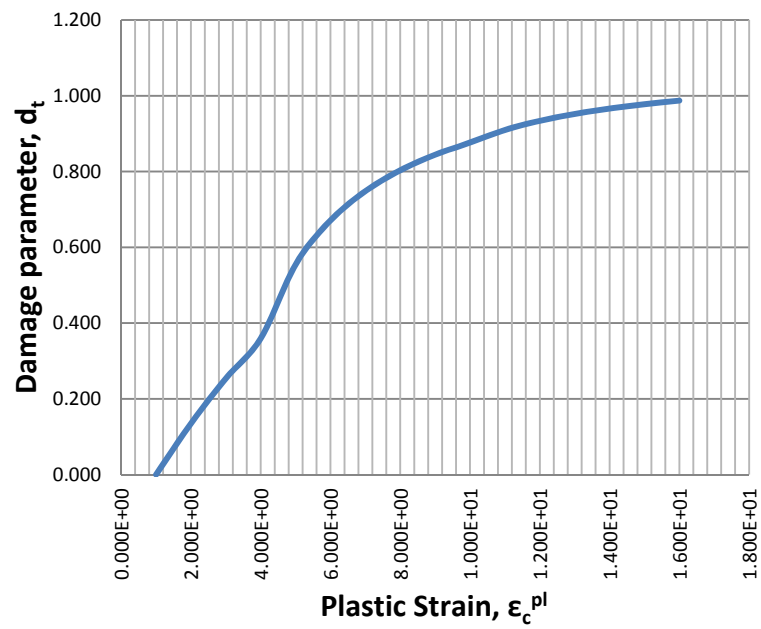


Figure 3-9 Damage Parameter. Concrete Under Tension

### 3.1.2 Reinforcing Steel

The reinforcing steel considered in the FEM performed is grade 60, with a yield strength of 60,000 psi (413.69 MPa). The following figure shows the strain-stress curves for different grades of steel. For a grade 60 steel, it can be seen that after the initial elastic behavior up to the yielding point, a perfectly plastic behavior take place followed by a strain hardening branch. Finally, a strain softening branch extends up to the ultimate strength of the material

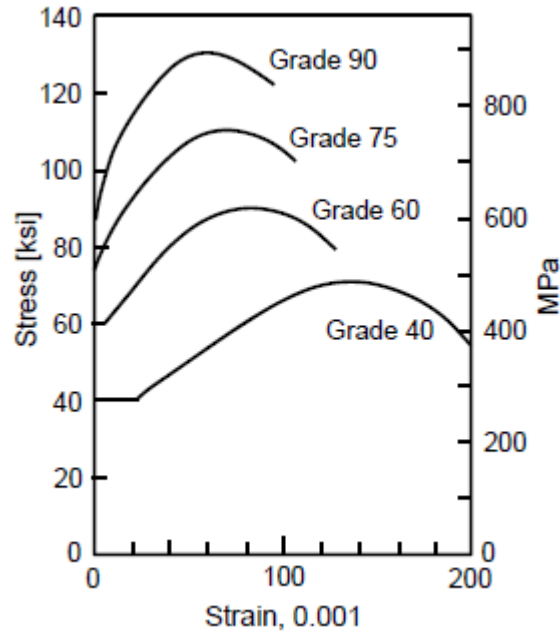


Figure 3-10 Typical Stress-Strain Curves for Reinforcing Steel

(Nilson, Darwin, & Dolan, 2004)

For the purpose of modelling the material, reinforcing steel has been considered an elastic-perfectly plastic material. Steel elastic properties have been taken as follows (AASHTO, 2012):



$$E = 29 \times 10^6 \text{ psi (200,000 MPa)}$$

$$\nu = 0.3$$

$$f_y = 60,000 \text{ psi (413.69 MPa)}$$

The material model considered for reinforcing steel is shown in the following figure:

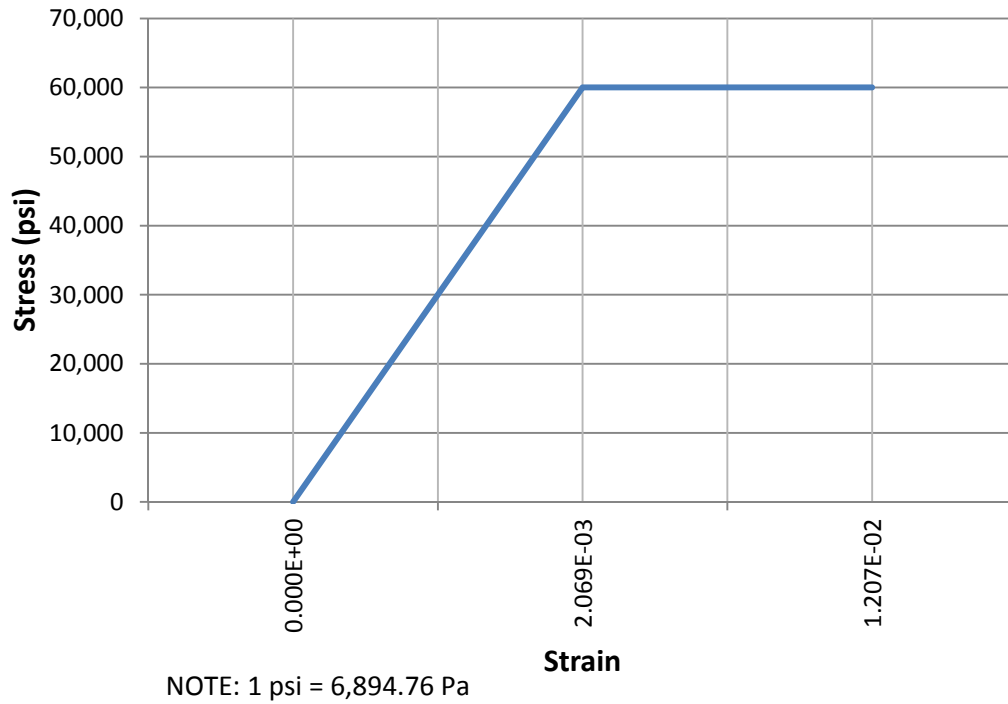


Figure 3-11 Grade 60 Reinforcing Steel. Stress-Strain Curve

### 3.1.3 Prestressing Steel

Unless reinforcing steel, in which the yielding stress can be clearly defined from the results of a uniaxial tension test, yielding stress limit for prestressing steels is not that clear. Different arbitrary methods that identify the yielding point as the stress reached at a certain strain are usually used. The following figures show the stress-strain curve for different prestressing steels and the 1% strain criteria to determine the yielding stress. Also, the criterion for determining the failure strain of the steel is included.

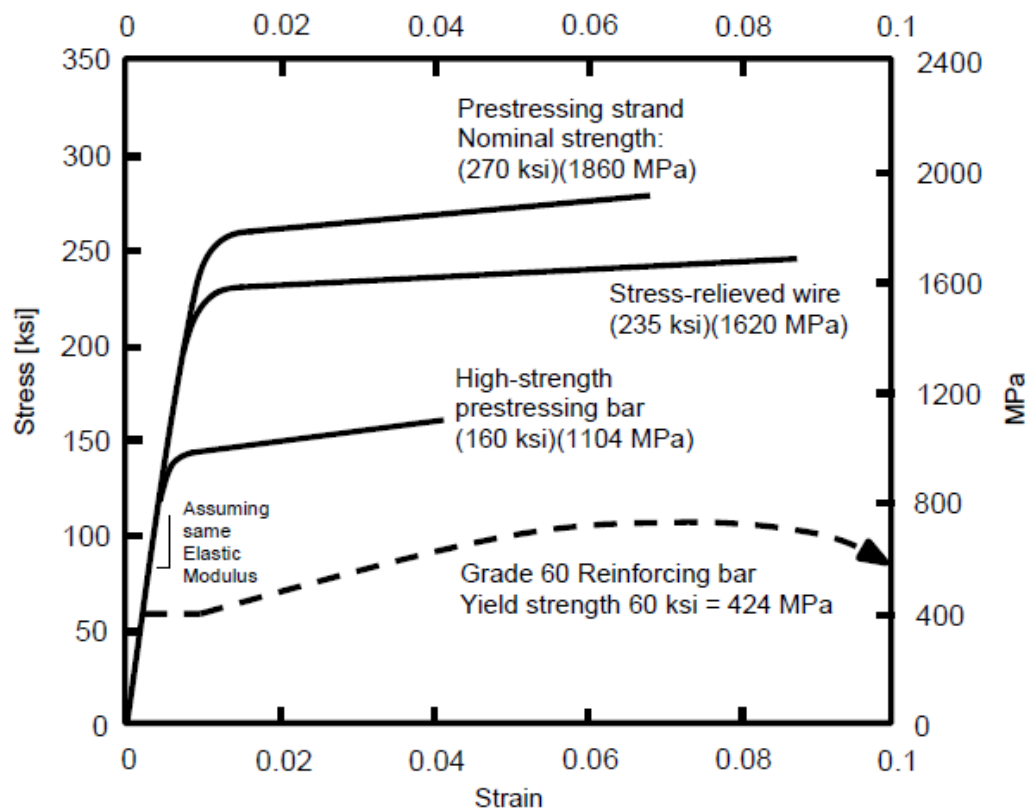


Figure 3-12 Typical Stress-Strain Curves for Prestressing Steel (Naaman, 2012)

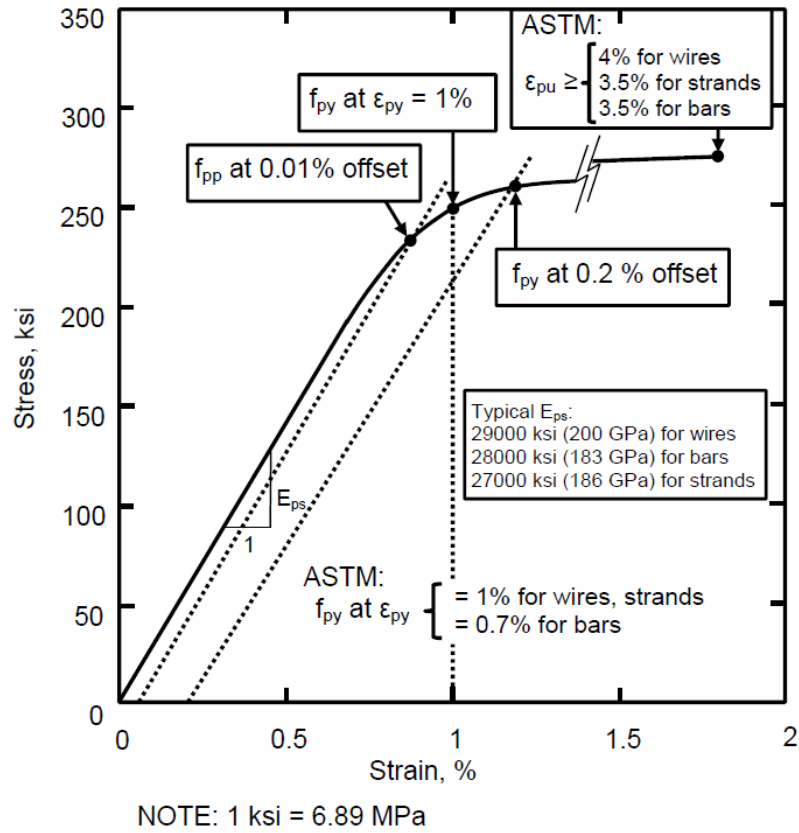


Figure 3-13 Typical Determination of Yield Strength for Prestressing Steel  
(Naaman, 2012)

Prestressing steel will be modelled as an elastic-plastic material, with the following properties (AASHTO, 2012):

Low relaxation Grade 270 prestressing steel

$$E = 28.5 \times 10^6 \text{ psi } (196,500.63 \text{ MPa})$$

$$\nu = 0.3$$

$$f_{pu} = 270,000 \text{ psi } (1,861.59 \text{ MPa})$$

$$\varepsilon_{pu} = 0.035$$

$$f_{py} = 243,000 \text{ psi (1,675.43 MPa)}$$

31-0.6" (15.24 mm)  $\Phi$  strands. Nominal area 6.727 in<sup>2</sup> (4,340 mm<sup>2</sup>) per tendon

The stress-strain curve obtained based on the previously described criteria and data for the prestressing steel is shown in the following figure:

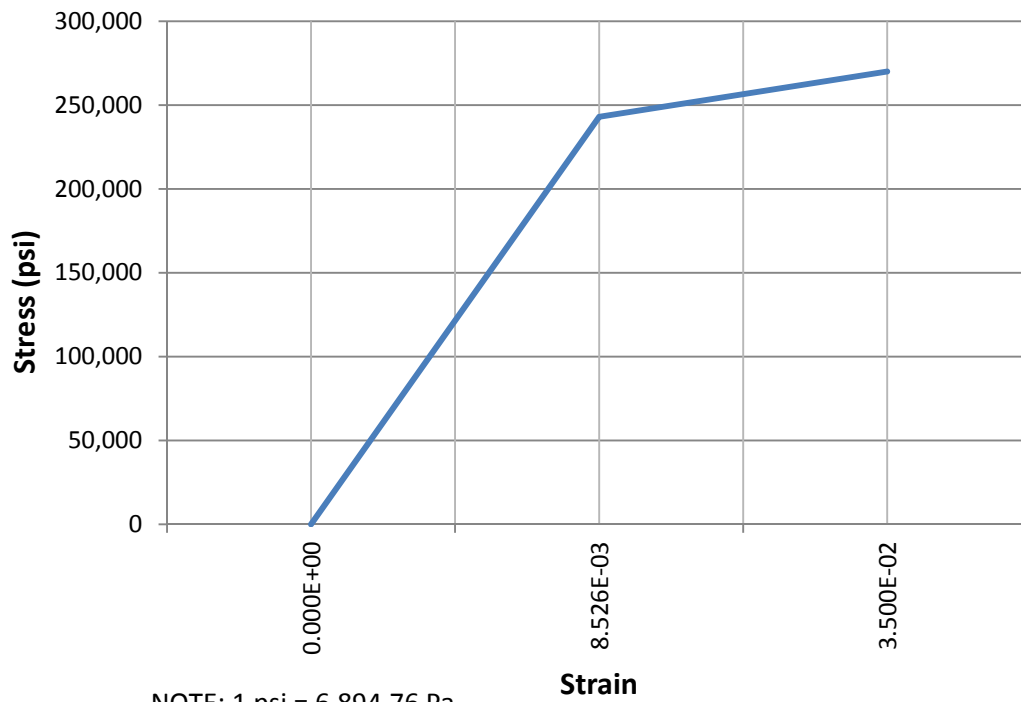


Figure 3-14 Grade 270 Low Relaxation Prestressing Steel.

Stress-Strain Curve

### 3.1.4 Structural Steel

Structural steels presents similar stress-strain curves to those obtained for reinforcing steel in uniaxial tension tests, with an elastic branch and a well-defined yielding point, followed by strain hardening and strain softening curves. The following figure shows the stress-strain curve for different structural steels.

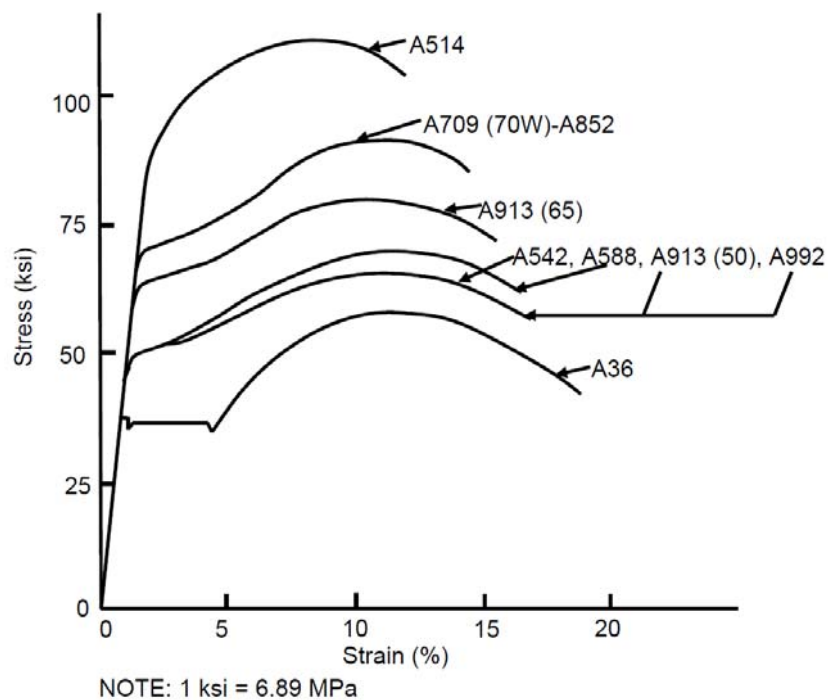


Figure 3-15 Typical Stress-Strain Curves Structural Steel

For the purpose of modelling the material, structural steel has been considered an elastic-perfectly plastic material. Steel properties have been taken as follows (AASHTO, 2012):

A709 Grade 50 steel

$$E = 29 \times 10^6 \text{ psi (200,000 MPa)}$$

$$\nu = 0.3$$

$$F_u = 65,000 \text{ psi (448.16 MPa)}$$

$$F_y = 50,000 \text{ psi (344.74 MPa)}$$

The material model considered for reinforcing steel is shown in the following figure:

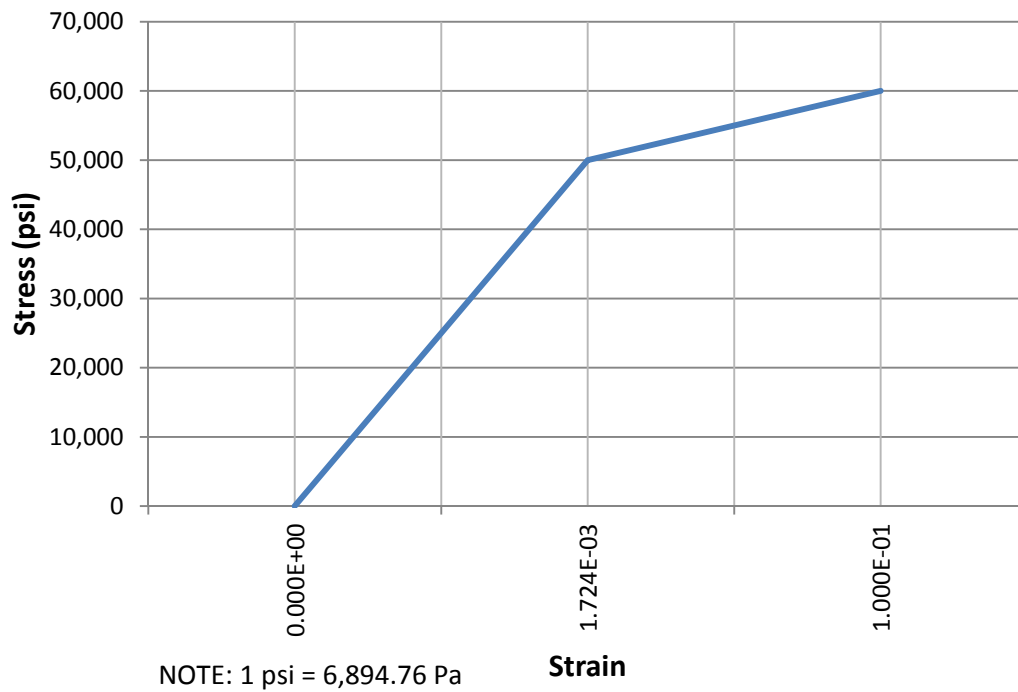


Figure 3-16 Grade 50 Structural Steel. Stress-Strain Curve

### 3.2 Loads

The two models have been analyzed subjected to HL-93 loading as per applicable code requirements (AASHTO, 2012). Therefore, the loads applied to the caps consist of the following:

- Girder reactions at supports for the controlling load combination (Strength I) obtained by considering the superstructure self-weight, the lane load and the truck or tandem per code provisions.
- Factored bent cap self-weight for the critical load combination (Strength I).

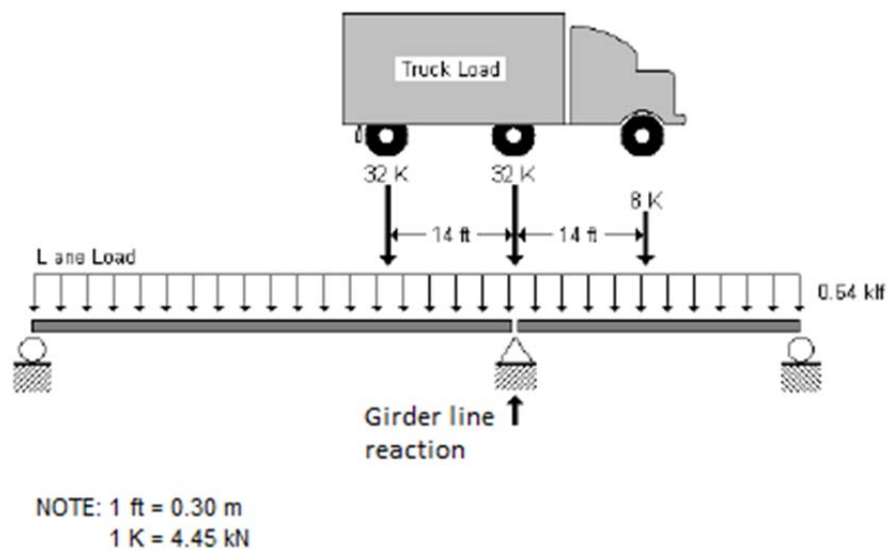


Figure 3-17 Live Load Model

The girder reactions at supports have been determined by modelling with the software PGSuper the two bridge spans that load the pier cap under analysis. The following table summarizes the results obtained in that model. Further information can be found in Appendix B.

Table 3-4 Summary of Girder Reactions at Support

GIRDER LINE	TOTAL REACTION, kip (kN)
1	285.69 (1,270.75)
2	336.87 (1,489.40)
3	433.27 (1,927.18)
4	531.15 (2,362.55)
5	556.31 (2,474.47)

Finally, the unfactored self-weight of the caps materials have been considered by using the following unit weights for the materials. A load factor  $\gamma_p$  of 1.25 (AASHTO, 2012) have been considered in the models.

- Normal weight concrete: 0.145 kcf (23.04 KN/m<sup>3</sup>).
- Structural steel 0.490 kcf (77.84 KN/m<sup>3</sup>).

### 3.3 Boundary Conditions

The post-tensioned and composite caps have been considered simply supported at both ends as shown in the figure below. This consideration translates as follows in terms of modelling with Abaqus:



- At both ends, movements along the x axis (oriented transversally to the element) are released. Constraining these movements generates additional stresses under the deformations caused by the Poisson effect, and does not properly model the actual behavior of the cap.
- At the left end, rotation about the x axis is released. This complies with the assumption of having a pin support at that end of the member.
- The support at the right end is modeled as a roller. Therefore, movement along the z axis and rotation about the x axis are released.



Figure 3-18 Boundary Conditions

### 3.4 Post-Tensioned Concrete Cap Model

#### 3.4.1 Introduction

The prestressed concrete cap has the following characteristics:

- It has been modeled as a simply supported beam, spanning between the two columns a total length of 74.5 ft. (22.71 m).
- The cross section of the concrete cap is 8.5 ft. (2.59 m) high by 6.33 ft. (1.93 m) wide.

- The cap serves as support for 10 girders (5 from the backward span and 5 from the forward span). The actual bridge has only three girders for span, but other two were considered in the design for future extension of the bridge.
- The cap is prestressed with 6 tendons following parabolic shapes. Each tendon is constituted by 31-0.6" (15.24 mm)  $\Phi$  grade 270 low relaxation steel strands.

The following figures summarize the main features of the prestressed concrete cap modeled. Additional information can be found in Appendix A.

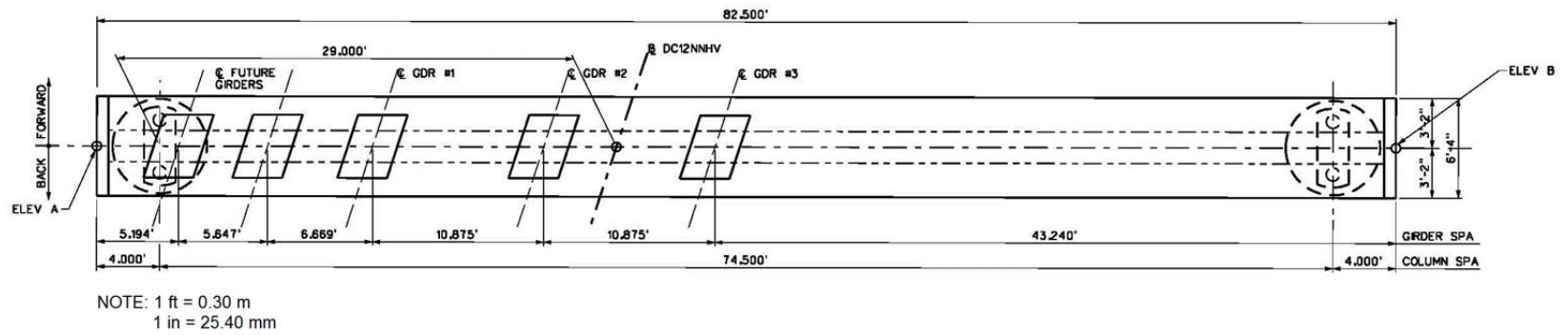


Figure 3-19 Plan View Geometry of Post-Tensioned Concrete Cap

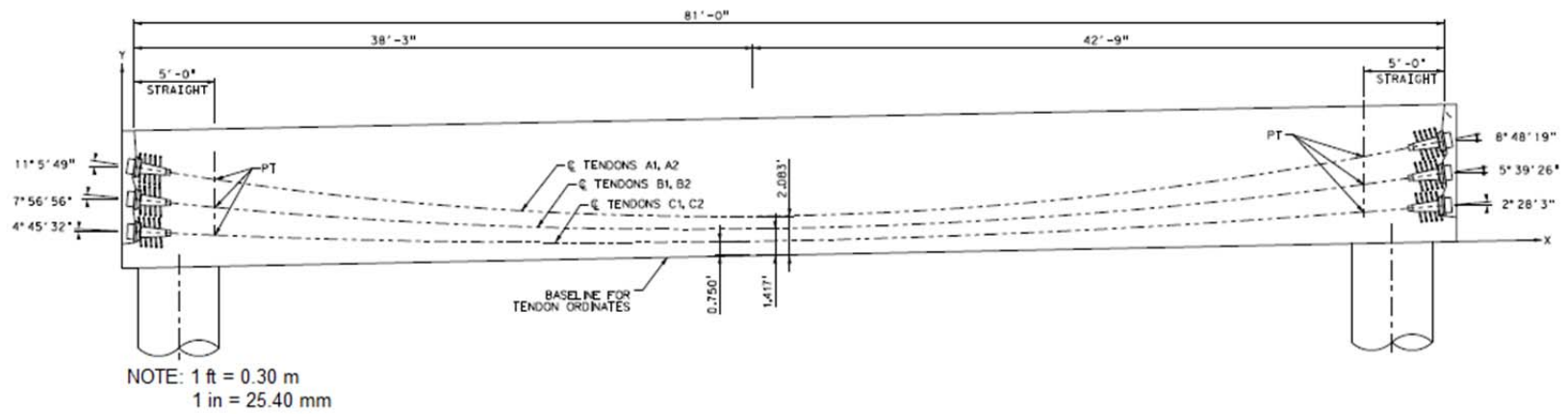


Figure 3-20 Tendons Profiles

Table 3-5 Tendons Elevations

$$Y_A = \begin{cases} 6.250 - 0.19614(X - 0.75) \\ 2.083 + 0.002882(39.00 - X)^2 \\ 2.083 + 0.002393(X - 39.00)^2 \\ 6.250 - 0.15490(81.75 - X) \end{cases}$$
$$Y_B = \begin{cases} 4.250 - 0.13963(X - 0.75) \\ 1.417 + 0.001931(39.00 - X)^2 \\ 1.417 + 0.001653(X - 39.00)^2 \\ 4.250 - 0.09906(81.75 - X) \end{cases}$$
$$Y_C = \begin{cases} 2.250 - 0.05325(X - 0.75) \\ 0.750 + 0.000980(39.00 - X)^2 \\ 0.750 + 0.000915(X - 39.00)^2 \\ 2.250 - 0.04309(81.75 - X) \end{cases}$$

$0.75 \leq X < 5.75$

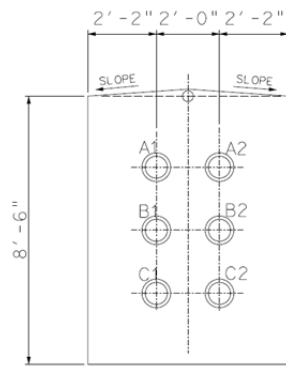
$5.75 \leq X < 39.00$

$39.00 \leq X < 76.00$

$76.00 \leq X < 81.75$

CG OF TENDONS AT 20TH POINTS ALONG THE CAP																				
	1	2	3	4	5	6	7	8	9	10	11	12	13	14	15	16	17	18	19	20
X (ft)	0.750	5.750	9.906	14.063	18.219	22.375	26.531	30.688	34.844	39.000	43.194	47.389	51.583	55.778	59.972	64.166	68.361	72.555	76.75	81.750
Y <sub>A</sub> (ft)	6.25	5.269	4.522	3.875	3.328	2.880	2.531	2.282	2.133	2.083	2.125	2.251	2.462	2.757	3.136	3.599	4.146	4.777	5.475	6.25
Y <sub>B</sub> (ft)	4.250	3.552	3.051	2.618	2.251	1.951	1.717	1.550	1.450	1.417	1.446	1.533	1.679	1.882	2.144	2.464	2.842	3.278	3.755	4.250
Y <sub>C</sub> (ft)	2.250	1.833	1.580	1.359	1.173	1.021	0.902	0.818	0.767	0.750	0.766	0.814	0.895	1.008	1.152	1.330	1.539	1.780	2.035	2.250

NOTE: 1 ft = 0.30 m



NOTE: 1 ft = 0.30 m  
1 in = 25.4 mm

Figure 3-21 Prestressed Concrete Cap Typical Section

The following parts have been included in the Abaqus model for the prestressed concrete bent cap:

- Concrete cap section. The concrete solid is modeled using a 3D deformable homogeneous solid element simply supported at its ends (pinned-roller boundary conditions).

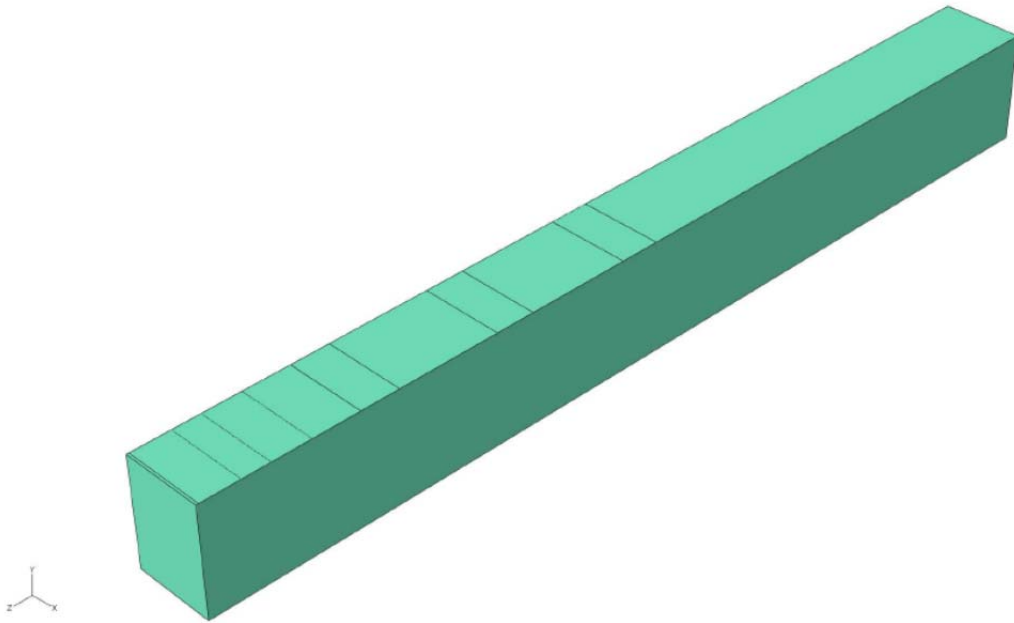


Figure 3-22 Concrete Cap Part in Abaqus Model

- Reinforcement. Both longitudinal and transverse reinforcement have been included in the model. The rebar has been modeled as 3D wire elements with truss sections (capable of developing only axial stresses) with a cross sectional area equal to the actual area of the rebar. To guarantee the deformation compatibility and a proper stress transmission between concrete

and rebar, the reinforcement is embedded into the concrete section (host region). By doing so, the degrees of freedom of the truss elements that form the reinforcement wires are constrained by the adjacent concrete solid elements.

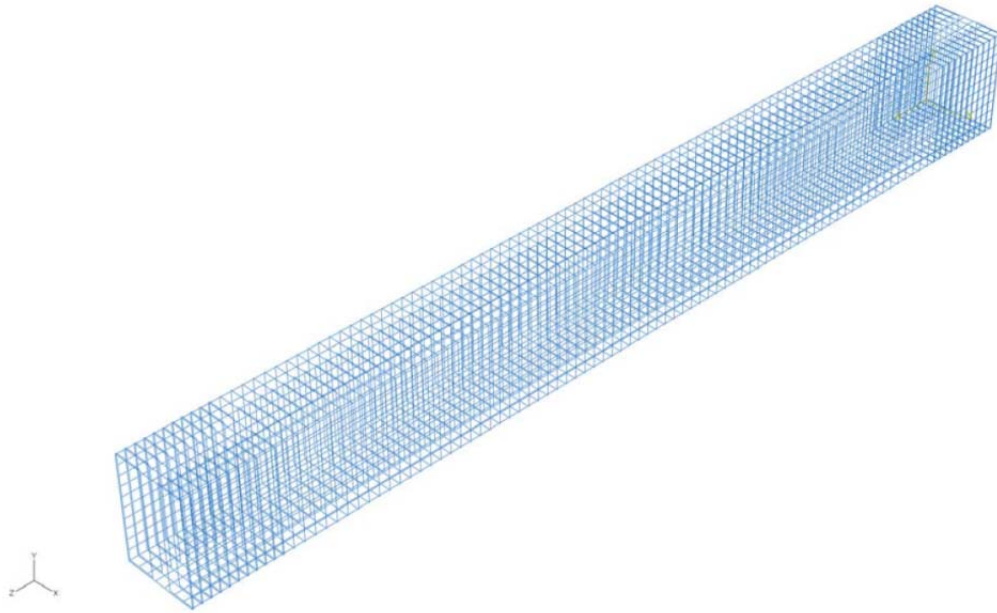


Figure 3-23 Reinforcement Parts in Abaqus Model

- Prestressing tendons. The effects of the prestressing tendons on the structure have been modeled as the combination of a homogeneous axial compressive stress and a vertical force obtained using the load-balancing method. Since the contribution of prestressing steel to the stiffness of the section is minimum (Saiedi, 2007), prestressing tendons have not been included in the FEM.

### 3.4.2 Prestressing Force

The effect of the post-tensioning tendons on the model will be taking into account by the introduction of two different loads:

- A compressive force applied at the ends of the member. This force has been determined by deducting the prestress losses to the jacking force to obtain the effective prestress force. This force is introduced into the model as a constant compressive pressure at both ends due to the fact that the center of gravity of the tendons coincides with the center of gravity of the section at both ends of the members.
- A vertical distributed load due to the load-balancing effect of the draped tendons. This force is obtained by imposing equilibrium at the tensioned tendon. The procedure followed is explained below.

#### 3.4.2.1 Prestress Loss

The prestress force at jacking per tendon for the post-tensioned concrete cap is defined in the drawings to be 972.97 kips (4,327.99 kN). However, to properly model the behavior of the structure, instantaneous and long term prestress losses shall be considered. For a post-tensioned member, the total losses can be obtained as (AASHTO, 2012):

$$\Delta f_{pT} = \Delta f_{pF} + \Delta f_{pA} + \Delta f_{pES} + \Delta f_{pLT} \quad (12)$$

where

$\Delta f_{pT}$  is the total loss (ksi).

$\Delta f_{pF}$  is the loss due to friction (ksi).

$\Delta f_{pA}$  is the loss due to anchorage set (ksi).

$\Delta f_{pES}$  is the sum of all losses or gains due to elastic shortening or extension at the time of application of prestress and/or external loads (ksi).

$\Delta f_{pLT}$  are the losses due to long-term shrinkage and creep of concrete, and relaxation of the steel (ksi).

The methodology followed to obtain the prestress losses is described below. The complete analysis performed is included in Appendix C. A total prestress loss of 57.83 ksi (398.74 MPa) has been obtained. Therefore, the long term prestress force to be considered in the FEM is 972.97 kips (4,327.78 kN) per tendon.

#### Friction Loss

The friction between the prestressing tendon and the duct in which it is placed reduces the prestress force applied to the tendon. This loss can be estimated as (AASHTO, 2012):

$$\Delta f_{pF} = f_{pj} (1 - e^{-(kx + \mu\alpha)}) \quad (13)$$

where

$f_{pj}$  is the stress in the prestressing steel at jacking (ksi).

$x$  is the length of a prestressing tendon from the jacking end to any point under consideration (ft).

$k$  wobble friction coefficient (per foot of tendon). Taken as 0.0002 per bridge drawings.

$\mu$  is the coefficient of friction. Taken as 0.23 per bridge drawings.

$\alpha$  is the sum of the absolute values of angular change of prestressing steel path from jacking end, or from the nearest jacking end if tensioning is done equally at both ends, to the point under investigation (rad).

The prestress loss caused by friction between the tendon and the duct obtained following the outlined procedure is 7.842 ksi (54.07MPa) per tendon.



#### Anchorage Set Loss

Anchorage set at release of the tendons is assumed to be 0.375 inches (0.95 cm) per the bridge drawings. With that information, the prestress loss due to anchorage set can be determined as follows:

$$\Delta f_{pA} = \frac{\Delta L}{L} E_s \quad (13)$$

where

$\Delta L$  is the anchorage set (in).

$L$  is the total length of tendon (in).

$E_s$  is the prestressing steel Young Modulus (ksi)

The prestress loss caused by setting of the anchorage at member ends obtained with the above explained procedure is 10.995 ksi (75.81 MPa) per tendon.

#### Elastic Shortening Loss

The loss caused by the elastic shortening of the element can be calculated as follows (AASHTO, 2012):

$$\Delta f_{pES} = \frac{N-1}{N} \frac{E_p}{E_{ci}} f_{cgp} \quad (14)$$

However, according to section C5.9.5.2.3B-1 of (AASHTO, 2012), the following alternative equation can be used to estimate the elastic shortening loss in post-tensioned members:

$$\Delta f_{pES} = \frac{N-1}{2N} \frac{A_{ps} f_{pbt} (I_g + e_m^2 A_g) - e_m M_g A_g}{A_{ps} (I_g + e_m^2 A_g) + \frac{A_g I_g E_{ci}}{E_p}} \quad (15)$$

where

$A_{ps}$  is the area of prestressing steel (in<sup>2</sup>).

$A_g$  is the gross area of section (in<sup>2</sup>).

$E_{ci}$  is the modulus of elasticity of concrete at transfer (ksi).

$E_p$  is the modulus of elasticity of prestressing tendons (ksi).

$e_m$  is the average eccentricity at midspan (in).

$f_{pbt}$  is the stress in prestressing steel immediately prior to transfer (ksi).

$I_g$  is the moment of inertia of the gross concrete section (in<sup>4</sup>).

$M_g$  is the midspan moment due to member self-weight (kip-in).

$N$  is the number of identical prestressing tendons.

$f_{pj}$  is the stress in the prestressing steel at jacking (ksi).

The prestress loss due to elastic shortening of the member when subjected to the prestressing force have been estimated to be 2.936 ksi (75.81 MPa) using the outlined procedure.

#### Creep, Shrinkage and Relaxation of Prestressing Steel Losses

Several methods of obtaining these losses are included in (AASHTO, 2012). The equation proposed in 5.9.5.3 is approximate and intended to be used only for standard precast pretensioned members. The procedure outlined in 5.9.5.4 is intended to be used when a more accurate estimation of time dependent losses is required. However, that procedure is not intended to be used for post-tensioned elements with no composite action. Therefore, time dependent losses due to creep and shrinkage will be determined using 5.4.3.2.

The creep coefficient is defined as (AASHTO, 2012):

$$\Psi(t, t_i) = 1.9 \cdot k_s \cdot k_{hc} \cdot k_f \cdot k_{td} \cdot t_i^{-0.118} \quad (16)$$

in which

$$k_s = 1.45 - 0.13(V/S) \geq 1.0 \quad (17)$$

$$k_{hc} = 1.56 - 0.008H \quad (18)$$

$$k_f = \frac{5}{1+f'_{ci}} \quad (19)$$

$$k_{td} = \left( \frac{t}{61 - 4f'_{ci} + t} \right) \quad (20)$$

where

H is the relative humidity (%).

$k_s$  is the factor for the effect of the volume-to-surface ratio of the component.

$k_f$  is the factor for the effect of concrete strength.

$k_{hc}$  is the humidity factor for creep.

$k_{td}$  is the time development factor.

t is the maturity of concrete (day) defined as age of concrete between time of loading for creep calculations, or end of curing for shrinkage calculations, and time being considered for analysis of creep or shrinkage effects.

$t_i$  is the age of concrete at time of load application (day).

V/S is the volume-to-surface ration (in).

$f'_{ci}$  is the specified compressive strength of concrete at time of prestressing for pretensioned members and at time of initial loading for nonprestressed members.

If concrete age at time of initial loading is unknown at design time,  $f'_{ci}$  may be taken as 0.80  $f'_c$  (ksi)

Once obtained the creep coefficient, the loss due to creep can be obtained as follows

$$\epsilon_{ci} = \frac{f_{pbt} \cdot A_{ps}}{A_g \cdot E_{ci}} \quad (21)$$

$$\epsilon_c = \Psi \cdot \epsilon_{ci} \quad (22)$$

$$\Delta f_{ps}(CR) = \epsilon_c \cdot E_p \quad (23)$$

where

$\epsilon_{ci}$  is the instantaneous strain (initial elastic strain) due to loading.

$\epsilon_c$  is the deformation due to creep.

The values obtained for different maturity times have been represented in the following figure. As can be observed in the figure below, the prestress loss caused by creep of the concrete tends quickly to a value close to 9 kips (62.05 MPa). The final value of 8.842 kips (90.97 MPa) obtained will be used in the calculations.

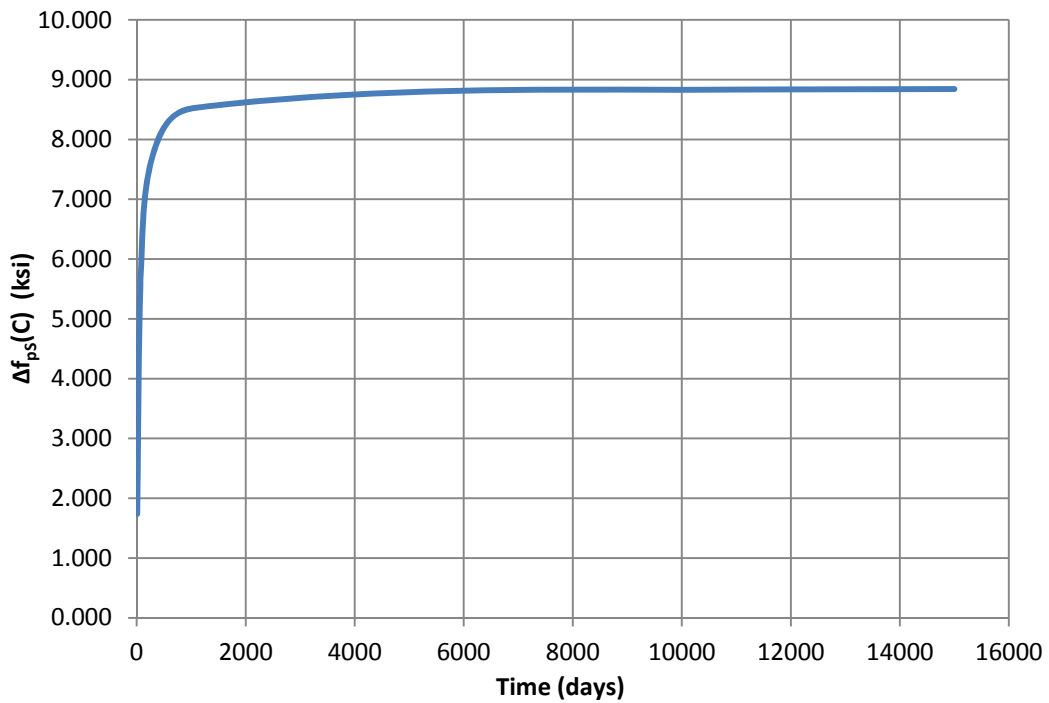


Figure 3-24 Prestress Loss per Tendon. Creep Loss  $\Delta f_{ps}(C)$

The strain due to shrinkage at a time  $t$  can be calculated as (AASHTO, 2012):

$$\varepsilon_{sh} = k_s k_{hs} k_f k_{td} 0.48 \cdot 10^{-3} \quad (24)$$

where

$$k_{hs} = 2 - 0.014H \quad (25)$$

And the total shrinkage loss is determined by:

$$\Delta f_{ps}(SH) = \varepsilon_{sh} \cdot E_{ps} \quad (26)$$

The prestress loss caused by shrinkage of the concrete has been calculated for different maturity times. The following figure, that summarize the results obtained, shows how shrinkage loss tends asymptotically to a value close to 13 ksi (89.63 MPa). The final value of 13.188 ksi (90.93 MPa) obtained has been used to determine the long term prestress force.

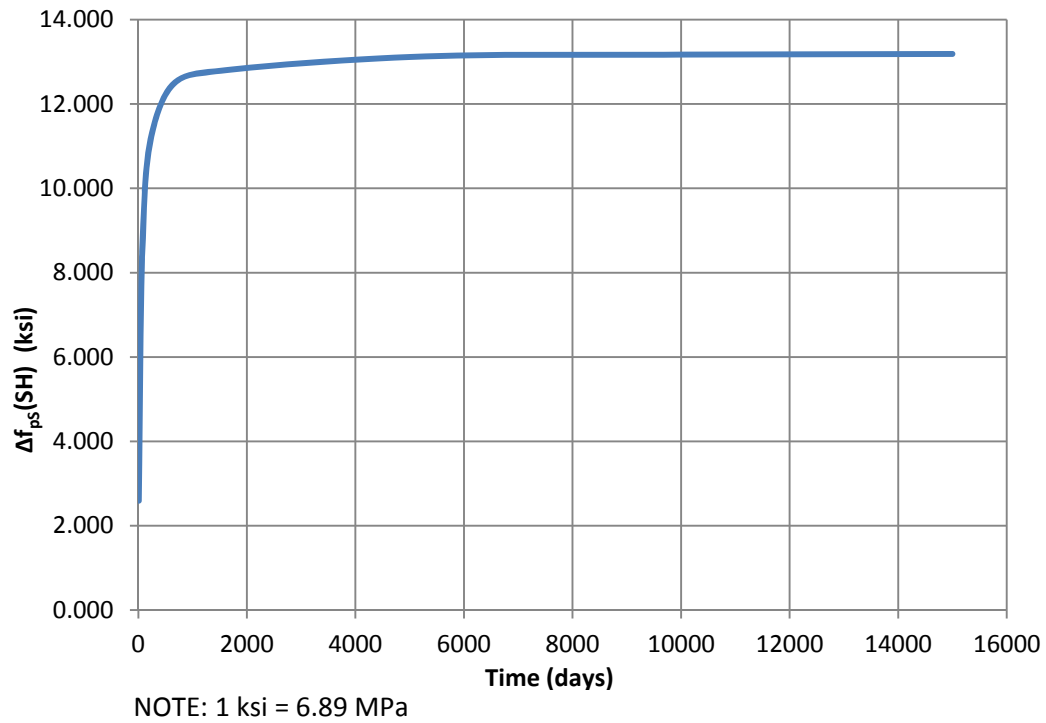


Figure 3-25 Prestress Loss per Tendon. Shrinkage Loss  $\Delta f_{ps}(SH)$

Finally, the loss caused by the relaxation of the strands is determined by the following equation:

$$\Delta f_{ps}(RL) = f_{pbt} - f_{ps}(t) \quad (27)$$

in which

$$f_{ps}(t) = f_{pbt} \left[ 1 - \frac{\log_{10}(t)}{K} \left( \frac{f_{pbt}}{f_{py}} - 0.55 \right) \right] \quad (28)$$

where

k is 30 for low relaxation strands.

t is the duration of loading in hours.

The values obtained for the steel relaxation loss for different times after loading are represented in the following graphic. A final value of 14.027 ksi (96.72 MPa) has been considered in the calculations.

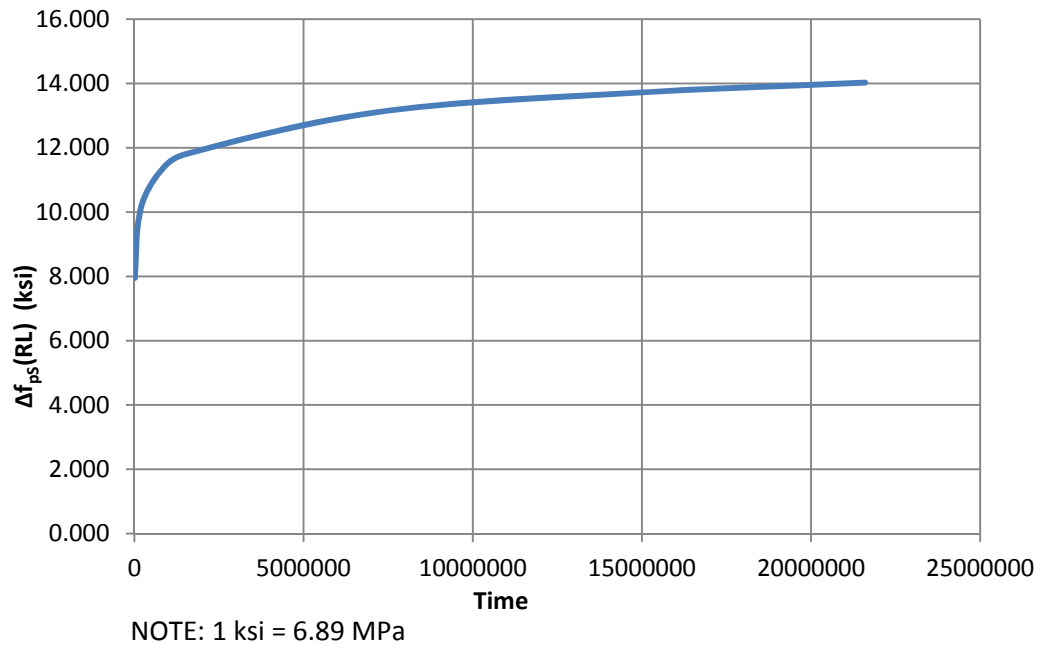


Figure 3-26 Prestress Loss per Tendon. Steel Relaxation Loss  $\Delta f_{ps}(RL)$

#### 3.4.2.2 Load-Balancing Force

An advantageous feature of draped post-tensioned tendons is that they develop a vertical force capable of counteracting or balancing the external loads applied to the prestressed member. This load is equal to the force required to keep the tendon in its draped shape at jacking. The following figure shows the load-balancing effect of a parabolic draped tendon.

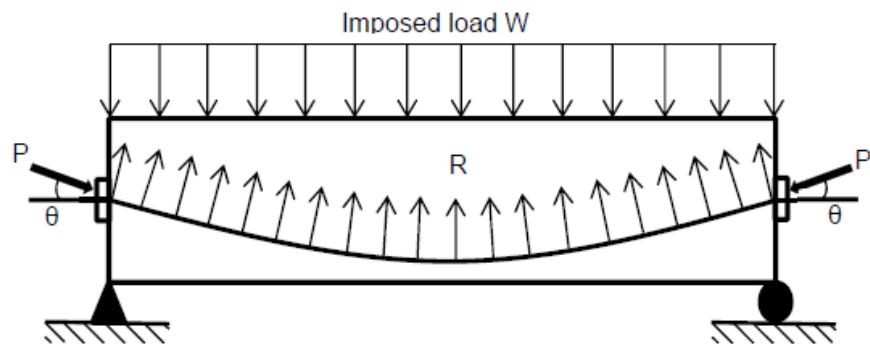


Figure 3-27 Load Balancing Force. Draped Tendons

The load-balancing force have been obtained considering the following simplifications

- The tendon force acts horizontally at the ends of the member and, therefore, vertical components of that force due to the inclination of the tendon are neglected.
- The load-balancing force is applied towards the center of curvature of the parabola that the tendons define. However, the radius of curvature of such parabolas is considered large enough to neglect that effect and assume that the load-balancing force is applied vertically along the tendon.

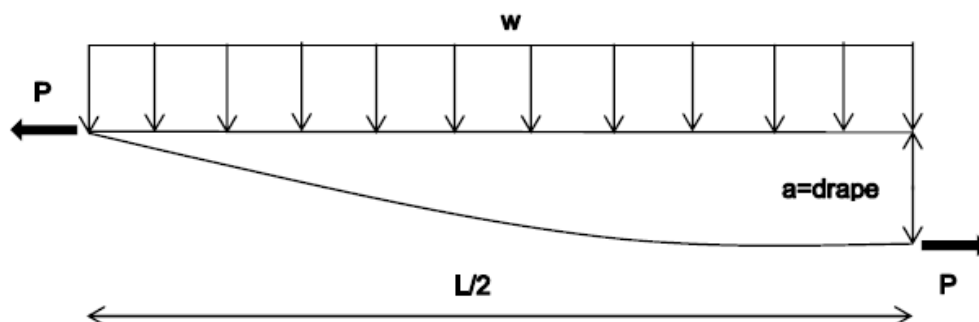


Figure 3-28 Parabolic Tendon Free Body Diagram



Figure 3-28 shows the free body diagram at mid-span of a parabolic tendon. By the application of equilibrium equations, taking summation of moments from the left end:

$$\sum M = 0 \quad (29)$$

$$\frac{wL}{2} * \frac{L}{4} = P * a \quad (30)$$

$$w = \frac{8Pa}{L^2} \quad (31)$$

Considering the previously exposed, the load-balancing force applied to the model for each type of tendon takes a value of:

$$w_a = \frac{8*972.971*4.167}{81^2} = 4.944 \text{ kip/ft (73.305 kN/m)} \quad (32)$$

$$w_b = \frac{8*972.971*2.833}{81^2} = 3.361 \text{ kip/ft (49.833 kN/m)} \quad (34)$$

$$w_c = \frac{8*972.971*1.5}{81^2} = 1.779 \text{ kip/ft (23.377 kN/m)} \quad (35)$$

And the total load-balancing force is:

$$w = 2 * w_a + 2 * w_b + 2 * w_c = 20.168 \text{ kip/ft (299.031 kN/m)} \quad (36)$$

### 3.3.3 Element Types

As explained above, two different types of parts have been included in the model: the 3D deformable homogeneous solid and 3D wires with truss sections. Abaqus library includes, for each type of part to be modeled, two types of finite elements (FE): linear

(constant strain elements) and quadratic (linear strain elements). Although the level of mesh refinement needed is usually smaller if quadratic elements are used, only linear elements have been utilized in the development of the model due to the fact that they are more accurate when modelling plastic behavior (Dassault Systemes Simulia Corp, Abaqus 6.9 Theory Manual).

With that into consideration, the 3D wires that form the steel reinforcement have been modeled using the linear FE T3D2.

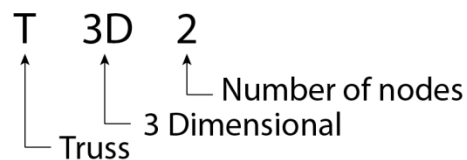


Figure 3-29 Abaqus Naming Convention for Truss Elements

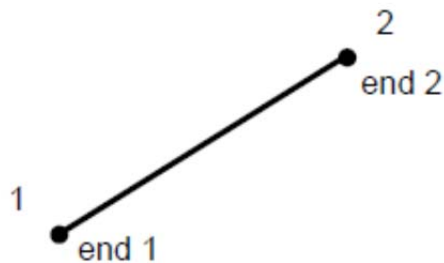


Figure 3-30 Abaqus 2 Nodes 3D Truss Element T3D2

For a 3D homogeneous solid part, Abaqus library includes two main types of elements: isoparametric (hexahedral) and tetrahedral. Tetrahedral elements have been used in this model due to their ability to better adapt to any member geometry.

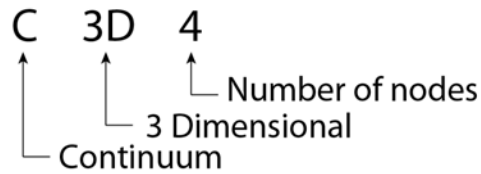


Figure 3-31 Abaqus Naming Convention for Continuum Elements

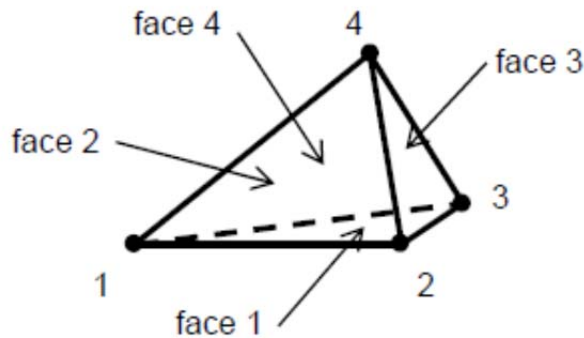


Figure 3-32 Abaqus 4 Nodes 3D Tetrahedral Element C3D4

### 3.3.4 Mesh Generation

Finite element models accuracy depends not only on the type of elements selected but also on the number of them. A smaller size of element and, consequently, a larger number of them, results in the development of more accurate models. Models with mesh maximum sizes varying from 15 to 5 inches (381 to 127 mm) have been generated and analyzed. It was found that the computer does not have capacity to run models with mesh sizes below 5 inches (127 mm), for a total of approximately 77,000 nodes. The following table summarizes the main characteristics of the meshes analyzed.

Table 3-6 Post-Tensioned Cap Model. Mesh Characteristics

Mesh size (in)	Number of nodes	Number of 3D truss elements	Number of 3D continuum elements
15	9,782	5,930	17,689
14	10,831	6,520	19,885
13	11,880	6,800	23,633
12	13,865	7,612	29,482
11	16,445	8,270	39,600
10	19,395	9,238	49,651
9	22,684	10,330	61,095
8	29,304	11,346	90,373
7	38,766	13,150	131,772
6	51,198	15,224	186,819
5	77,506	18,112	315,285

The following figure represents the variation in the number of nodes in the model when the maximum element size decreases. As can be observed, the number of nodes and therefore the computational cost and the accuracy of the model, grow exponentially as the maximum mesh size decreases.

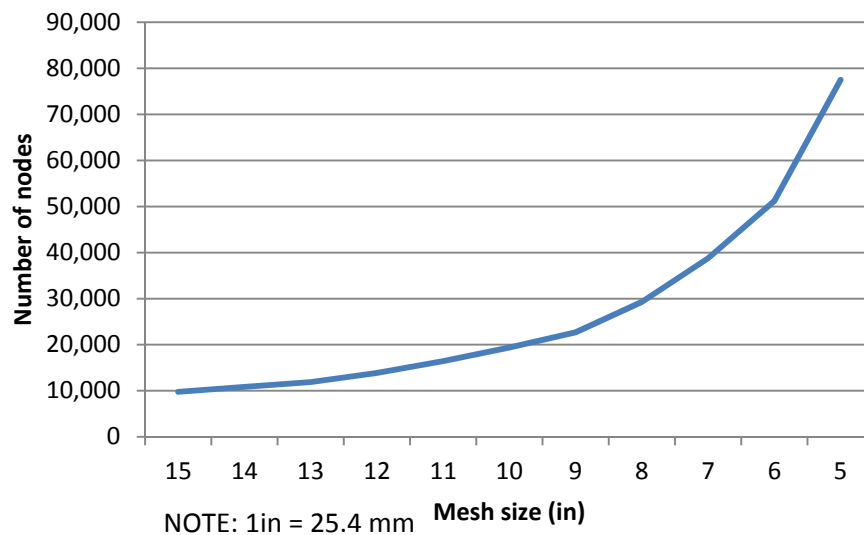


Figure 3-33 Post-Tensioned Cap Model. Number of Nodes vs. Mesh Size

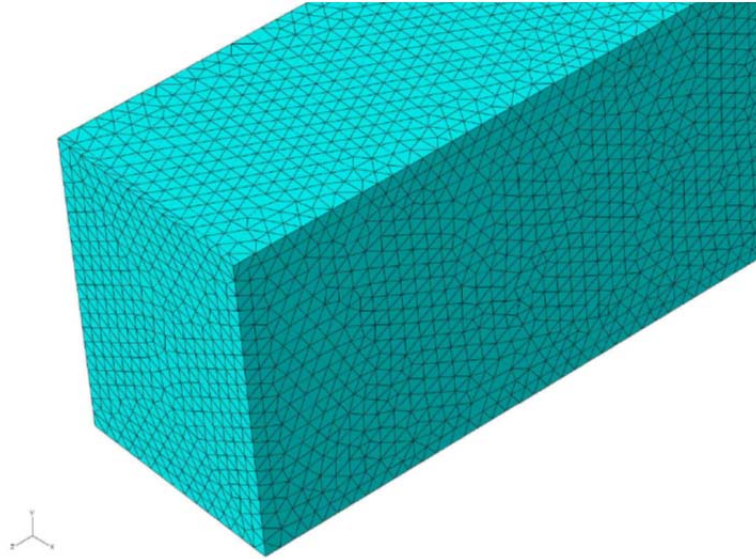


Figure 3-34 Post-Tensioned Cap Model.5 Inches (127 mm) Mesh Size Detail

### 3.3.5 FEM validation

To determine if the model developed tends to the correct solution when the mesh is refined, one of the results obtained has to be checked using alternative procedures. To optimize the model development procedure, the result to be confirmed has to be chosen so that the time required in that verification is limited to the minimum.

The solution obtained implies that the concrete element remains within the elastic limits for both top and bottom fiber stresses under the bending action:

- The top fiber compression stress at maximum moment section is found to be 2,106.2 psi (14.52 MPa), below the elastic limit of 3,000 psi (20.684 MPa) defined in the material model.

- The bottom fiber compression stress at maximum moment section is found to be 539.4 psi (3.72 MPa), below the elastic and fracture limit of 587.88 psi (4.053 MPa).

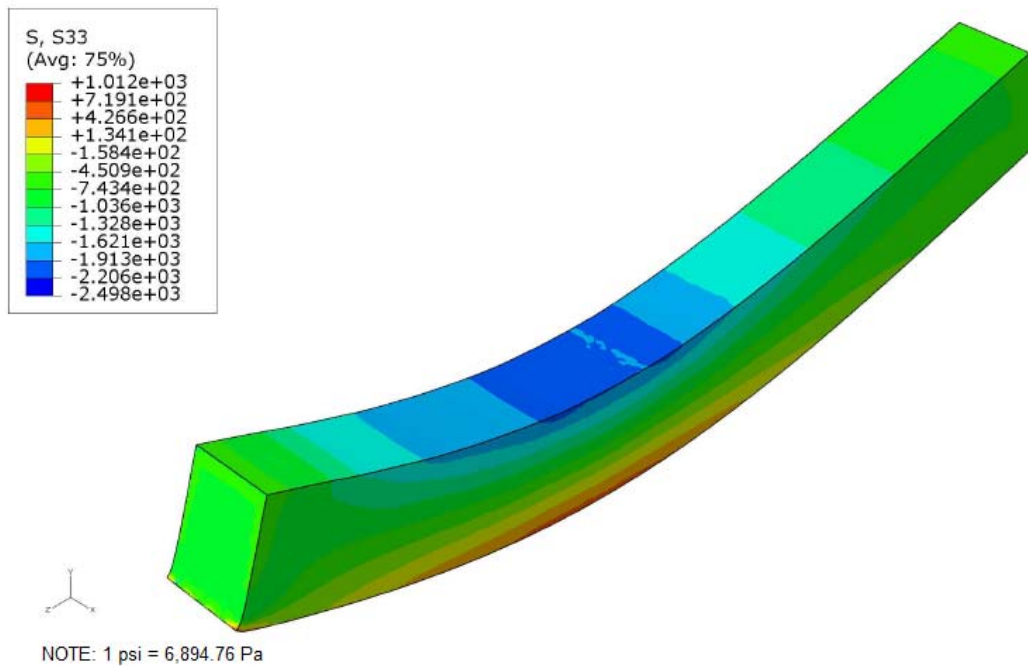


Figure 3-35 Post-Tensioned Cap. Bending Stresses (psi) Distribution.

5 Inches (127 mm) Mesh Model

Under those circumstances, simplified hand calculations performed with the following assumptions provide accurate enough reference values to check the adequacy of the results obtained:

- The structure behaves elastically and, therefore, the superposition principle is applicable.

- Straight sections before deformation remain straight after deformation (Bernoulli's hypothesis).
- The contribution of the longitudinal steel to the section strength will be neglected, so that there is no need of transforming the different materials that form the structural section.

The calculations performed under these hypotheses are included in Appendix E. The results obtained are shown in the following table. There are small differences due to already mentioned approximations in the hand calculations. As can be seen, the model developed adequately simulates the structural behavior of the bent cap.

Table 3-7 Post-tensioned Concrete Cap Model. Validation Analysis. US Units

<b>Max. Bottom Fiber Stress. Model (psi)</b>	<b>Max. Bottom Fiber Stress. Hand Calculations (psi)</b>	<b>Difference (psi)</b>
539.4	560.5	21.1
<b>Max. Top Fiber Stress. Model (psi)</b>	<b>Max. Top Fiber Stress. Hand Calculations (psi)</b>	<b>Difference (psi)</b>
-2,106.2	-2,066.7	39.5

Table 3-8 Post-Tensioned Concrete Cap Model. Validation Analysis. SI Units

<b>Max. Bottom Fiber Stress. Model (MPa)</b>	<b>Max. Bottom Fiber Stress. Hand Calculations (MPa)</b>	<b>Difference (MPa)</b>
0.4	0.4	0.0
<b>Max. Top Fiber Stress. Model (MPa)</b>	<b>Max. Top Fiber Stress. Hand Calculations (MPa)</b>	<b>Difference (MPa)</b>
-1.5	-1.4	0.1

### 3.4 Steel-Concrete Composite Cap Model

#### 3.4.1 Introduction

The steel-concrete composite concrete cap has the following characteristics:

- It has been modeled as a simply supported beam, spanning between the two columns a total length of 74.5 ft. (22.708 m).
- The cross section of cap consists of a steel box girder with a top slab 10 inches (254 mm) thick. The connection between these two elements is achieved by the use of studs embedded in the concrete section after pouring.
- The cap serves as support for 10 girders (5 from the backward span and 5 from the forward span). Although the bridge built has only three girders per span, its section is planned to be widened in the future by the addition of two new girders.

The following figures summarize the main features of the steel-concrete composite cap modeled. Additional information can be found in Appendix A.



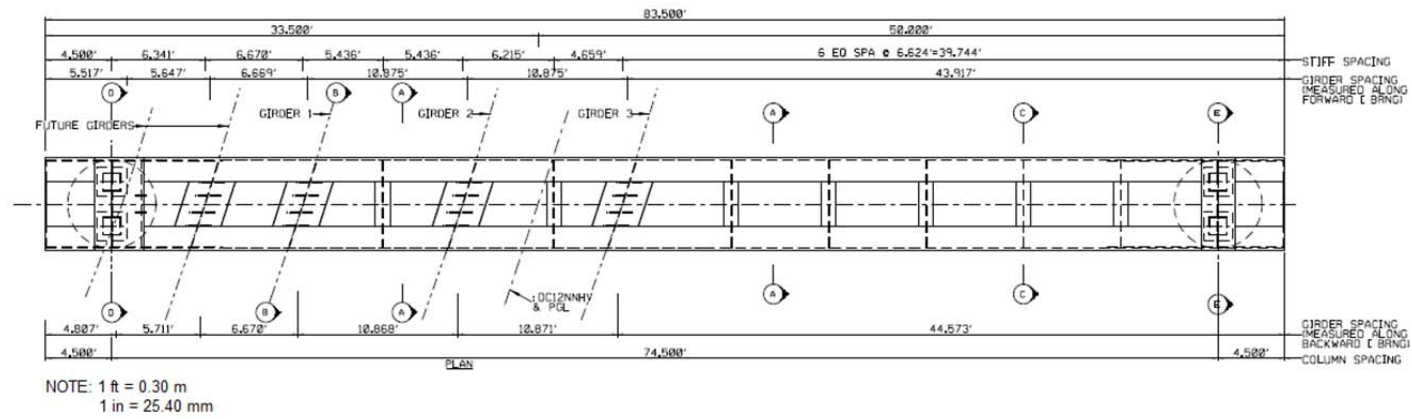


Figure 3-36 Plan View Geometry of Steel-Concrete Composite Cap

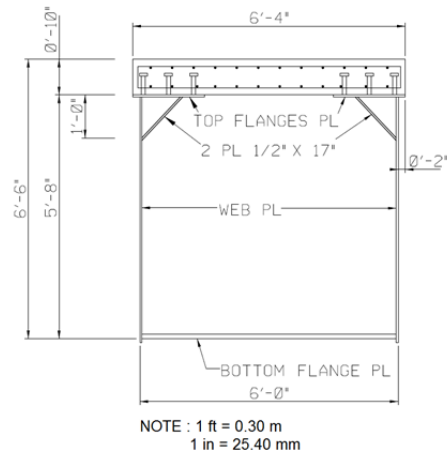


Figure 3-37 Composite Cap Typical Section

The following parts have been included in the Abaqus model for the steel-concrete composite bent cap:

- Concrete slab section. The concrete solid is modeled using a 3D deformable homogeneous solid element.

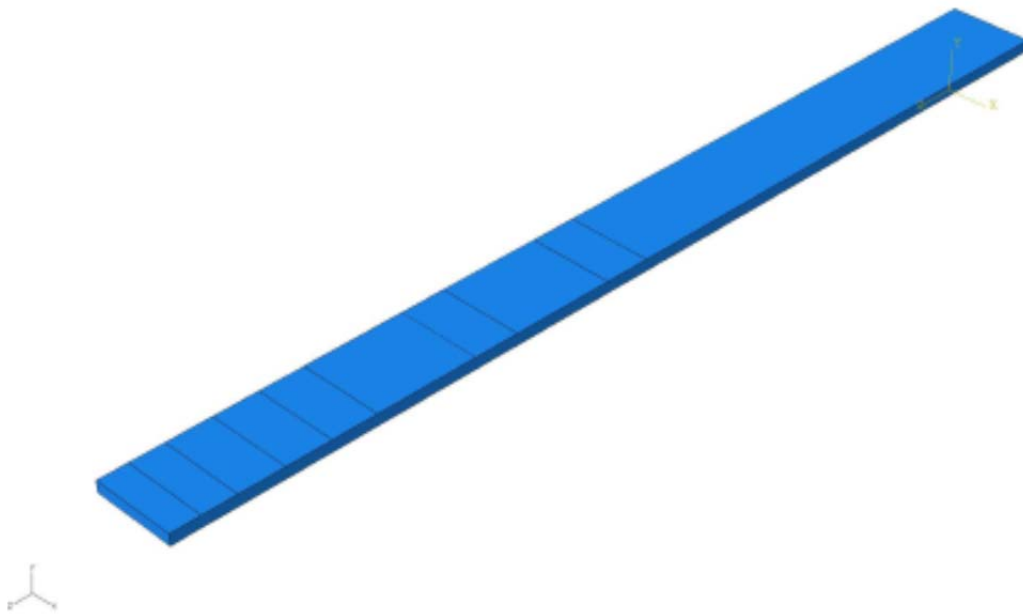


Figure 3-38 Concrete Slab Part in Abaqus Model

- Reinforcement. Following the same criteria used in the previous model, concrete slab reinforcement has been modeled as 3D wire elements with truss sections (capable of developing only axial stresses) with a cross sectional area equal to the actual area of the rebar. This reinforcement is embedded into the concrete section to guarantee the deformation compatibility and a proper stress transmission between concrete and rebar.

In that way, the degrees of freedom of the truss elements that form the reinforcement wires are constrained by the adjacent concrete solid elements.

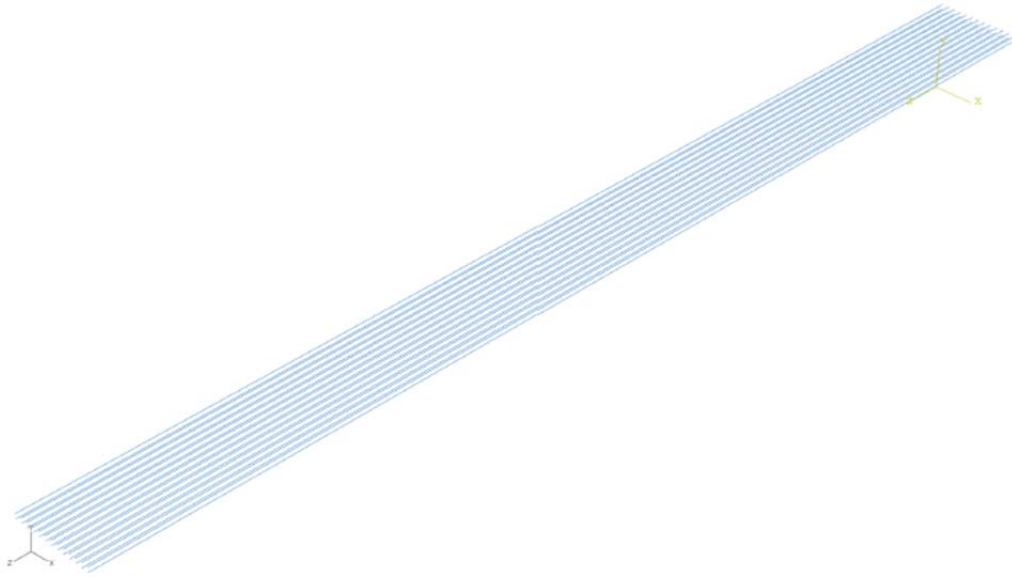


Figure 3-39 Reinforcement Parts in Concrete Slab

- Steel cap section. The steel section is modeled using 3D deformable shell elements. It is considered simply supported at both ends (pinned-roller boundary conditions). The top flange of the steel cap section is tied to the bottom surface of the concrete slab to guarantee compatibility in the deformations and a correct stress transmission between the two elements. Using the tie interaction, the degrees of freedom of the nodes in the concrete slab surface are constrained by the degrees of freedom of the nodes in the steel cap surface.

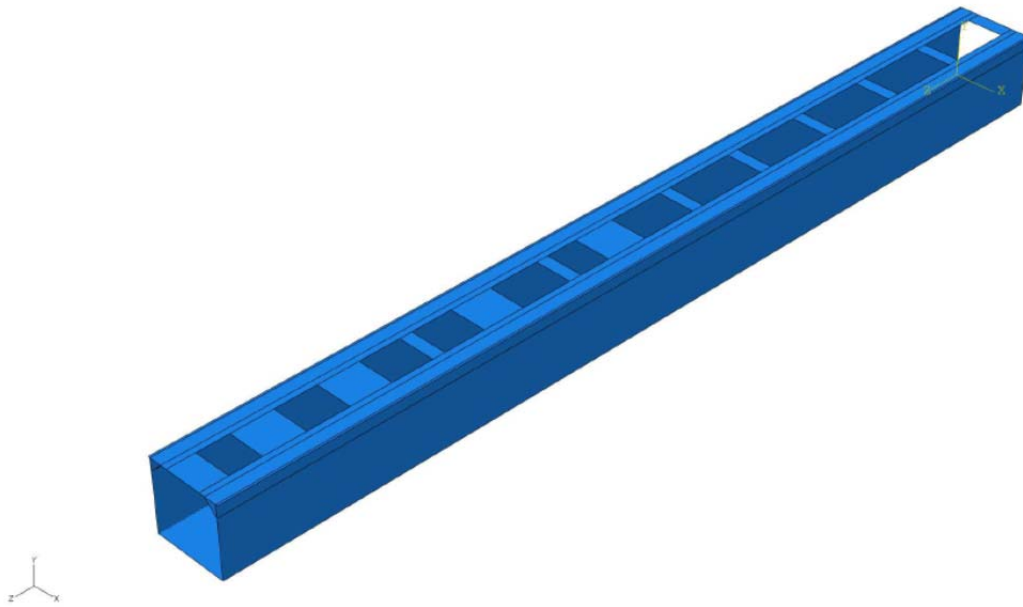


Figure 3-40 Steel Cap Part in Abaqus Model

- Stiffeners and diaphragms. Stiffeners have to be added to the model to prevent the failure of the steel plates due to instabilities when subjected to compressive stresses. Three types of stiffeners have been included: diaphragms at support locations, girder stiffeners at girder locations and interior stiffeners distributed along the length of the member. In all the cases, stiffeners are modeled as 3D deformable homogeneous shells. The correct interaction between the steel cap section and the stiffeners is achieved by merging both stiffeners and steel cap section. After the merging process, the combination of the different elements behaves as a single part.

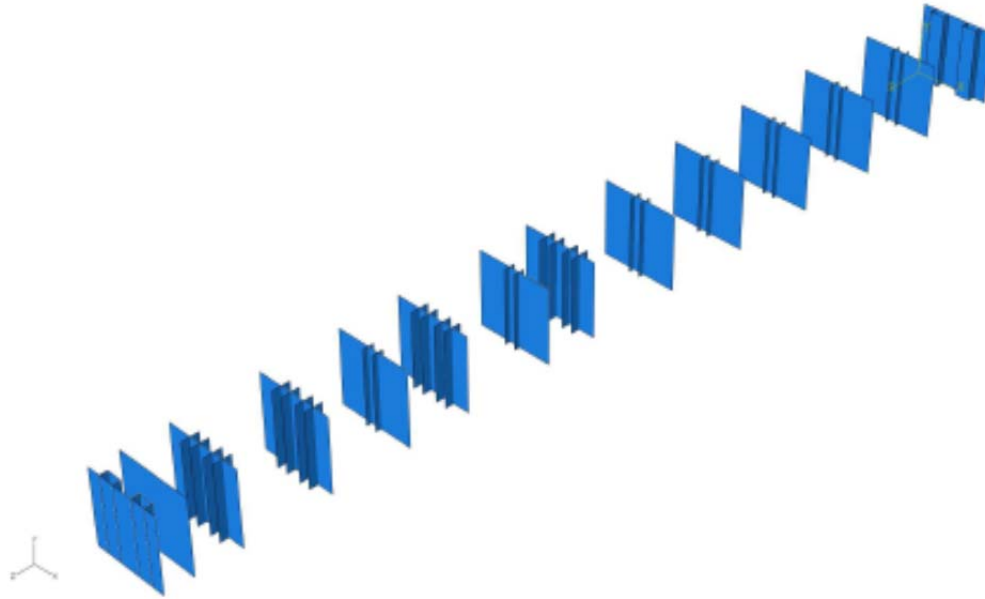


Figure 3-41 Stiffeners and Diaphragms Parts in Abaqus Model

### 3.4.2 Element Types

For this model, three different types of elements have been used: 3D deformable homogeneous solid, 3D wires with truss sections and 3D deformable shells. The first two types have been previously described. For the 3D shell elements, like for the rest of the element types to be used in structural analyses, Abaqus library includes two types of finite elements (FE): linear (constant strain elements) and quadratic (linear strain elements). Although the level of mesh refinement needed is usually smaller if quadratic elements are used, only linear elements have been utilized in the development of the model due to the fact that they are more accurate when modelling plastic behavior (Dassault Systemes Simulia Corp, Abaqus 6.9 Theory Manual).

For a 3D conventional shell element, Abaqus library includes two main types of elements: triangular and rectangular. Triangular elements have been used in this model

due to their ability to better adapt to any member geometry. With that into consideration, the 3D shells that form the steel cap, the stiffeners and the diaphragms have been modeled using the linear FE S3.

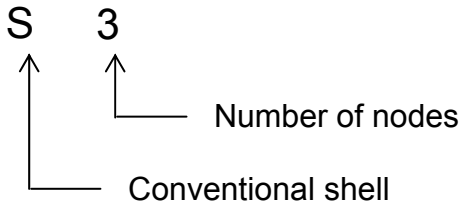


Figure 3-42 Abaqus Naming Convention for  
Conventional Shell Elements

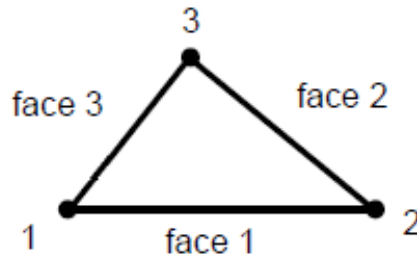


Figure 3-43 Abaqus 3 Nodes 3D Conventional Shell Element S3

### 3.4.3 Mesh Generation

Following the same procedure described for the post-tensioned cap model, meshes varying from 15 to 3 inches (381 to 76.2 mm) have been investigated. The computer utilized reached its computational capacity limit for the 3 inches (76.2 mm) model, for a total of approximately 93,000 nodes. The following table summarizes the main characteristics of the meshes analyzed.

Table 3-9 Composite Bent Cap Model. Mesh Characteristics

Mesh size (in)	Mesh size (mm)	Number of nodes	Number of 3D truss elements	Number of 3D shell elements	Number of 3D continuum elements
15	381.0	4,675	1,534	5,139	2,062
14	355.6	5,153	1,664	5,746	2,211
13	330.2	5,479	1,768	5,895	2,609
12	304.8	6,517	1,924	7,445	3,014
11	279.4	7,187	2,106	7,902	3,839
10	254.0	8,600	2,314	9,547	5,416
9	228.6	10,134	2,574	11,110	7,876
8	203.2	12,812	2,886	13,794	12,453
7	177.8	16,089	3,302	16,627	18,402
6	152.4	20,456	3,848	21,030	24,900
5	127.0	30,332	4,628	33,079	38,735
4	101.6	49,154	5,798	50,679	82,148
3	76.2	93,025	7,722	93,336	185,470

The following figure represents how the number of nodes in the model varies when decreasing the maximum element size. As can be observed, the number of nodes and therefore the computational cost and the accuracy of the model, grow exponentially as the maximum mesh size decreases.

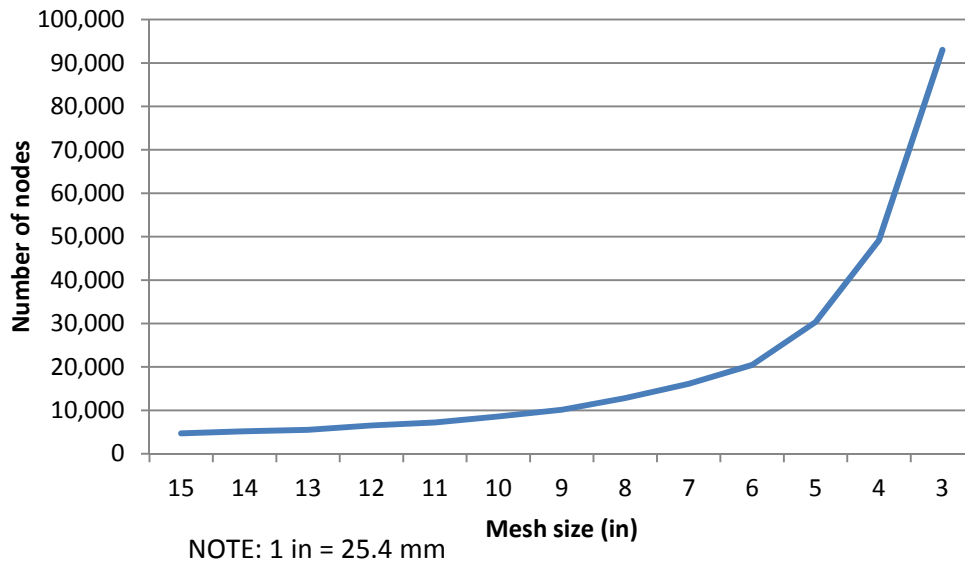


Figure 3-44 Composite Cap Model. Number of Nodes vs. Mesh Size

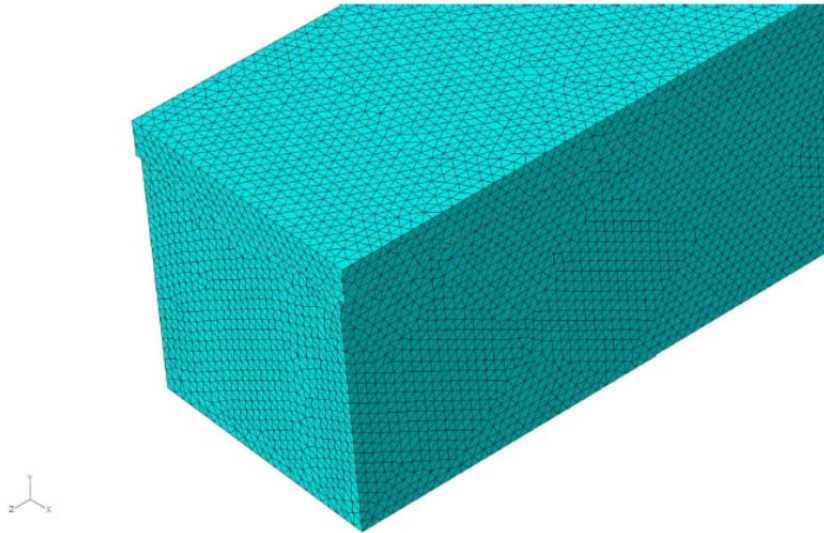


Figure 3-45 Composite Cap Model. 3 Inches (76.2 mm) Mesh Detail

#### *3.4.4 FEM Validation*

Following the same procedure outlined for the previous model, the composite cap model will be validated by the determination of the bending stresses using alternative methods. The following figures show the bending stresses distribution in both the concrete slab and the steel section.



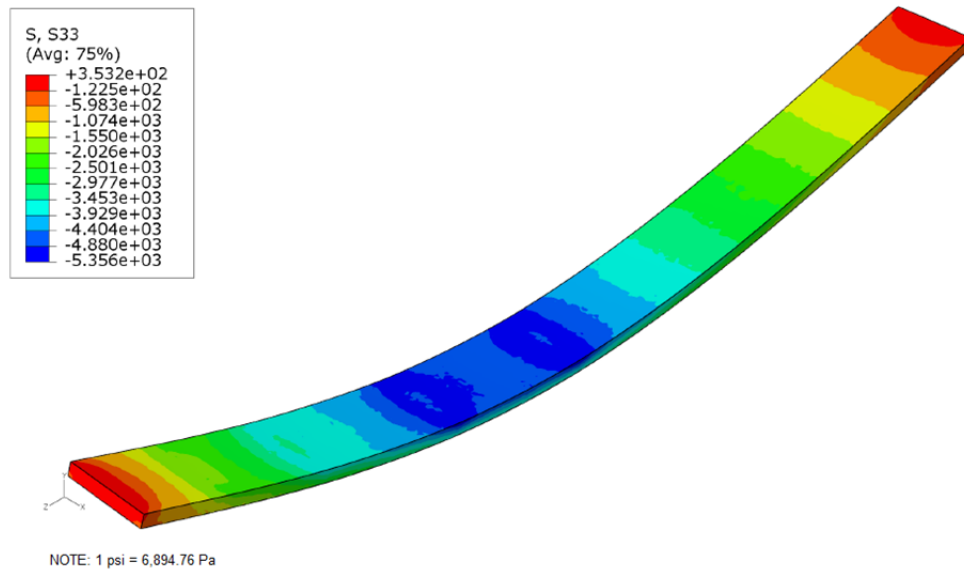


Figure 3-46 Bending Stresses (psi) Distribution in Concrete Slab.

3 Inches (76.2 mm) Mesh Model

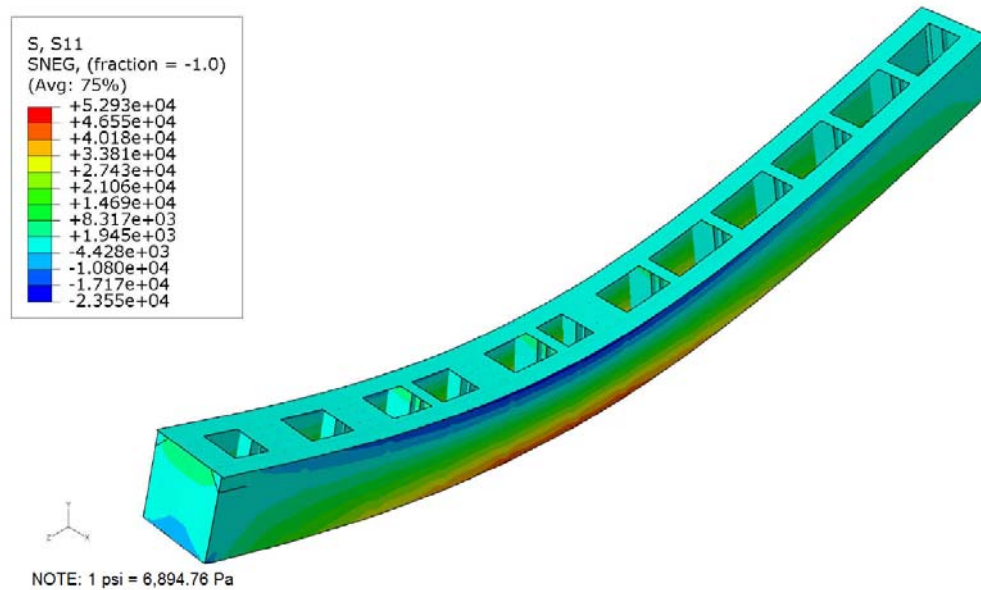


Figure 3-47 Bending Stresses (psi) Distribution in Steel Section.

3 Inches (76.2 mm) Mesh Model

Simplified hand calculations to check the accuracy of the model developed have been performed with the following assumptions:

- The structure behaves elastically and, therefore, the superposition principle is applicable. Also, this assumption allows the consideration of a homogeneous section after the transformation of the concrete slab into an equivalent structural steel section.
- Straight sections before deformation remain straight after deformation (Bernoulli's hypothesis).
- The contribution of the longitudinal steel to the section strength will be neglected.

The calculations performed under these hypotheses are included in Appendix E. The results obtained are shown in the following table. There are small differences due to simplifications adopted in the hand calculations. As can be seen, the model developed adequately simulates the structural behavior of the bent cap.

Table 3-10 Composite Cap Model. Validation Analysis. US Units

<b>Max. Bottom Fiber Stress. Model (psi)</b>	<b>Max. Bottom Fiber Stress. Hand Calculations (psi)</b>	<b>Difference (psi)</b>
52,930.0	49,908.6	3,021.4
<b>Max. Top Fiber Stress. Model (psi)</b>	<b>Max. Top Fiber Stress. Hand Calculations (psi)</b>	<b>Difference (psi)</b>
-5,356.0	-5,099.4	256.6

Table 3-11 Composite Cap Model. Validation Analysis. SI Units

<b>Max. Bottom Fiber Stress. Model (MPa)</b>	<b>Max. Bottom Fiber Stress. Hand Calculations (MPa)</b>	<b>Difference (MPa)</b>
36.5	34.4	2.1
<b>Max. Top Fiber Stress. Model (MPa)</b>	<b>Max. Top Fiber Stress. Hand Calculations (MPa)</b>	<b>Difference (MPa)</b>
-3.7	-3.5	0.2

## Chapter 4

### COST ESTIMATE AND SCHEDULE

This chapter describes the methods followed in the estimation of the cost and construction time of the two structural typologies described. First, the materials and activities involved are identified. In the second part of the chapter, actual unit costs for the LBJ project are applied to obtain the corresponding estimates. Finally, the time required for the construction of the two solutions and the time the traffic will be impacted for both of them are determined.

#### 4.1. Materials and Activities Identified

##### *4.1.1 Post-Tensioned Bent Cap*

The following materials are to be used in the construction of the post-tensioned concrete bent cap:

- Concrete with a nominal compressive strength of 6,000 psi (41.37 MPa).
- Grade 60 reinforcing steel.
- Grade 270 low relaxation prestressing steel.
- Other materials and elements, such as grout, plastic ducts and end anchorages.

The construction process for the post-tensioned concrete bent cap consists of the following activities:

- Shoring structure placement. A shoring structure will be required to resist the self-weight of the post-tensioned cap until the moment it has enough strength to become a self-supporting structure. A long term closure to traffic has to be performed in the roadway below the bent cap. This closure will extend up to the end of the bent cap construction process.
- Form work. This activity consists of the placement of the forms that will provide the concrete element the desired shape.
- Rebar placement. Working inside the forms previously placed to layout the rebar will be difficult and time consuming. For that reason, the cage formed by the rebar is prepared at ground level and then lifted to its final position inside the forms. This activity is performed simultaneously to the previous one.
- Placement of additional elements for prestressing tendons (ducts and end anchorages). This activity is performed simultaneously to the previous one.
- Concrete pouring. After the rebar, ducts and end anchorages are placed, the concrete is poured and vibrated. Enough curing time has to be provided for the concrete to achieve the minimum required strength to perform the following activity. For typical concretes fabricated with cement Type I and moist-cured, the variation of strength with time is defined by (Wight & MacGregor, 2012):

$$f'_{ci} = \frac{t}{4.00 + 0.85t} f'_c \quad (37)$$

where

$f'_{ci}$  is the concrete strength at time  $t$  (psi).

$t$  is the curing time (days).

$f'_c$  is the nominal concrete strength (psi).

Solving for  $t$  in the previous equation,

$$t = \frac{4f'_{ci}}{(f'_c - 0.85f'_{ci})} \quad (38)$$

Considering a nominal concrete strength of 6,000 psi (41.37 MPa) and a required strength at jacking of 5,000 psi (34.47 MPa), the stressing of the tendons cannot occur before 12 days after pouring of the concrete.

- Tendons placement, stressing and ducts grouting. Once the concrete has achieved the required strength, tendons are placed in the ducts. After tensioning them to its final stress, the ducts are grouted to prevent corrosion and ensure adherence between tendons and ducts and the surrounding concrete.
- Form work and shoring structure removal. After tensioning the tendons, the structure is ready to sustain its own self-weight. Both forms and auxiliary structure are removed, and traffic can be restored in the roadway below the bent cap.

#### *4.2.2 Composite Bent Cap*

The following materials are to be used in the construction of the composite bent cap:

- Concrete with a nominal compressive strength of 6,000 psi (41.37 MPa).

- Grade 60 reinforcing steel.
- A709 Grade 50 structural steel.

The construction process of the composite bent cap comprises a lower number of activities when compare with the post-tensioned concrete cap process. The activities identified are:

- Concrete slab form work. After the delivery of the steel section to the construction site, the forms that will allow the pouring of the concrete slab are placed. This activity is performed at ground level prior to the placement of the cap on its final location, so traffic is not impacted.
- Rebar placement. The concrete slab reinforcement is placed. This activity is also performed prior the lifting and placement of the pier cap on top of the columns.
- Concrete pouring. After the rebar is placed, the concrete is poured and vibrated. Enough curing time has to be provided prior to removing the form work. This activity is performed at ground level. To proceed with the lifting and placement activity, a minimum concrete strength in the slab is required so the section is capable of supporting its self-weight. Considering a minimum required strength of 3,000 psi (20.68 MPa) and a nominal concrete strength of 6,000 psi (41.37 MPa), following the same procedure outlined before, the lifting and placement of the cap cannot occur before 4 days after pouring the concrete slab.
- Form work removal. Once the concrete slab has developed enough form work can be removed. This is the last activity to be performed at ground

level. After the form work is removed, the pier cap is ready to be place on its final position.

- Lifting and placement of the composite cap in place supported by the already built cast in place columns. IH35E shall be closed to traffic during this operation, but it can be restored after finishing the operation. Because of the short time required to place the cap on its final position, only a night closure of IH35E is required.



Figure 4-1 Composite Bent Cap Ready to be Placed





Figure 4-2 Lifting of Composite Bent Cap

#### 4.2. Unit Costs and Cost Estimate

The cost of developing a project can be obtained as the summation of the following costs for each of the materials and activities identified:

- Direct cost. It can be defined as the cost of material, labor and equipment directly used for the construction of a unit measurement of the activities identified for the project. This cost, provided that the construction processes are optimized, should not significantly vary depending on the company performing the work.

- Indirect cost or general expenses. It is included in this category the cost of all the auxiliary items that the contractor needs to properly develop his activity but that are not specifically related to any of the construction activities identified for the project. This cost may greatly vary depending on the construction company policies and internal methods of operation.

To make the results obtained independent from the company performing the activities, only direct cost will be evaluated. Two set of values are needed in order to estimate the direct cost of the bent cap construction:

- Unit cost for each of the materials and activities identified. A problem that the cost estimator has to face when approaching the development of a cost estimate for a given project is the lack of accurate unit costs. The main reason for this lack of information is the construction companies' refusal to make public their costs of operation in a highly competitive market. The unit costs used in this study are actual costs
- Quantity takeoff for each of the materials and activities. Quantities have been calculated based on the project drawings. A summary of the values obtained is shown in Appendix F.

For cost estimation purposes, the previously described activities have been grouped in some cases. The direct cost consequence of the time the IH35E freeway shall be closed for the construction of both solutions (lane rentals) and the indirect cost caused to the city economic activity have not been considered in the estimates. However, the time during which traffic will be affected has been determined as explained in the

following subchapter. Considering that these direct and indirect costs are proportional to the time the traffic is impacted, a comparison can be established.

Maintenance cost for the two alternatives analyzed has not been considered. In general, because of the need of restoring the corrosion protective coating in the steel section, the composite cap will have a higher maintenance cost during its life cycle than the post-tensioned solution. However, an accurate actual unit cost for the replacement of such coating was not available.

A total direct cost of \$207,373.36 have been obtained for the post-tensioned bent cap compare to a total of \$199,867.37 calculated for the composite solution. Detailed calculations are shown in Appendix F.

#### 4.3 Activities Duration

Different construction scheduling techniques with varying accuracy and complexity were identified during the literature review phase of this research. Because of the short amount of time and reduced number of operations that the construction of the two proposed solutions imply, the bar (Gantt) chart technique has been used.

The duration of the activities to be performed for the construction of both solutions have been obtained by directly surveying construction engineers working on the project.

Because of the importance of the roadway affected by the bridge construction, it has been assumed that the work is performed during the seven days of the week. In order to estimate the time in which the traffic on IH35E will be impacted during the construction of the two solutions, activities that imply a conflict with the traffic below the

bridge have been differentiated from those that do not. The following Gantt charts show the time required for the construction of each of the solutions proposed.

ACTIVITY	DAYS																						
	1	2	3	4	5	6	7	8	9	10	11	12	13	14	15	16	17	18	19	20	21	22	23
Shoring structure placement																							
Form work																							
Rebar work																							
Post-tensioning additional elements																							
Concrete pouring																							
Tendons placement, stressing and grouting																							
Form work removal																							
Shoring structure removal																							



 Activities requiring traffic closure  
 Activities not requiring traffic closure

Figure 4-3 Post-Tensioned Bent Cap Construction Schedule

ACTIVITY	DAYS									
	1	2	3	4	5	6	7	8	9	10
Concrete slab form work										
Rebar placement										
Concrete pouring										
Form work removal										
Lifting and placement										



 Activities requiring traffic closure  
 Activities not requiring traffic closure

Figure 4-4 Composite Bent Cap Construction Schedule

Based on the results obtained, the construction of the post-tensioned solution requires 23 days and affects the traffic below during the complete construction time. However, the composite solution requires only 10 days to be finished once the steel section have arrived to the site, with only one day (actually, a few hours during a night) impacting the IH-35E traffic. Therefore, the alternative proposed improves the construction time required a limits to the minimum the interferences with traffic on the existing roadway.

## Chapter 5

### SUMMARY AND RESULTS DISCUSSION

A summary of the topic investigated in this research is included in this chapter together with a description and analysis of the results obtained. In the first part of the chapter, a summary of the case under study and the analysis performed is presented. The second part describes the modelling techniques and validation methods used. Also, results obtained are discussed and the main differences between the two structures modeled are established. The third part presents the results obtained in the cost estimation performed. Finally, the construction schedules and times of impact to traffic are compared.

#### 5.1 Summary

Bridges constitute one of the most important elements in transportation projects because of their impact in the cost and schedule of such projects. Properly determining the most appropriate structural typology in the design of a bridge involves the contribution of skilled and experienced professionals with different backgrounds. As a result, bridge design can be optimized to obtain the expected outcome in terms of quality, safety, cost and schedule.

The increasing competitiveness scenario construction companies have to deal with due to the current market conditions have made the design optimization even more important for the project's success. In that sense, the availability of comprehensive and detailed guidance documents describing the new processes, techniques and structural

typologies is extremely important to ensure that engineers properly comply with their commitment with the society.

The evolution of pier typologies is a consequence of the intensive use of bridges caused by the changes in our transportation infrastructures (Zhao & Tonia, 2012). The evolution of the urban areas and consequently the increase in their population, translates into increasing traffic volumes that, eventually, may overcome the existing transportation infrastructures capacity. The construction of new projects to increase the capacity of the transportation system in consolidated urban areas generates conflicts with existing infrastructures that requires the development of new construction processes, techniques and structural typologies to limit the impact on the traffic.

Structural prefabricated systems have been successfully used in different structure typologies with the well-known advantages:

- Reduction of the construction time and the number of operations to be performed in situ.
- Improved in plant quality control.
- Work zone safety improvement.
- Lower environmental impact.

The development of bridge substructure prefabricated structural systems will add to the previously exposed advantages a reduction in the number and time of traffic detours and closures.

Researches proposing different bridge substructure precast systems using concrete as main material are available, and different systems have been already used in actual projects. For example, precast post-tensioned simply supported bent caps with an inverted T section and with spans up to 58 ft. (17.68 m.) have been successfully used for the u-section bridges along the managed lanes in the LBJ project. However, there is a



practical limit for the span length of these precast elements due to their self-weight to allow for their safely lifting and placement.

The IH-635 Managed Lanes Project is located in North Dallas (Texas) and comprises works on both IH-35 and IH-635 freeways. Started in early 2011, it is expected to be completed and opened to public on summer 2015. After its completion, expected for the end of summer 2015, it will increase noticeably the traffic capacity of this important east-west corridor in Dallas.

Because of its complexity and the extensive use of bridges, the IH-35 IH-635 interchange became one of the major landmarks of the project. To provide direct access from both Loop 12 to the new managed lanes, a new Loop 12-IH 635 WB direct connector has been built. Its crossing over IH-35E has been solved with the construction of Bridge 4.

The IH-35 and its existing interchange with IH-635 is a major traffic corridor in Dallas area, supporting high traffic volumes, particularly during peak hours. The construction of a new bridge using conventional design and construction methodologies over this important corridor may imply closing the highway to the traffic and, therefore, seriously impacting the traffic and overall economic activity in this important area of the Metroplex.

The solution to be adopted may have to be prefabricated and simply supported on the columns to limit to the minimum the impact to the traffic. With spans varying from 74.5 ft. to 86 ft. (22.71 to 26.21 m.) between supports, a precast prestressed concrete bent cap would have been too heavy to be safely lifted. A composite steel-concrete bent cap, consisting of a rectangular shaped section of steel with a top compression concrete slab, was designed and built as a lighter alternative complying with the previously mentioned requirements.

Two pier cap typologies have been presented in this dissertation. The first one consist of the use of cast in place posttensioned concrete pier cap with a rectangular section, and simply supported on concrete columns built at both sides of the affected roadway. In this case, the pier cap will work as a prestressed concrete girder simply supported at both ends. The original design of Bridge 4 used this typology in the crossing over IH-35E in the LBJ project.

The second proposed typology tries to solve the weight problem that concrete has as a material when used to fabricate substructure precast systems. This is achieved by using a different material applied to the same structural concept: the use of a composite steel-concrete section, constituted by a rectangular steel section topped by a cast in place concrete slab to resist the top compression, and again simply supported at both ends. This solution has also the advantage of simplifying the construction process by changing the always arduous construction process of a post-tensioned concrete cap on site on an elevated position by simply lifting and placing the steel-concrete section once the concrete slab has reached enough strength to support its self-weight.

## 5.2 FEM Modelling and Results

Finite element models have been developed using the commercial software Abaqus with the objective of accurately simulating the theoretical structural behavior of both solutions reducing the computational cost to the minimum. These two models have been developed under the following hypotheses:

- The concrete have been modeled as an elastic-plastic material with damage simulation by using the concrete damage plasticity model (CDP model) available in Abaqus.
- Three different types of steel have been used in the two models developed: reinforcing steel, prestressing steel and structural steel. The three of them have been modeled as elastic-plastic materials.
- Linear finite elements have been used in both models following the software developer recommendations when modeling structures in which plastic behavior may be encountered. Using linear elements improves the convergence of the model and, therefore, reduces the computational cost.
- The contact surfaces between different elements and materials in the two models have been modeled by directly constraining the degrees of freedom of the nodes in contact to guarantee the deformation compatibility and an adequate stress transfer between elements. Modeling these surfaces with the method described reduces considerably the computational resources required to run the model and does not affect noticeably the accuracy of the model developed.
- In the case of the post-tensioned bent cap model, the prestressing tendons have not been included in the model because of their low contribution to the total stiffness of the section (Saiedi, 2007). Tendons overall effects on the structure have been simulated by properly determining an equivalent set of forces. In addition to a compressive force, a vertical force has been determined by the application of the load balancing method. The equivalent forces obtained using this procedure have been proof adequate to be used in the modelling of post-tensioned bent cap structures.

The models developed with the previously described assumptions have been validated by comparing the results obtained to alternative hand calculations. The parameters chosen to validate the model were the bending stresses. This selection allows reducing the time required for the validation process. The small differences obtained are caused by the simplifications assumed in the hand calculations, like neglecting the contribution of the rebar working in compression to the overall bending capacity of the section.

Therefore, based on the results obtained, the models developed are considered adequate to accurately simulate the structural behavior of the two alternative solutions proposed.

The results obtained show that, for the post-tensioned concrete bent cap alternative, the concrete section remains in the elastic range. Therefore, for the given loading case and with the objective of optimizing the computational cost of running the model, only the elastic behavior of the material needs to be considered. However, if future lab tests are performed to determine the postfailure performance of the solution, the concrete damage plasticity model is proposed to be used to account for the plastic behavior of the material.

On the other hand, both concrete and steel sections are found to be working in the plastic range in the composite bent cap model for the given loading case, so the material properties cannot be simplified.

In terms of structural strength, both solutions show the capability of properly resisting the imposed loads. The main difference in the structural response of the two solutions is related to deformations. For that reason, the structural behavior comparison has been performed in terms of serviceability instead of in terms of strength.

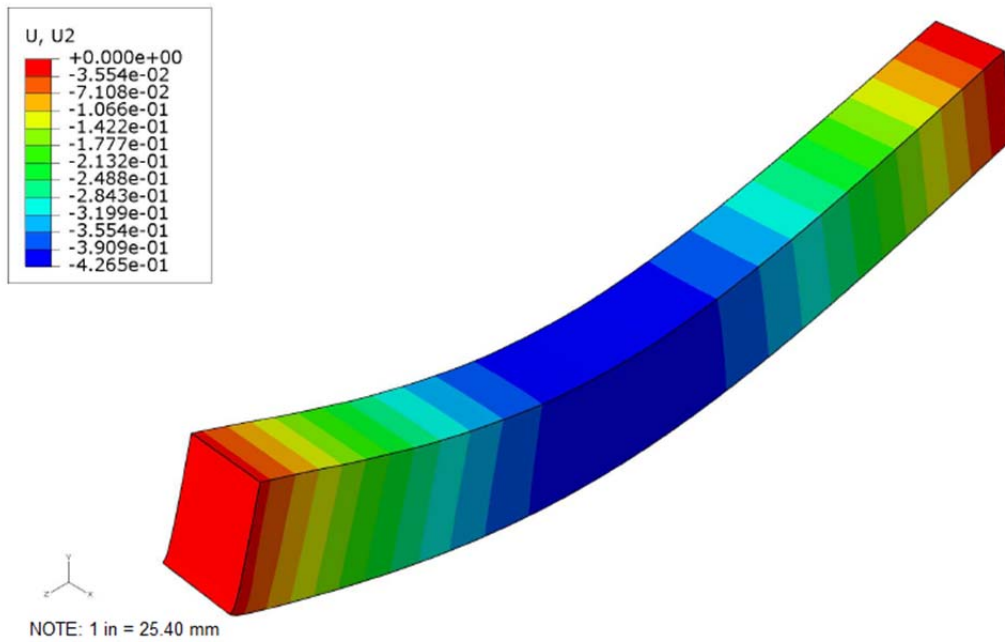


Figure 5-1 Post-Tensioned Cap Model. Deflections (inches)

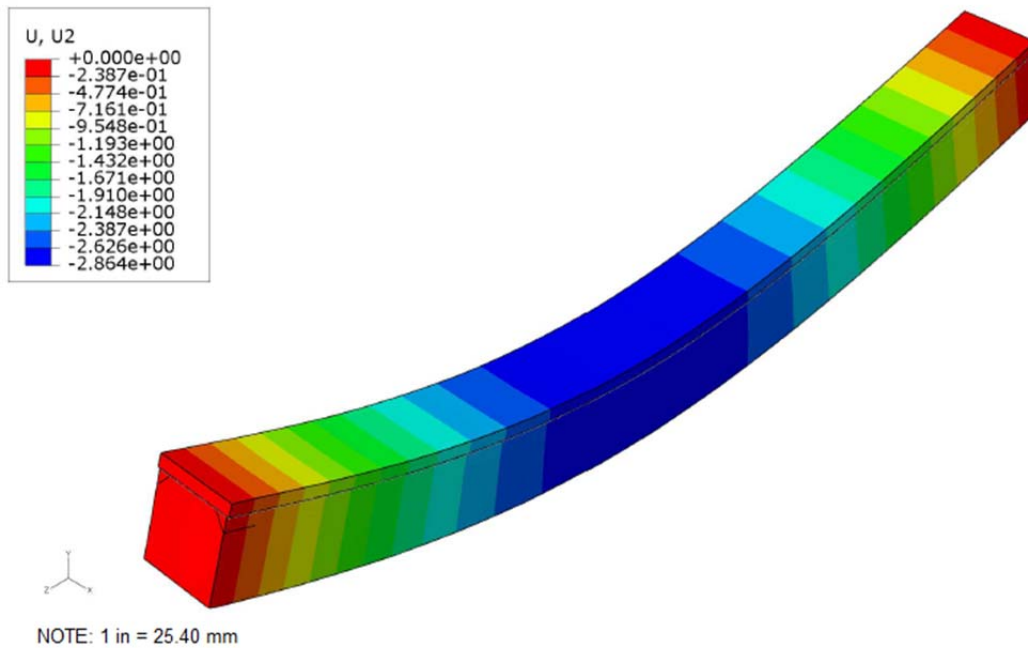


Figure 5-2 Composite Cap Model. Deflections (inches)

Figures 5-1 and 5-2 show the deflection obtained for the two alternative solutions. Maximum deflections values of 2.864 inches (72.75 mm) and 0.426 inches (10.82 mm) are obtained, respectively, for the composite and post-tensioned solutions. Based on the results obtained for the vertical displacement, it can be seen how the composite bent cap design has a more flexible behavior than the post-tensioned cap alternative.

Complying with the serviceability provisions about maximum deflection (AASHTO, 2012) may not be a problem when using the post-tensioned solution. However, the design of the composite bent cap solution has to account for that issue by providing the steel section with a camber to counteract the deflection caused by the loads.

### 5.3 Cost and Schedule Comparison

The cost of developing a project can be divided into two types. The first one, direct cost, is defined as the cost of material, labor and equipment directly used for the construction of a unit measurement of the construction activities identified for the project. Since this cost is established directly by the market based on the supply and demand rules, it is intrinsically independent from the company developing the project. The second one, indirect cost, is defined as the cost of all auxiliary items the contractor needs to perform the works but that are not specifically related to any of the construction activities identified for the project. This cost, unlike direct cost, depends on particular structure and methods of operation of the company in charge of developing the project.

To make the results obtained independent from the company performing the activities, only direct cost have been evaluated. The cost of the two solutions proposed have been obtained using real unit cost of the LBJ project and the quantities determined based on the project drawings. Also, as stated before, the cost incurred by the possible impacts on IH35E traffic have not been considered in the determination of the detailed estimates shown in Appendix F, although the time of impact on the traffic has been determined. Finally, the maintenance cost for the structural typologies studied has not been considered because of a lack of actual unit costs. Due to the requirement of replacing the corrosion protective coating of the steel section, the maintenance cost during the life cycle of the composite solution will be higher than for the post-tensioned alternative.

A total direct cost of \$207,373.36 have been obtained for the post-tensioned bent cap compare to a total of \$199,867.37 calculated for the composite solution. The results obtained show that, if traffic impact cost is not considered, the direct cost is very similar for the two proposed solutions. However, for the particular project in hand, the lane rental cost of closing IH35E makes the cast in place option unviable.

The main difference between the uses of one of the proposed alternatives is found after evaluating the construction time required and the duration of the traffic closure needed. A total of 23 days are required to build the post-tensioned solution, with a traffic closure needed for the total duration of the construction activities. However, and provided that the steel section is delivered to the site at the proper timing, casting the concrete slab and lifting the bent cap to its final position only takes 10 days, with only one night impacting the traffic on IH-35E.

Therefore, after the evaluation of the direct cost, construction schedule and traffic impacts, the proposed composite structural typology is considered a valid alternative to

be used as a prefabricated system in long span bridge substructure elements to limit impact caused to existing transportation structures.



## Chapter 6

### CONCLUSIONS AND RECOMMENDATIONS FOR FUTURE RESEARCH

#### 6.1 Conclusions

The following conclusions can be drawn from the research conducted:

- The modelling techniques applied during the performance of this dissertation are adequate and serve to the purpose of accurately modeling the structural behavior of the two structural typologies analyzed.
- The composite prefabricated bent cap has a more flexible behavior than the post-tensioned cast in place one. Special attention needs to be paid to the serviceability limits in the design of such bent cap typology.
- In the cases in which no conflicts with traffic are expected, the construction cost (maintenance cost has not been considered) is very similar for the two solutions proposed.
- The construction time for the composite alternative (10 days), provided that the steel section has been ordered in advance and has been delivered as required, is half of the time required to finish the construction of the cast in place solution (23 days).
- While the construction of the post-tensioned solution requires closing IH-35E for 23 days, with the traffic closure associated cost and impacts on the traffic, the prefabricated composite alternative limits it to one night.
- Based on the results obtained, the composite bent cap typology presented in this research is considered adequate to be proposed as a bridge

substructure prefabricated system to limit the impact on existing transportation infrastructures for the use in cases in which the span length required impedes the use of concrete based solutions.

## 6.2 Recommendations for Future Research

The following recommendations are presented as proposal for future researches about bridge substructure elements in general and about the two pier caps typologies analyzed in this study in particular:

1. The concrete damage plasticity model have been used in the development of the two finite element models included in this research because of its capability of modeling the inelastic behavior of concrete both in tension and compression. The accuracy of the parameters used to define the concrete material model is essential to properly simulate the structural behavior of the element under analysis. Developing a database of values to be used as a function of the concrete nominal strength in the application of the CDP model will be useful for future researches.
2. Bridge substructure precast systems have been widely analyzed in previous researches. However, all the solutions found are based on the use of concrete as main construction material. Concrete precast elements, although easier to implement as standardized systems, have as a counterpart their weight, that limits the size of element that can be safely lifted and placed. Lighter solutions may be explored in order to propose prefabricated or semi-prefabricated systems capable of

spanning longer distances to be used in beyond the limits of application of such precast systems. The composite section analyzed in this research is proposed as an economic feasible alternative to be further investigated in future studies about prefabricated bridge substructure systems.

3. The connection between the post-tensioned concrete cap and the cast in place columns has been modeled as a pin support. Releasing the rotation at both ends of the member minimizes the moment transferred to the columns. Typically, the idealized pin support is achieved in actual structures by the use of elastomeric bearing pads. However, the design and construction of a connection system that behaves similarly to the idealized pin support and that, at the same time, allows for the application of the prestress force in situ is not always easy. The connection detail proposed by the project design team could not be included in the model developed because of the computation limitations of the computer used. In order to confirm the adequacy of the system proposed, and to improve it if possible, further analyses should be performed. Additional information regarding the proposed connection can be found in Appendix A.

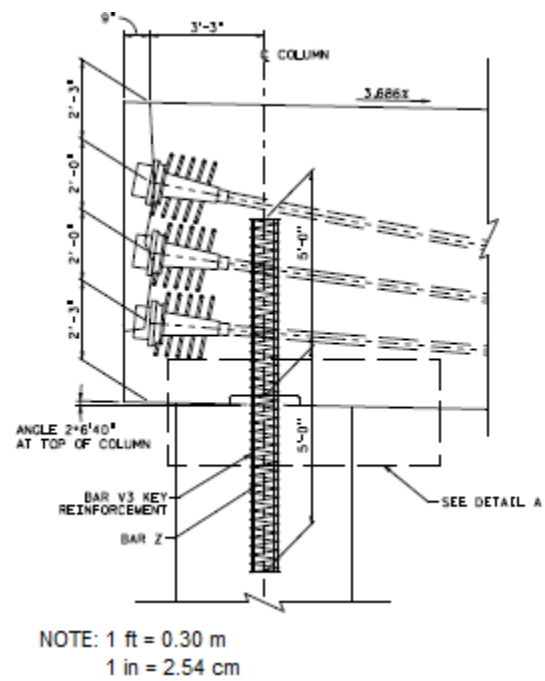


Figure 6-1 Post-Tensioned Cap. End and Support Detail

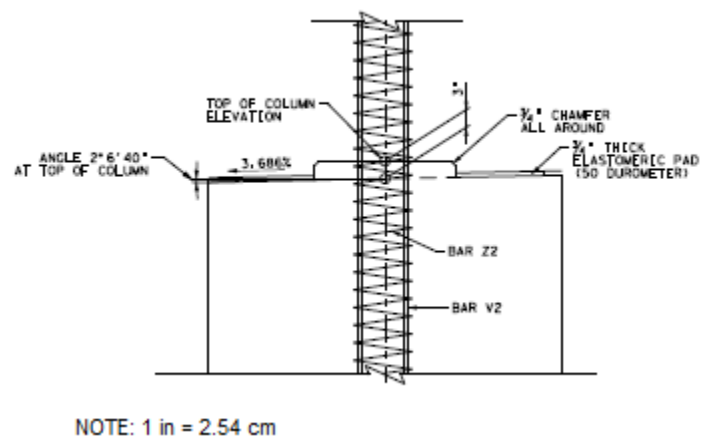


Figure 6-2 Post-Tensioned Cap. Detail A

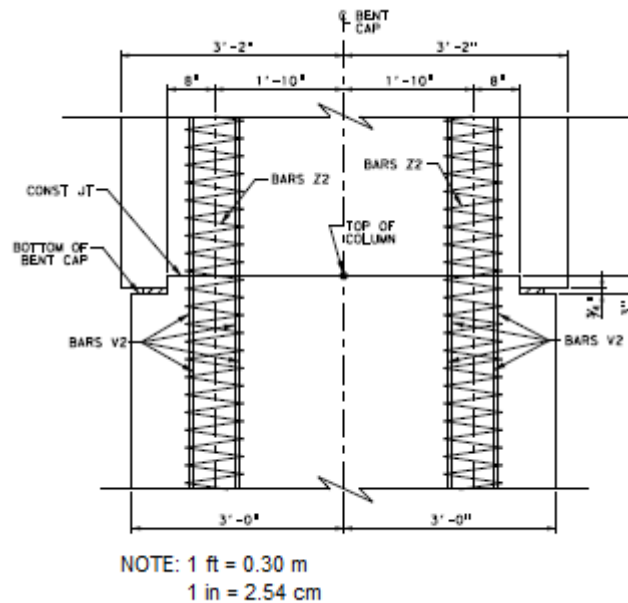


Figure 6-3 Post-Tensioned Cap. Transverse Section at Support

4. Determining the most suitable structural typology for a given case is a difficult task that involves the participation of skilled and experienced professionals with different backgrounds. The importance of properly selecting the bridge substructure typology to be used for the success of a project has been sufficiently justified in the research conducted. Example of factors that may determine the optimum design are: superstructure typology, height of the pier cap, availability of space for the pier cap foundation, possible impacts to traffic in existing roadways and scheduling and cost constraints. In order to help the Structural Engineer in taking such important decisions, the development of a comprehensive database and selection model for optimum bridge substructure design and construction is proposed for future researches.

5. The main disadvantage of the composite bent cap solution proposed is the flexibility of the element. The development of large deflections under the application of the design loads requires the fabrication of the steel section with a predefined camber in order to comply with the serviceability limits established in the applicable codes provisions. In those cases in which different structural typologies are used in the two pier caps supporting a span, the difference in the deflection developed at each end can generate additional stresses in the bridge superstructure and slab joints. This effect can be amplified in cases in which, like in the span 7 of the bridge studied, the exterior girders are alternatively located at the point of maximum deflection of the bent cap. The analysis of the importance of the torsional stresses introduced in the bridge superstructure and slab joints is proposed for a future research.

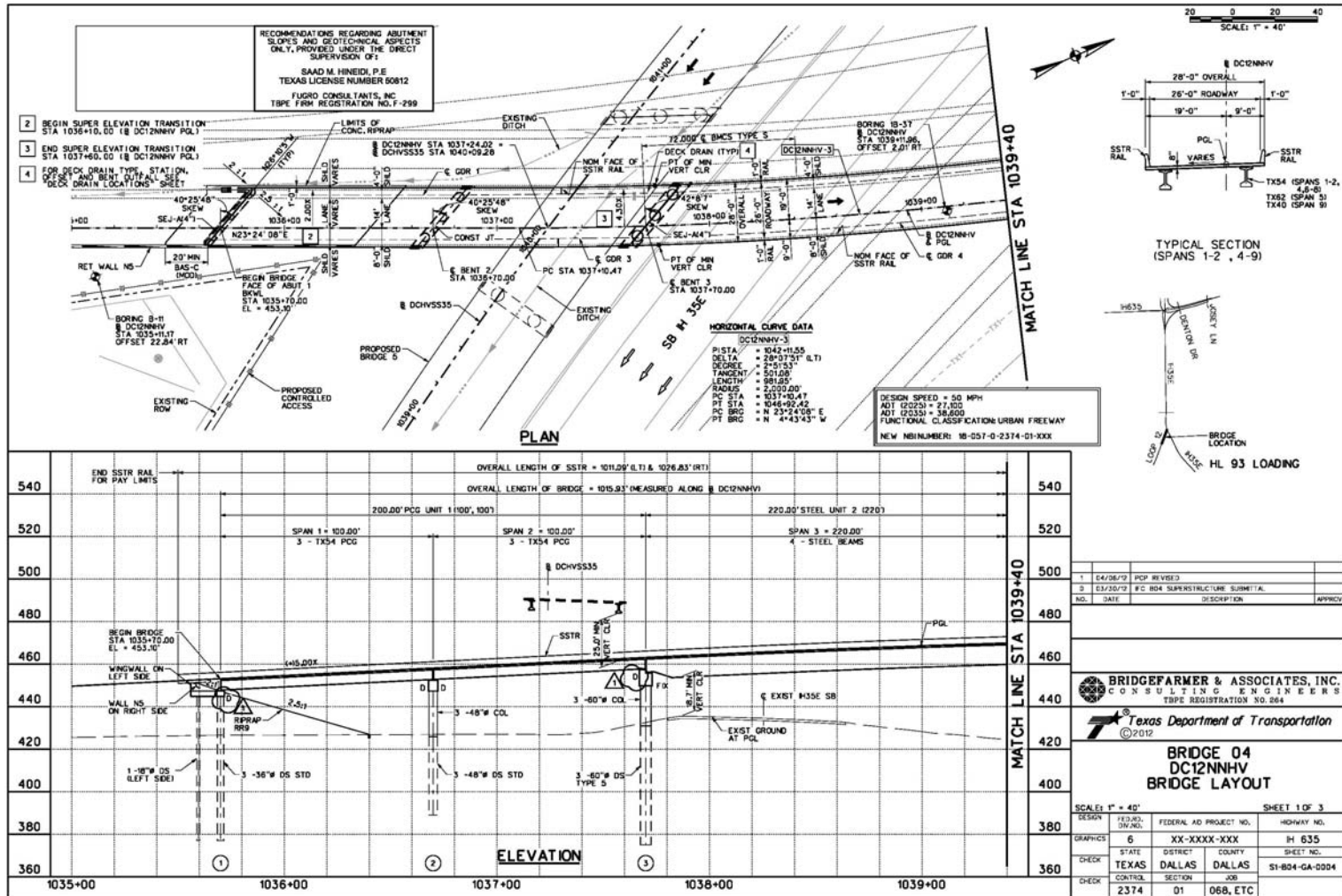
Appendix A  
Bridge 4 Drawings

The following drawings show the preliminary design of the post-tensioned concrete bent cap and the final design for the composite steel-concrete bent cap. All names and initials have been removed from the sheets for privacy purposes.

Unit conversion factors: 1 ft. = 0.30 m.

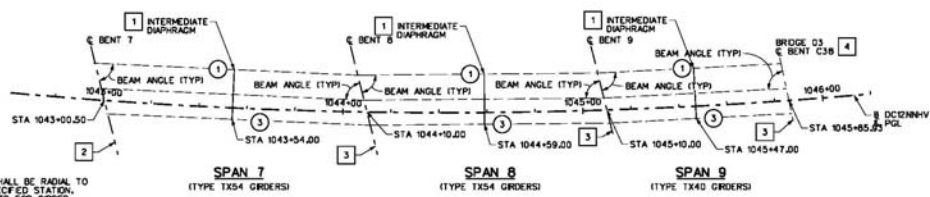
1 in = 25.40 mm









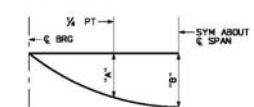


- 1 INTERMEDIATE DIAPHRAGM SHALL BE RADIAL TO BASELINE DC12NNHV AT SPECIFIED STATION. SEE 100 (M02) (2 SHEETS) STD FOR ORDER DETAILS.
- 2 SEE ELASTOMERIC BEARING PAD DETAIL SHEET 1 OF 1 FOR PAD DETAILS AND NOTE (1) FOR ADDITIONAL TESTING REQUIREMENT.
- 3 SEE ELASTOMERIC BEARING PAD DETAIL SHEET 1 OF 1 FOR PAD DETAILS AND NOTE 1 FOR ADDITIONAL TESTING REQUIREMENT.

**FRAMING PLAN**

- DENOTES ORDER NUMBER
- 4 SEE BRIDGE GSC PLANS FOR DETAILS NOT SHOWN.

\* ALL BEAM LENGTHS SHOWN ARE HORIZONTAL DISTANCES, WITHOUT ANY ADJUSTMENT MADE FOR LONGITUDINAL SLOPE. THE EXCEPTION IS THE TRUE DISTANCE, WHERE THE LENGTHS SHOWN ARE BOTTOM BEAM FLANGE LENGTHS WITH ADJUSTMENT MADE FOR THE BEAM SLOPE. ALL DIMENSIONS ARE IN FEET UNLESS OTHERWISE SHOWN.



NOTE: DEFLECTIONS SHOWN ARE CALCULATED VALUES DUE TO ALL DEAD LOADS, EXCLUDING ALLOWANCE FOR FUTURE OVERLAY AND FUTURE UTILITY LOADS. FIELD DEFLECTIONS MAY BE LESS THAN THE CALCULATED VALUES SHOWN. THESE VALUES MAY REQUIRE FIELD VERIFICATION. CALCULATIONS ARE BASED ON AN EC OF 5,000 KSI.

**BENT REPORT**

BENT NO. 7 (S 78 21 44 W)  
DISTANCE BETWEEN STATION LINE AND BEAM 1 15,966 L

BEAM SPAC.	BEAM ANGLE
(C.L. BENT)	D M S
SPAN 7 BEAM 1	0.000 73 20 40
BEAM 2	10.876 73 24 41
BEAM 3	10.876 73 28 42
TOTAL	21.753

BENT NO. 8 (S 78 21 44 W)  
DISTANCE BETWEEN STATION LINE AND BEAM 1 15,792 L

BEAM SPAC.	BEAM ANGLE
(C.L. BENT)	D M S
SPAN 7 BEAM 1	0.000 73 20 40
BEAM 2	10.743 73 24 41
BEAM 3	10.743 73 28 42
TOTAL	21.486

BEAM REPORT, SPAN 7

HORIZONTAL DISTANCE *	TRUE LENGTH	BEAM	DEFLECTIONS
C-C BENT E-E BM C-C BRG.	BOT. BM FLG.	SLOPE	A B
BEAM 1 108.536 109.01 107.448	108.03	-0.0176	0.116 0.162
BEAM 2 108.498 108.98 107.411	108.99	-0.0178	0.141 0.198
BEAM 3 108.460 108.94 107.374	108.96	-0.0180	0.130 0.182
TOTAL	326.93		

BENT NO. 8 (S 78 21 44 W)  
DISTANCE BETWEEN STATION LINE AND BEAM 1 15,792 L

BEAM SPAC.	BEAM ANGLE
(C.L. BENT)	D M S
SPAN 8 BEAM 1	0.000 76 28 07
BEAM 2	10.743 76 28 10
BEAM 3	10.743 76 28 13
TOTAL	21.486

BENT NO. 9 (S 78 21 44 W)  
DISTANCE BETWEEN STATION LINE AND BEAM 1 15,857 L

BEAM SPAC.	BEAM ANGLE
(C.L. BENT)	D M S
SPAN 8 BEAM 1	0.000 76 28 07
BEAM 2	10.741 76 28 10
BEAM 3	10.741 76 28 13
TOTAL	21.482

BEAM REPORT, SPAN 8

HORIZONTAL DISTANCE *	TRUE LENGTH	BEAM	DEFLECTIONS
C-C BENT E-E BM C-C BRG.	BOT. BM FLG.	SLOPE	A B
BEAM 1 99.974 99.46 97.917	99.50	-0.0267	0.080 0.113
BEAM 2 99.974 99.46 97.917	99.49	-0.0265	0.099 0.139
BEAM 3 99.974 99.46 97.917	99.49	-0.0264	0.089 0.125
TOTAL	298.38		

BENT NO. 9 (S 78 21 44 W)  
DISTANCE BETWEEN STATION LINE AND BEAM 1 15,857 L

BEAM SPAC.	BEAM ANGLE
(C.L. BENT)	D M S
SPAN 9 BEAM 1	0.000 78 52 23
BEAM 2	10.741 78 55 35
BEAM 3	10.741 78 58 49
TOTAL	21.482

ABUT NO. 10 (S 80 24 12 W)  
DISTANCE BETWEEN STATION LINE AND BEAM 1 15,650 L

BEAM SPAC.	BEAM ANGLE
(ABUT. BEAM)	D M S
SPAN 9 BEAM 1	0.000 80 54 52
BEAM 2	10.602 80 58 03
BEAM 3	10.602 81 01 17
TOTAL	21.203

BEAM REPORT, SPAN 9

HORIZONTAL DISTANCE *	TRUE LENGTH	BEAM	DEFLECTIONS
C-C BENT E-E BM C-C BRG.	BOT. BM FLG.	SLOPE	A B
BEAM 1 76.514 76.01 74.482	76.02	-0.0212	0.060 0.084
BEAM 2 76.115 75.61 74.084	75.62	-0.0209	0.072 0.100
BEAM 3 75.717 75.21 73.686	75.23	-0.0207	0.062 0.087
TOTAL	226.82		

HL 93 LOADING

1	08/08/10	SPAN 8-9 REVISED	
3	03/20/12	FIG. 804 SUPERSTRUCTURE SUBMITTAL	
NO.	DATE	DESCRIPTION	APPROVED

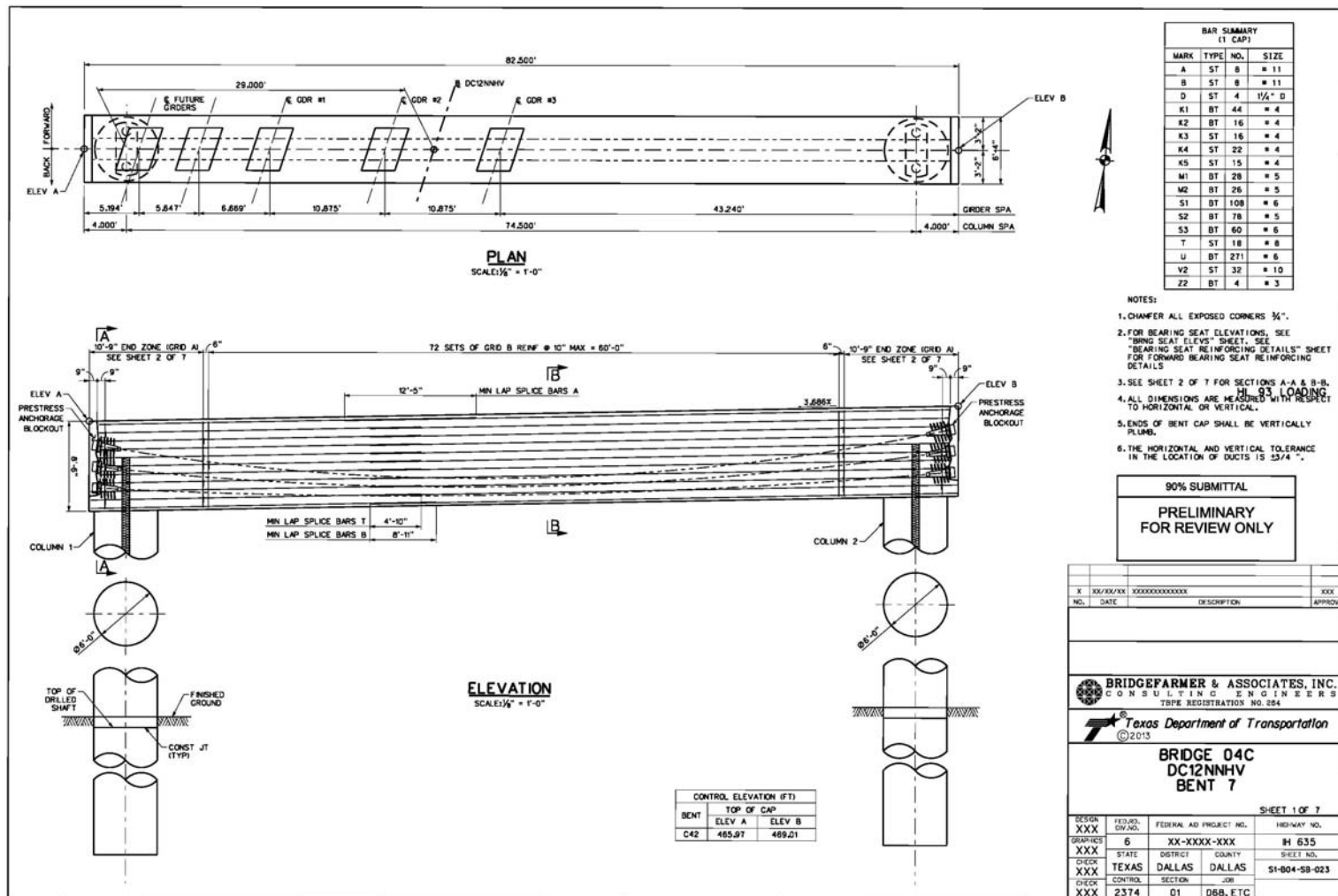
**BRIDGEFARMER & ASSOCIATES, INC.**  
CONSULTING ENGINEERS  
TXPE REGISTRATION NO. 044

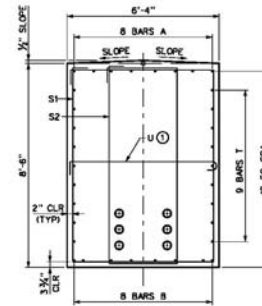
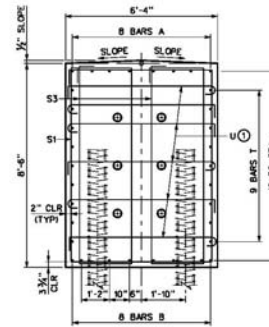
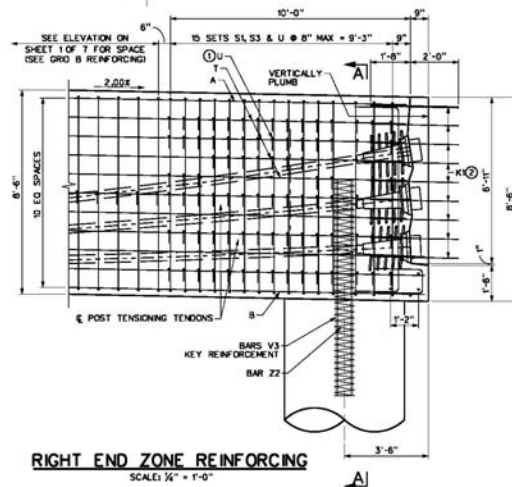
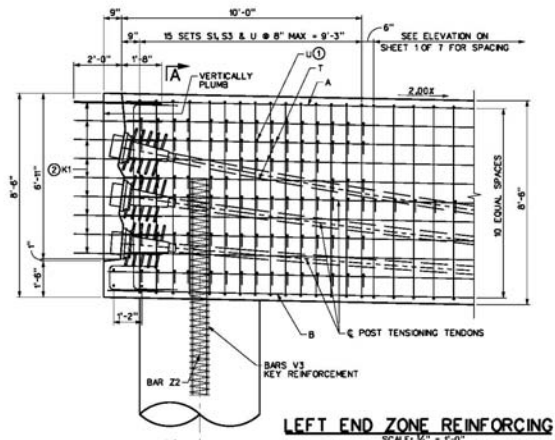
**Texas Department of Transportation**  
© 2012

**BRIDGE 04**  
**DC12NNHV**  
**PSTR CONC GRDR LAYOUT**  
**SPAN NO. 07-09**

SCALE: 1" = 40'	FED. AD. PROJECT NO.	HIGHWAY NO.
DESIGN	6	XX-XXXX-XXX
GRAPHICS	STATE	DISTRICT
CHECK	TEXAS	DALLAS
CHECK	CONTROL	SECTION
	2374	01
		068, ETC

SHEET 3 OF 3  
IH 635  
SHEET NO.  
S1-804-SP-0006

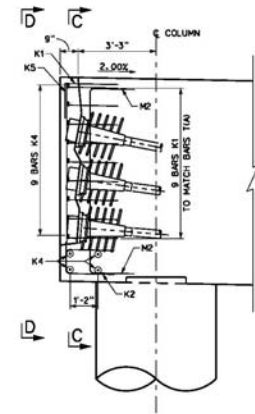




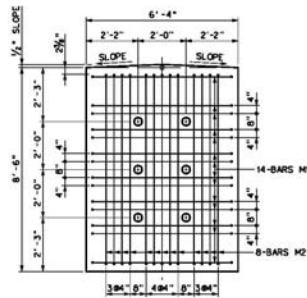
HL 93 LOADING

90% SUBMITTAL  
PRELIMINARY  
FOR REVIEW ONLY

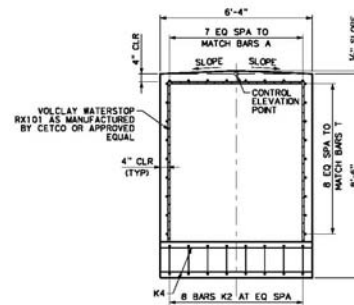
DESIGN	XXX	FED. AID PROJECT NO.	XXX	HIGHWAY NO.	XXX
GRAPHICS	XXX	STATE	TEXAS	COUNTY	DALLAS
CHECK	XXX	DISTRICT	DALLAS	COUNTY	DALLAS
CHECK	XXX	SECTION	01	JOB	06B, ETC
CHECK	XXX	SECTION	01	JOB	06B, ETC



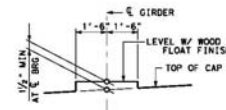
**BLOCKOUT REINFORCING DETAIL**  
SCALE: 1/4" = 1'-0"



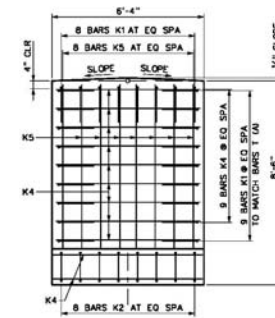
**MESH REINFORCEMENT**  
SCALE: 1/4" = 1'-0"



**SECTION C-C**  
SCALE: 1/4" = 1'-0"



**BEARING SEAT DETAIL**  
NOT TO SCALE  
(BEARING SURFACE SHALL BE CLEAN AND FREE OF ALL LOOSE MATERIAL BEFORE PLACING BEARING PAD).

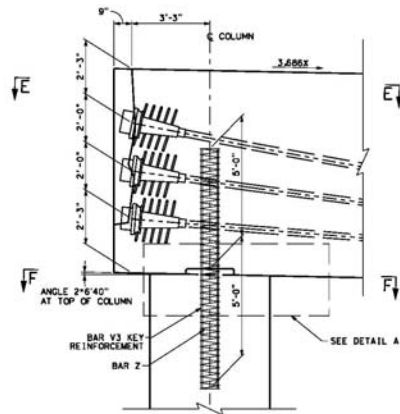


**SECTION D-D**  
SCALE: 1/4" = 1'-0"

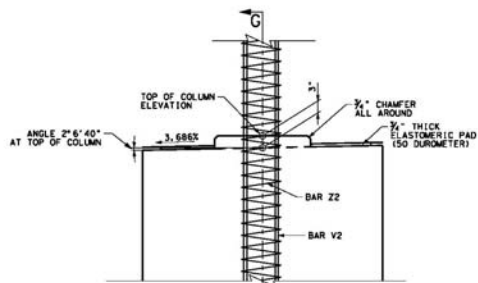
HL 93 LOADING

90% SUBMITTAL  
PRELIMINARY  
FOR REVIEW ONLY

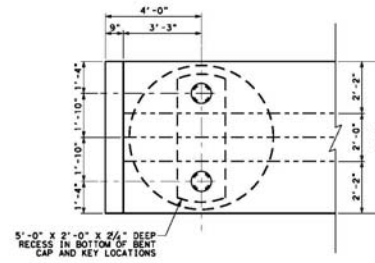
XX	XX/XX/XX	XXXXXXXXXXXXXXXXXXXX	XXX
NO.	DATE	DESCRIPTION	APPROV.
BRIDGEFARMER & ASSOCIATES, INC. CONSULTING ENGINEERS TYPE REGISTRATION NO. 064			
Texas Department of Transportation ©2013			
BRIDGE 04 DC12NNHV BENT 7			
SHEET 3 OF 7			
DESIGN XXX	FIELD NO. 6	FEDERAL AID PROJECT NO. XX-XXXX-XXX	HIGHWAY NO. IH 635
CHECK XXX	STATE TEXAS	DISTRICT DALLAS	COUNTY DALLAS
CHECK XXX	CONTROL 2374	SECTION 01	JOB 06B, ETC
SHEET NO. S1-804-SB-025			



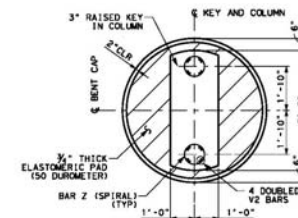
**END DETAIL**  
SCALE: 1/4" = 1'-0"



**DETAIL A**  
SCALE: 1/4" = 1'-0"



**SECTION E-E**  
SCALE: 1/4" = 1'-0"



**SECTION F-F**  
SCALE: 1/4" = 1'-0"

HL 93 LOADING

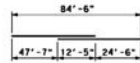
90% SUBMITTAL  
PRELIMINARY  
FOR REVIEW ONLY

DESIGN	XXX	FED. AD. PROJECT NO.	XX-XXXX-XXX	HIGHWAY NO.	IH 635
GRAPHICS	XXX	STATE	DALLAS	COUNTY	DALLAS
CHECK	XXX	CITY	DALLAS	SECTION	S1-804-SB-028
CHECK	XXX	DATE	01	JOB	06B, ETC

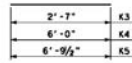
**BRIDGEFARMER & ASSOCIATES, INC.**  
CONSULTING ENGINEERS  
TYPE REGISTRATION NO. 064  
Texas Department of Transportation  
©2013  
**BRIDGE 04**  
**DC12NNHV**  
**BENT 7**

SHEET 4 OF 7

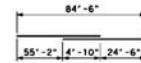




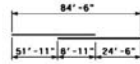
**BAR A**



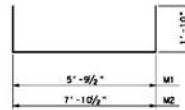
**BARS K3, K4 & K5**



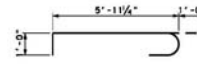
**BAR T**



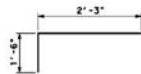
**BAR B**



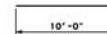
**BARS M1 & M2**



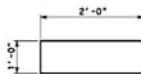
**BAR U**



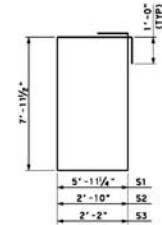
**BAR K1**



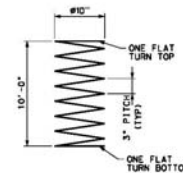
**BAR V2**



**BAR K2**



**BARS S1, S2 & S3**



**BAR Z2**

HL 93 LOADING

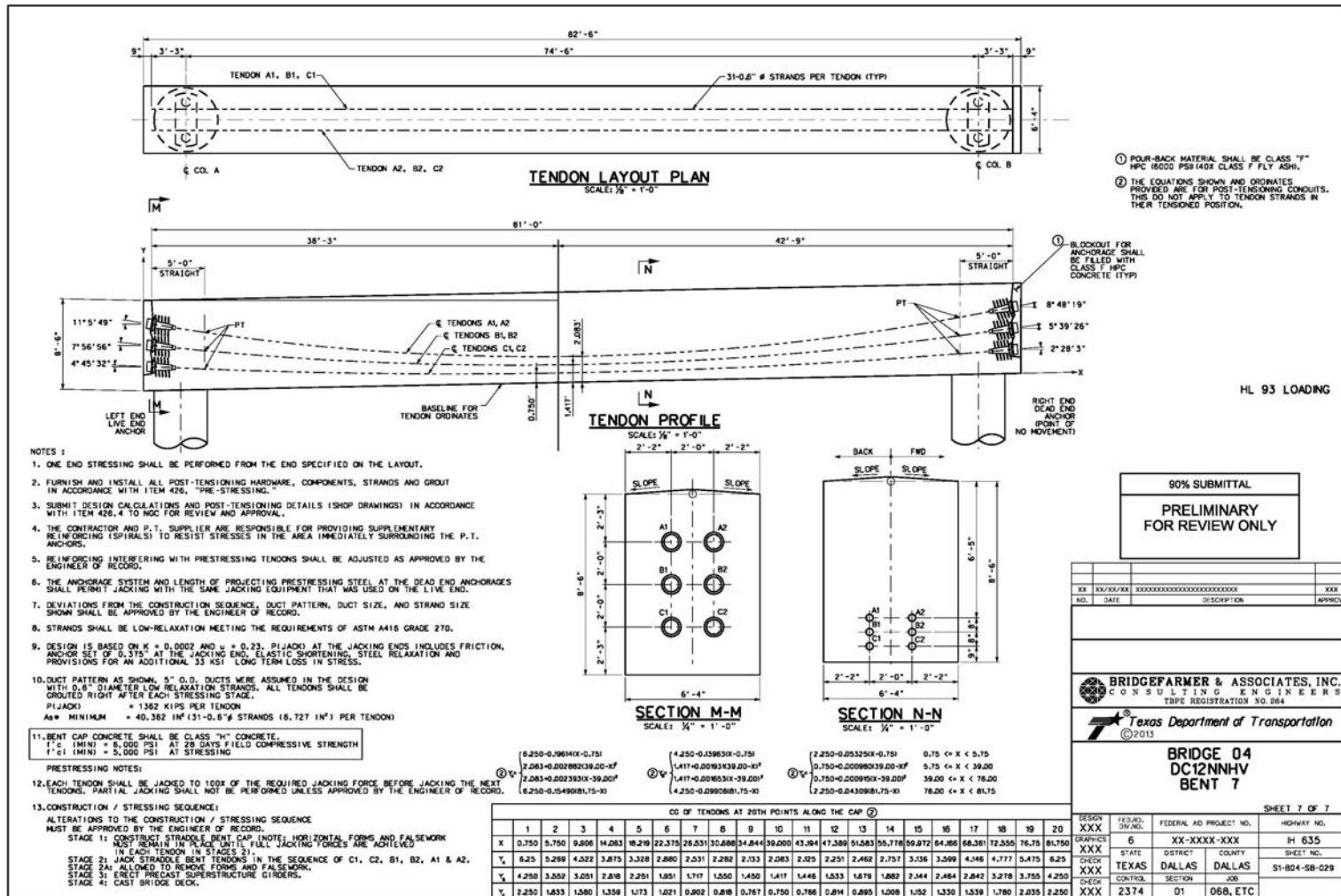
90% SUBMITTAL  
PRELIMINARY  
FOR REVIEW ONLY

DESIGN	XXX	FED. AID PROJECT NO.	XX-XXXX-XXX	HIGHWAY NO.	IH 635
GRAPHICS	XXX	STATE	DALLAS	COUNTY	DALLAS
CHECK	XXX	SECTION	01	JOB	06B, ETC
CHECK	XXX	SECTION	01	JOB	06B, ETC

BRIDGEFARMER & ASSOCIATES, INC.  
CONSULTING ENGINEERS  
TYPE REGISTRATION NO. 064  
Texas Department of Transportation  
©2013

BRIDGE 04  
DC12NNHV  
BENT 7

SHEET 6 OF 7



- POUR-BACK MATERIAL SHALL BE CLASS "F" HPC (M30) PER 1403 CLASS F FLY ASH.
- THE EQUATIONS SHOWN AND ORDINATES PROVIDED ARE FOR POST-TENSIONING CONDUITS. THIS DOES NOT APPLY TO TENDON STRANDS IN THEIR TENSIONED POSITION.

1. BLOCKOUT FOR ANCHORAGE SHALL BE FILLED WITH CLASS F HPC CONCRETE (TYP)

RIGHT END DEAD END ANCHOR (POINT OF NO MOVEMENT)

90% SUBMITTAL  
PRELIMINARY FOR REVIEW ONLY

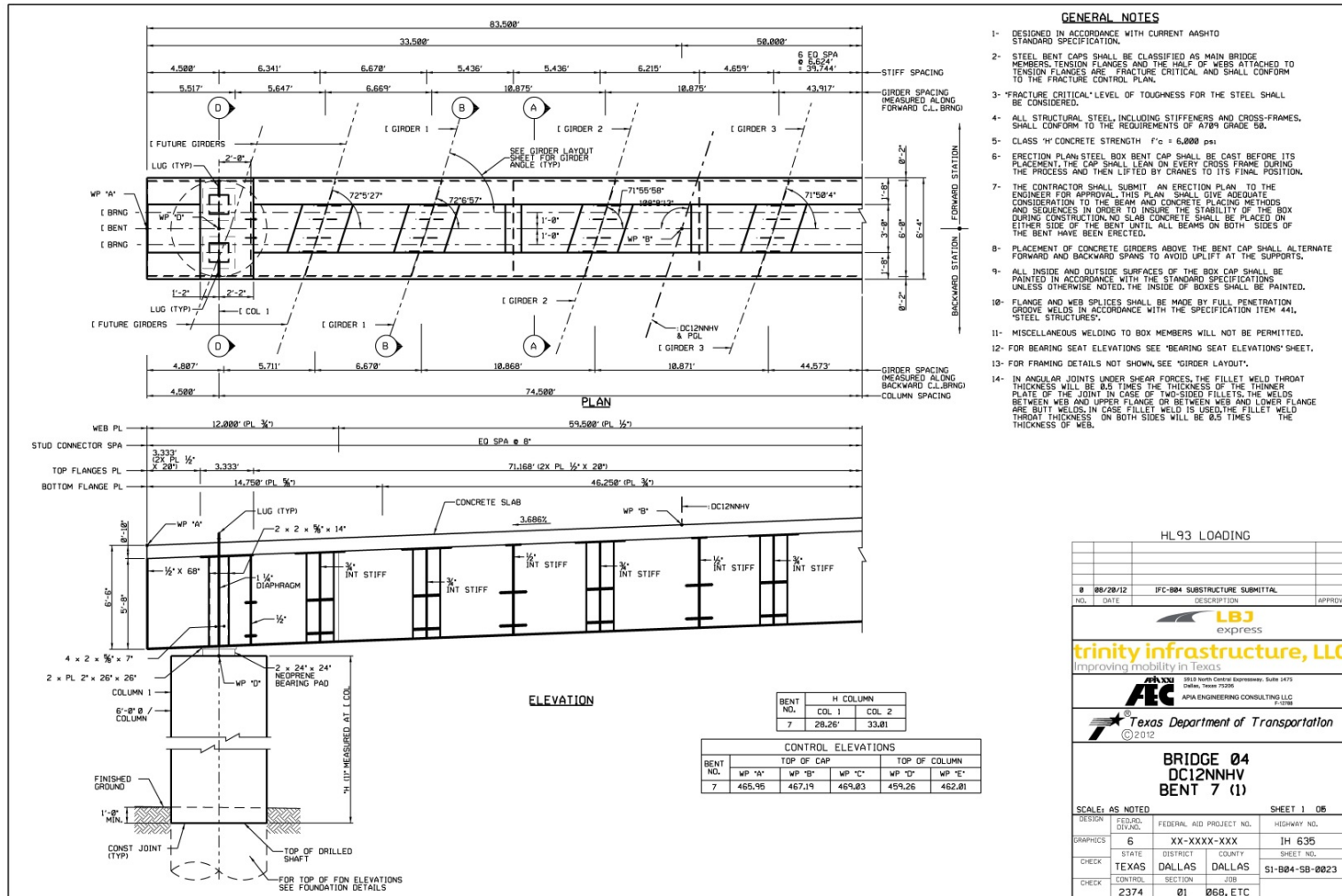
XX	XX/XX/XX	XXXXXXXXXXXXXXXXXXXXXXXXXXXX	XXX
NO.	DATE	DESCRIPTION	APPROVED

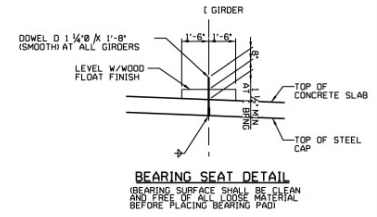
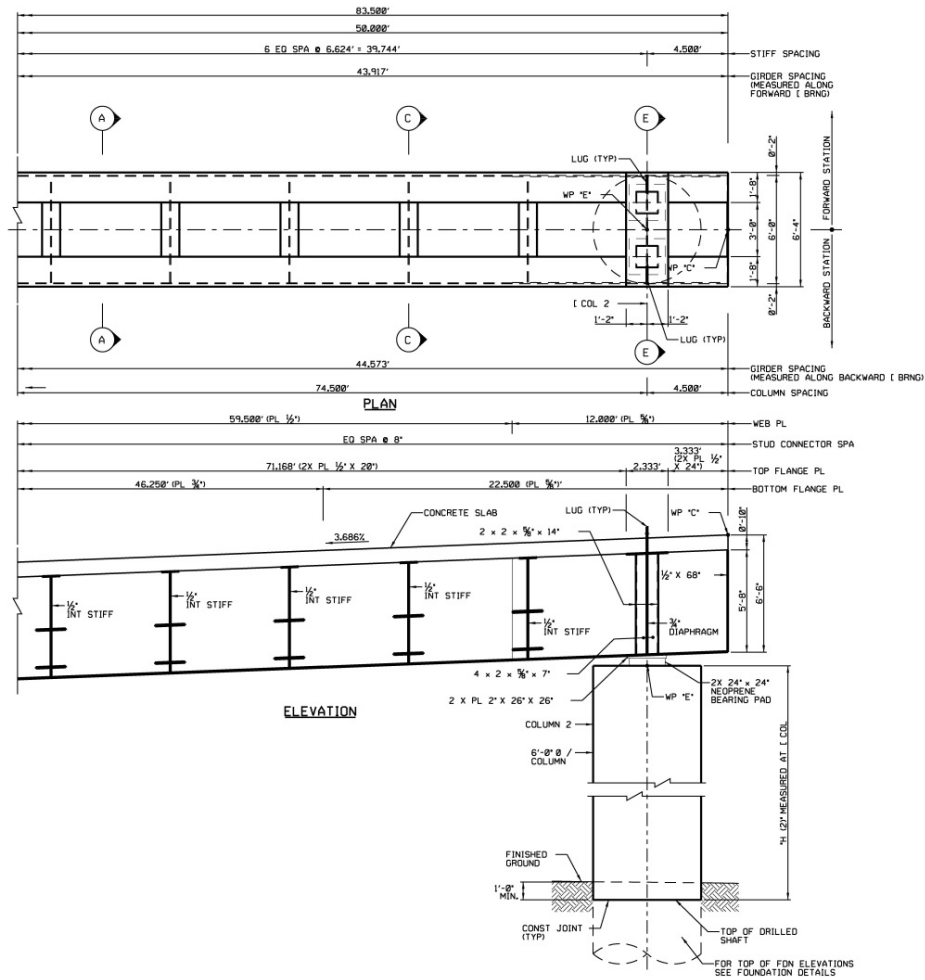
**BRIDGEFARMER & ASSOCIATES, INC.**  
CONSULTING ENGINEERS  
TYPE REGISTRATION NO. 064

**Texas Department of Transportation**  
©2015

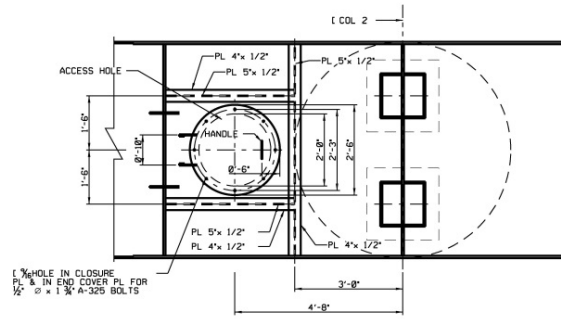
**BRIDGE 04 DC12NNHV BENT 7**

DESIGN	XXX	FEEDBACK	STATE	FEDERAL AID PROJECT NO.	HIGHWAY NO.
GRAPHICS	XXX	6	XX-XXXX-XXX	IH 635	
CHECK	XXX	STATE	DISTRICT	COUNTY	SHEET NO.
CONTRACT	XXX	TEXAS	DALLAS	DALLAS	S1-804-SB-029
CHECK	XXX	SECTION	01	06B, ETC	

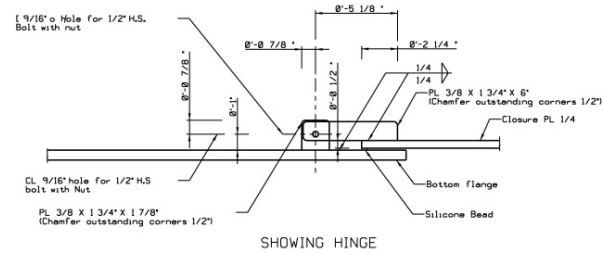


[illegible]

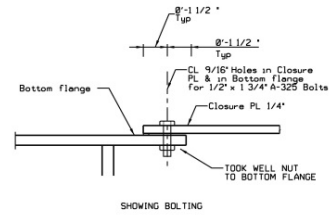




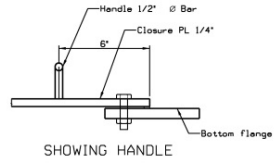
PLAN VIEW OF ACCESS HOLE IN  
BOTTOM FLANGE AND CLOSURE PLATE



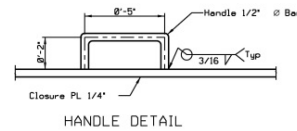
SHOWING HINGE



SHOWING BOLTING



SHOWING HANDLE



HANDLE DETAIL

WHEN SECURING BOTTOM FLANGE,  
THE BOLTS SHALL BE SNUG TIGHT ONLY.  
A SILICONE BEAD SHALL BE UNIFORMLY  
APPLIED AROUND EDGE OF CLOSURE  
PLATE BEFORE SECURING

HL 93 LOADING			
NO.	DATE	DESCRIPTION	APPROV.
0	08/28/12	IFC-804 SUBSTRUCTURE SUBMITTAL	
<b>trinity infrastructure, LLC</b> Improving mobility in Texas			
1910 North Central Expressway, Suite 1415 Dallas, Texas 75236 APIA ENGINEERING CONSULTING LLC P. 0308			
<b>BRIDGE 04</b> <b>DC12NNHV</b> <b>BENT 7 (4)</b>			
SCALE: AS NOTED		SHEET 4 OF 5	
DESIGN	FEDERAL AID PROJECT NO.	HIGHWAY NO.	
GRAPHICS	6	XX-XXXX-XXX	IH 635
CHECK	STATE	DISTRICT	COUNTY
	TEXAS	DALLAS	DALLAS
CHECK	CONTROL	SECTION	JOB
	2374	01	068, ETC



Appendix B  
Load Calculations



The following pages have been extracted from the Bridge Analysis Reports for each girder line in the Bridge 4 model generated using the software PGSUPER. Only the pages regarding to the calculation of girder lines reactions are reproduced in this Appendix.

Unit conversion factor: 1 kip = 4.448 kN.

# Bridge Analysis Report

For

Girder Line A

July 4, 2015 6:20:29 pm

**PGSuper™**

Copyright © 2015, WSDOT, All Rights Reserved

Version 2.7.2 - Built on Nov 9 2012



## Project Properties

Bridge Name	Bridge 4
Bridge ID	
Company	Your Company
Engineer	Your Name
Job Number	001
Comments	
File	C:\Users\FranciscoDavid\Desktop\Thesis\Pran\PGSuper\Bridge4\DesignLoads.pgs

Bridge: Bridge 4

Job: 001

04/07/2015

Location from Left Support (ft)	Design							
	Service I		Service III		Fatigue I		Strength I	
	Max (kip-ft)	Min (kip-ft)	Max (kip-ft)	Min (kip-ft)	Max (kip-ft)	Min (kip-ft)	Max (kip-ft)	Min (kip-ft)
Span 2 Girder A <sub>1</sub> (0.9L <sub>g</sub> ) 97.760	-68.73	-130.86	-69.37	-119.07	-32.62	-99.51	-57.77	-194.40
Span 2 Girder A <sub>1</sub> 98.193	-69.61	-131.93	-70.22	-120.08	-33.15	-100.26	-58.69	-195.93
Span 2 Girder A <sub>1</sub> (1.5H) 101.331	-76.00	-139.72	-76.37	-127.35	-36.97	-105.69	-65.32	-207.04
Span 2 Girder A <sub>1</sub> 101.872	-77.10	-141.07	-77.43	-128.61	-37.63	-106.63	-66.47	-208.96
Span 2 Girder A <sub>1</sub> (H) 103.581	-80.50	-145.33	-80.73	-132.59	-39.63	-109.61	-69.94	-215.05
Span 2 Girder A <sub>1</sub> (CB) 103.725	-80.77	-145.69	-80.99	-132.93	-39.79	-109.86	-70.21	-215.57
Span 2 Girder A <sub>1</sub> 104.664	-82.56	-148.04	-82.74	-135.12	-40.80	-111.50	-71.98	-218.92
Span 2 Girder A <sub>1</sub> 105.247	-83.67	-149.50	-83.82	-136.48	-41.43	-112.53	-73.07	-221.00
Span 2 Girder A <sub>1</sub> (PSXFR) 106.664	-86.35	-153.05	-86.44	-139.80	-42.94	-115.02	-75.72	-226.08
Span 2 Girder A <sub>1</sub> (FoS) 108.081	-89.04	-156.61	-89.06	-143.12	-44.46	-117.52	-78.36	-231.17
Span 2 Girder A <sub>1</sub> (1.0L <sub>g</sub> ) 108.622	-90.07	-157.98	-90.07	-144.40	-45.03	-118.48	-79.37	-233.13

Total Girderline Reactions at Abutments and Piers

	DC		DW		ΣDC		ΣDW	
	Max (kip)	Min (kip)	Max (kip)	Min (kip)	Max (kip)	Min (kip)	Max (kip)	Min (kip)
Abutment 1	0.00	0.00	2.32	2.32	29.25	29.25	2.32	2.32
Pier 2	0.00	0.00	9.22	9.22	114.12	114.12	9.22	9.22
Abutment 3	0.00	0.00	6.85	6.85	84.22	84.22	6.85	6.85

Total Girderline Reactions at Abutments and Piers - Design Vehicles (Including Impact)

	Total Live Load					
	* LL+IM Design		* LL+IM Fatigue		* LL+IM Permit	
	Max (kip)	Min (kip)	Max (kip)	Min (kip)	Max (kip)	Min (kip)
Abutment 1	67.68	0.00	49.80	0.00	53.15	0.00
Pier 2	73.83	0.00	56.06	0.00	61.79	0.00
Abutment 3	68.20	0.00	51.33	0.00	56.09	0.00

\* Live Load values are per girder and include impact.

Total Girderline Reactions at Abutments and Piers (Including Impact)

	Design							
	Service I		Service III		Fatigue I		Strength I	
	Max (kip)	Min (kip)	Max (kip)	Min (kip)	Max (kip)	Min (kip)	Max (kip)	Min (kip)
Abutment 1	99.25	31.57	85.72	31.57	90.48	157.79	158.48	27.83
Pier 2	197.18	123.34	182.41	123.34	145.75	61.67	285.69	108.70
Abutment 3	159.27	91.07	145.63	91.07	122.53	45.54	234.51	80.25

Live Load Reactions without Impact

Total Girderline Reactions at Abutments and Piers - Design Vehicles (Without Impact)

	Total Live Load					
	* LL Design		* LL Fatigue		* LL Permit	
	Max (kip)	Min (kip)	Max (kip)	Min (kip)	Max (kip)	Min (kip)
Abutment 1	53.15	0.00	44.30	0.00	53.15	0.00
Pier 2	61.79	0.00	51.49	0.00	61.79	0.00
Abutment 3	56.09	0.00	46.74	0.00	56.09	0.00

\* Live Load values are per girder and do not include impact.

Total Girderline Reactions at Abutments and Piers - Rating Vehicles (Without Impact)

	* LL Design		* LL Legal Routine		* LL Legal Special	
	Max (kip)	Min (kip)	Max (kip)	Min (kip)	Max (kip)	Min (kip)
Abutment 1	53.15	0.00	32.93	0.00	41.21	0.00

Maximum Reaction for Girder Line A

	* LL Design		* LL Legal Routine		* LL Legal Special	
	Max (kip)	Min (kip)	Max (kip)	Min (kip)	Max (kip)	Min (kip)
Pier 2	61.79	0.00	35.04	0.00	39.94	0.00
Abutment 3	56.09	0.00	34.80	0.00	38.95	0.00

\* Live Load values are per girder and do not include impact.

# Bridge Analysis Report

For

Girder Line B

July 4, 2015 6:22:43 pm

**PGSuper™**

Copyright © 2015, WSDOT, All Rights Reserved

Version 2.7.2 - Built on Nov 9 2012



## Project Properties

Bridge Name	Bridge 4
Bridge ID	
Company	Your Company
Engineer	Your Name
Job Number	001
Comments	
File	C:\Users\FranciscoDavid\Desktop\Thesis\Pran\PGSuper\Bridge4DesignLoads.pgs

Bridge: Bridge 4

Job: 001

04/07/2015

Location from Left Support (ft)	Design							
	Service I		Service III		Fatigue I		Strength I	
	Max (kip-ft)	Min (kip-ft)	Max (kip-ft)	Min (kip-ft)	Max (kip-ft)	Min (kip-ft)	Max (kip-ft)	Min (kip-ft)
Span 2 Girder B, 65.014	4.63	-61.12	-0.17	-52.76	5.21	-35.79	24.88	-97.63
Span 2 Girder B, (0.7L <sub>g</sub> ) 75.723	-21.84	-88.98	-25.03	-78.74	-9.03	-51.01	-5.43	-137.50
Span 2 Girder B, 75.940	-22.37	-89.54	-25.52	-79.26	-9.31	-51.32	-6.03	-138.31
Span 2 Girder B, (0.8L <sub>g</sub> ) 86.541	-47.11	-117.38	-48.93	-105.15	-22.50	-66.61	-33.65	-178.34
Span 2 Girder B, 86.866	-47.82	-118.24	-49.61	-105.94	-22.88	-67.08	-34.42	-179.57
Span 2 Girder B, (0.9L <sub>g</sub> ) 97.358	-70.47	-146.00	-71.25	-131.68	-34.80	-82.40	-58.76	-219.67
Span 2 Girder B, 97.791	-71.39	-147.15	-72.13	-132.74	-35.28	-83.04	-59.74	-221.34
Span 2 Girder B, (1.5H) 100.884	-77.93	-155.37	-78.39	-140.34	-38.71	-87.59	-66.71	-233.24
Span 2 Girder B, (FoB) 101.426	-79.06	-156.81	-79.48	-141.67	-39.30	-88.39	-67.92	-235.33
Span 2 Girder B, (H) 103.134	-82.56	-161.35	-82.84	-145.87	-41.13	-90.91	-71.59	-241.93
Span 2 Girder B, (CG) 103.291	-82.86	-161.77	-83.13	-146.26	-41.28	-91.14	-71.90	-242.54
Span 2 Girder B, (FoB) 107.634	-84.65	-164.24	-84.87	-148.54	-42.21	-92.51	-73.70	-246.11
Span 2 Girder B, 104.801	-85.78	-165.79	-85.96	-149.97	-42.79	-93.37	-74.83	-248.37
Span 2 Girder B, (PSKFR) 106.217	-88.50	-169.56	-88.60	-153.46	-44.19	-95.47	-77.57	-253.85
Span 2 Girder B, (FoB) 107.634	-91.20	-173.34	-91.23	-156.94	-45.59	-97.57	-80.29	-259.34
Span 2 Girder B, (1.0L <sub>g</sub> ) 108.176	-92.23	-174.78	-92.23	-158.27	-46.12	-98.37	-81.32	-261.44

## Total Girderline Reactions at Abutments and Piers

	DC		DW		ΣDC		ΣDW	
	Max (kip)	Min (kip)	Max (kip)	Min (kip)	Max (kip)	Min (kip)	Max (kip)	Min (kip)
Abutment 1	0.00	0.00	3.27	3.27	40.42	40.42	3.27	3.27
Pier 2	0.00	0.00	10.10	10.10	127.43	127.43	10.10	10.10
Abutment 3	0.00	0.00	6.82	6.82	86.38	86.38	6.82	6.82

## Total Girderline Reactions at Abutments and Piers - Design Vehicles (Including Impact)

	Total Live Load					
	* LL+IM Design		* LL+IM Fatigue		* LL+IM Permit	
	Max (kip)	Min (kip)	Max (kip)	Min (kip)	Max (kip)	Min (kip)
Abutment 1	77.75	0.00	50.26	0.00	61.64	0.00
Pier 2	92.82	0.00	64.12	0.00	78.14	0.00
Abutment 3	82.90	0.00	56.60	0.00	68.16	0.00

\* Live Load values are per girder and include impact.

## Total Girderline Reactions at Abutments and Piers (Including Impact)

	Design							
	Service I		Service III		Fatigue I		Strength I	
	Max (kip)	Min (kip)	Max (kip)	Min (kip)	Max (kip)	Min (kip)	Max (kip)	Min (kip)
Abutment 1	121.44	43.69	105.89	43.69	97.23	21.84	191.49	38.50
Pier 2	230.35	137.53	211.78	137.53	164.95	68.77	336.87	121.25
Abutment 3	176.10	93.20	159.52	93.20	131.50	46.60	263.25	82.18

## Live Load Reactions without Impact

## Total Girderline Reactions at Abutments and Piers - Design Vehicles (Without Impact)

	Total Live Load					
	* LL Design		* LL Fatigue		* LL Permit	
	Max (kip)	Min (kip)	Max (kip)	Min (kip)	Max (kip)	Min (kip)
Abutment 1	61.64	0.00	44.92	0.00	61.64	0.00
Pier 2	78.14	0.00	59.08	0.00	78.14	0.00
Abutment 3	68.16	0.00	51.53	0.00	68.16	0.00

\* Live Load values are per girder and do not include impact.

Maximum Reaction for Girder Line B

**Total Girderline Reactions at Abutments and Piers -  
Rating Vehicles (Without Impact)**

	* LL Design		* LL Legal Routine		* LL Legal Special	
	Max (kip)	Min (kip)	Max (kip)	Min (kip)	Max (kip)	Min (kip)
Abutment 1	61.64	0.00	36.95	0.00	47.89	0.00
Pier 2	78.14	0.00	42.98	0.00	49.29	0.00
Abutment 3	68.16	0.00	42.31	0.00	47.38	0.00

\* Live Load values are per girder and do not include impact.

# Bridge Analysis Report

For

Girder Line C

July 4, 2015 6:23:15 pm

**PGSuper™**

Copyright © 2015, WSDOT, All Rights Reserved

Version 2.7.2 - Built on Nov 9 2012



## Project Properties

Bridge Name	Bridge 4
Bridge ID	
Company	Your Company
Engineer	Your Name
Job Number	001
Comments	
File	C:\Users\FranciscoDavid\Desktop\Thesis\Pran\PGSuper\Bridge4DesignLoads.pgs

Bridge: Bridge 4

Job: 001

04/07/2015



Location from Left Support (ft)	Design									
	Service I		Service II		Fatigue I		Strength I		Strength II	
	Max (kip-ft)	Min (kip-ft)	Max (kip-ft)	Min (kip-ft)	Max (kip-ft)	Min (kip-ft)	Max (kip-ft)	Min (kip-ft)	Max (kip-ft)	Min (kip-ft)
Span 2 Girder C, 3.958	202.44	99.22	182.08	99.50	112.91	49.48	305.53	86.53	240.13	87.55
Span 2 Girder C, (CS) 4.854	199.49	97.12	179.36	97.47	111.28	48.40	301.22	84.38	236.53	85.64
Span 2 Girder C, (H) 5.042	198.87	96.68	178.79	97.04	110.94	48.17	300.32	83.93	235.78	85.24
Span 2 Girder C, 6.750	193.25	92.42	173.62	92.95	107.85	45.96	292.12	79.41	228.92	81.34
Span 2 Girder C, (1.5H) 7.292	191.47	91.03	171.98	91.63	106.87	45.23	289.53	77.91	226.75	80.07
Span 2 Girder C, 10.379	181.34	83.09	162.65	84.05	101.31	41.09	274.78	69.33	214.39	72.76
Span 2 Girder C, (0.1L <sub>y</sub> ) 10.812	179.92	81.96	161.34	82.98	100.53	40.50	272.71	68.11	212.66	71.73
Span 2 Girder C, 21.299	145.80	54.47	129.85	56.79	81.83	26.09	223.15	38.15	171.09	46.27
Span 2 Girder C, (0.2L <sub>y</sub> ) 21.634	144.75	53.61	128.88	55.96	81.25	25.64	221.62	37.20	169.81	45.47
Span 2 Girder C, 32.219	110.73	23.61	97.40	27.71	62.70	9.73	172.42	3.17	128.44	17.31
Span 2 Girder C, (0.3L <sub>y</sub> ) 32.436	110.04	22.97	96.76	27.11	62.32	9.39	171.43	2.43	127.60	16.71
Span 2 Girder C, 43.139	76.19	-9.07	65.36	-2.85	43.95	-7.76	122.67	-34.92	86.52	-13.69
Span 2 Girder C, (0.4L <sub>y</sub> ) 43.248	75.85	-9.40	65.04	-3.16	43.76	-7.93	122.18	-35.31	86.11	-14.01
Span 2 Girder C, (HP) 48.654	58.97	-25.83	49.35	-18.49	34.63	-16.76	97.94	-54.59	65.65	-29.69
Span 2 Girder C, 48.659	58.96	-25.84	49.33	-18.50	34.62	-16.76	97.91	-54.61	65.63	-29.70
Span 2 Girder C, (0.5L <sub>y</sub> ) 54.060	42.34	-42.41	33.77	-33.94	25.60	-25.68	73.99	-74.18	45.43	-45.61
Span 2 Girder C, 59.461	25.67	-59.12	18.34	-49.50	16.68	-34.70	54.45	-98.13	29.56	-65.84
Span 2 Girder C, (HP) 59.466	25.66	-59.14	18.32	-49.51	16.67	-34.71	54.45	-98.15	29.54	-65.86
Span 2 Girder C, (0.6L <sub>y</sub> ) 64.872	9.25	-76.01	3.01	-65.19	7.86	-43.84	35.18	-122.38	13.88	-86.31
Span 2 Girder C, 64.980	8.92	-76.35	2.70	-65.51	7.68	-44.02	34.79	-122.86	13.96	-86.72
Span 2 Girder C, (0.7L <sub>y</sub> ) 75.684	-23.06	-110.13	-27.20	-96.85	-9.43	-62.37	-2.50	-171.54	-16.78	-127.72
Span 2 Girder C, 75.900	-23.70	-110.82	-27.79	-97.49	-9.77	-62.74	-3.25	-172.54	-17.39	-128.56
Span 2 Girder C, 86.496	-53.59	-144.74	-55.95	-128.87	-25.63	-81.25	-37.19	-221.61	-45.46	-169.80
Span 2 Girder C, 86.821	-54.45	-145.78	-56.77	-129.84	-26.08	-81.82	-38.14	-223.13	-46.26	-171.07
Span 2 Girder C, (0.8L <sub>y</sub> ) 97.307	-81.81	-179.76	-82.82	-161.18	-40.42	-100.45	-67.98	-272.51	-71.59	-212.46
Span 2 Girder C, 97.741	-82.92	-181.18	-83.88	-162.48	-41.01	-101.22	-69.18	-274.56	-72.62	-214.18
Span 2 Girder C, (1.5H) 100.828	-90.81	-191.25	-91.41	-171.76	-45.13	-106.76	-77.73	-289.25	-79.88	-226.47
Span 2 Girder C, 101.369	-92.19	-193.02	-92.73	-173.39	-45.85	-107.74	-79.22	-291.83	-81.15	-228.63
Span 2 Girder C, (H) 103.078	-96.42	-198.61	-96.78	-178.54	-48.04	-110.82	-83.71	-299.99	-85.02	-235.45
Span 2 Girder C, (CS) 103.265	-96.86	-199.23	-97.21	-179.10	-48.27	-111.16	-84.16	-300.89	-85.42	-236.20
Span 2 Girder C, 104.161	-98.95	-202.16	-99.23	-181.80	-49.34	-112.77	-86.29	-305.17	-87.31	-239.78
Span 2 Girder C, 104.744	-100.30	-204.08	-100.54	-183.56	-50.04	-113.83	-87.68	-307.97	-88.54	-242.11
Span 2 Girder C, (PSXPR) 106.161	-103.59	-208.73	-103.72	-187.83	-51.73	-116.39	-91.02	-314.76	-91.52	-247.79
Span 2 Girder C, (FoS) 107.578	-106.85	-213.38	-106.89	-192.11	-53.41	-118.96	-94.34	-321.57	-94.48	-253.47
Span 2 Girder C, (1.0L <sub>y</sub> ) 108.119	-108.10	-215.16	-108.10	-193.75	-54.05	-119.94	-95.60	-324.17	-95.60	-255.65

## Total Girderline Reactions at Abutments and Piers

	DC		DW		ΣDC		ΣDW	
	Max (kip)	Min (kip)	Max (kip)	Min (kip)	Max (kip)	Min (kip)	Max (kip)	Min (kip)
Abutment 1	0.00	0.00	4.17	4.17	56.30	56.30	4.17	4.17
Pier 2	0.00	0.00	10.95	10.95	159.33	159.33	10.95	10.95
Abutment 3	0.00	0.00	6.82	6.82	102.47	102.47	6.82	6.82

## Total Girderline Reactions at Abutments and Piers - Design Vehicles (Including Impact)

	Total Live Load					
	* LL+IM Design		* LL+IM Fatigue		* LL+IM Permit	
	Max (kip)	Min (kip)	Max (kip)	Min (kip)	Max (kip)	Min (kip)
Abutment 1	98.70	0.00	61.02	0.00	78.93	0.00
Pier 2	124.39	0.00	78.53	0.00	105.27	0.00
Abutment 3	107.52	0.00	66.90	0.00	88.40	0.00

\* Live Load values are per girder and include impact.

## Total Girderline Reactions at Abutments and Piers (Including Impact)

Bridge: Bridge 4

Job: 001

04/07/2015

	Design									
	Service I		Service III		Fatigue I		Strength I		Strength II	
	Max (kip)	Min (kip)	Max (kip)	Min (kip)	Max (kip)	Min (kip)	Max (kip)	Min (kip)	Max (kip)	Min (kip)
Abutment 1	159.17	60.47	139.43	60.47	121.77	80.23	349.36	59.38	183.19	53.38
Pier 2	294.67	170.28	269.79	170.28	202.94	85.14	433.27	150.51	357.71	150.51
Abutment 3	216.81	109.29	195.31	109.29	155.00	54.66	376.89	96.66	257.66	96.66

## Live Load Reactions without Impact

## Total Girderline Reactions at Abutments and Piers - Design Vehicles (Without Impact)

	Total Live Load					
	* LL Design		* LL Fatigue		* LL Permit	
	Max (kip)	Min (kip)	Max (kip)	Min (kip)	Max (kip)	Min (kip)
Abutment 1	78.93	0.00	54.79	0.00	78.93	0.00
Pier 2	105.27	0.00	72.54	0.00	105.27	0.00
Abutment 3	88.40	0.00	60.92	0.00	88.40	0.00

\* Live Load values are per girder and do not include impact.

## Total Girderline Reactions at Abutments and Piers - Rating Vehicles (Without Impact)

	* LL Design		* LL Legal Routine		* LL Legal Special	
	Max (kip)	Min (kip)	Max (kip)	Min (kip)	Max (kip)	Min (kip)
Abutment 1	78.93	0.00	49.03	0.00	60.74	0.00
Pier 2	105.27	0.00	56.76	0.00	64.71	0.00
Abutment 3	88.40	0.00	54.88	0.00	61.46	0.00

\* Live Load values are per girder and do not include impact.

Maximum Reaction  
for Girder Line C

# Bridge Analysis Report

For

Girder Line D

July 4, 2015 6:24:48 pm

**PGSuper™**

Copyright © 2015, WSDOT, All Rights Reserved

Version 2.7.2 - Built on Nov 9 2012



**Washington State  
Department of Transportation**



**TEXAS DEPARTMENT OF TRANSPORTATION**



## Project Properties

Bridge Name	Bridge 4
Bridge ID	
Company	Your Company
Engineer	Your Name
Job Number	001
Comments	
File	C:\Users\FranciscoDavid\Desktop\Thesis\Pran\PGSuper\Bridge4DesignLoads.pgs

Bridge: Bridge 4

Job: 001

04/07/2015

Location from Left Support (ft)	Design									
	Service I		Service III		Fatigue I		Strength I		Strength II	
	Max (kip-ft)	Min (kip-ft)	Max (kip-ft)	Min (kip-ft)	Max (kip-ft)	Min (kip-ft)	Max (kip-ft)	Min (kip-ft)	Max (kip-ft)	Min (kip-ft)
Span 2 Girder D, (H) 103.040	-106.04	-224.97	-106.46	-201.60	-52.85	-124.61	-92.12	-341.16	-93.64	-266.04
Span 2 Girder D, (CS) 103.325	-106.78	-226.02	-107.17	-202.57	-53.23	-125.19	-92.88	-342.70	-94.31	-267.32
Span 2 Girder D, 104.123	-108.85	-228.98	-109.18	-205.28	-54.29	-126.81	-95.01	-347.03	-96.20	-270.92
Span 2 Girder D, 104.706	-110.36	-231.14	-110.64	-207.26	-55.07	-127.99	-96.56	-350.19	-97.57	-273.55
Span 2 Girder D, (PSKFR) 106.123	-114.02	-236.38	-114.18	-212.07	-56.94	-130.87	-100.31	-357.89	-100.89	-279.94
Span 2 Girder D, (FoS) 107.540	-117.66	-241.64	-117.70	-216.89	-58.81	-133.75	-104.03	-365.60	-104.20	-286.35
Span 2 Girder D, (1.0L <sub>u</sub> ) 108.081	-119.04	-243.65	-119.04	-218.73	-59.52	-134.86	-105.45	-368.55	-105.45	-288.80

Total Girderline Reactions at Abutments and Piers

	DC		DW		ΣDC		ΣDW	
	Max (kip)	Min (kip)	Max (kip)	Min (kip)	Max (kip)	Min (kip)	Max (kip)	Min (kip)
Abutment 1	0.00	0.00	5.63	5.63	82.58	82.58	5.63	5.63
Pier 2	0.00	0.00	12.29	12.29	197.06	197.06	12.29	12.29
Abutment 3	0.00	0.00	6.82	6.82	113.57	113.57	6.82	6.82

Total Girderline Reactions at Abutments and Piers - Design Vehicles (Including Impact)

	Total Live Load					
	* LL+IM Design		* LL+IM Fatigue		* LL+IM Permit	
	Max (kip)	Min (kip)	Max (kip)	Min (kip)	Max (kip)	Min (kip)
Abutment 1	126.95	0.00	75.87	0.00	102.81	0.00
Pier 2	152.22	0.00	92.54	0.00	129.78	0.00
Abutment 3	125.14	0.00	74.70	0.00	102.88	0.00

\* Live Load values are per girder and include impact.

Total Girderline Reactions at Abutments and Piers (Including Impact)

	Design									
	Service I		Service III		Fatigue I		Strength I		Strength II	
	Max (kip)	Min (kip)	Max (kip)	Min (kip)	Max (kip)	Min (kip)	Max (kip)	Min (kip)	Max (kip)	Min (kip)
Abutment 1	215.16	88.20	189.77	88.20	157.90	34.10	333.89	71.98	250.46	77.98
Pier 2	361.57	209.35	331.13	209.35	243.48	104.68	531.15	185.34	439.97	185.34
Abutment 3	245.52	120.38	220.49	120.38	172.34	50.19	371.71	106.64	291.08	106.64

Live Load Reactions without Impact

Total Girderline Reactions at Abutments and Piers - Design Vehicles (Without Impact)

	Total Live Load					
	* LL Design		* LL Fatigue		* LL Permit	
	Max (kip)	Min (kip)	Max (kip)	Min (kip)	Max (kip)	Min (kip)
Abutment 1	102.81	0.00	68.55	0.00	102.81	0.00
Pier 2	129.78	0.00	85.79	0.00	129.78	0.00
Abutment 3	102.88	0.00	68.01	0.00	102.88	0.00

\* Live Load values are per girder and do not include impact.

Total Girderline Reactions at Abutments and Piers - Rating Vehicles (Without Impact)

	* LL Design		* LL Legal Routine		* LL Legal Special	
	Max (kip)	Min (kip)	Max (kip)	Min (kip)	Max (kip)	Min (kip)
Abutment 1	102.81	0.00	64.68	0.00	76.20	0.00
Pier 2	129.78	0.00	67.73	0.00	76.24	0.00
Abutment 3	102.88	0.00	63.87	0.00	71.53	0.00

\* Live Load values are per girder and do not include impact.

Maximum Reaction  
for Girder Line D

# Bridge Analysis Report

For

Girder Line E

July 4, 2015 6:25:17 pm

**PGSuper™**

Copyright © 2015, WSDOT, All Rights Reserved

Version 2.7.2 - Built on Nov 9 2012



## Project Properties

Bridge Name	Bridge 4
Bridge ID	
Company	Your Company
Engineer	Your Name
Job Number	001
Comments	
File	C:\Users\FranciscoDavid\Desktop\Thesis\Pran\PGSuper\Bridge4DesignLoads.pgs

Bridge: Bridge 4

Job: 001

04/07/2015

Location from Left Support (ft)	Design									
	Service I		Service III		Fatigue I		Strength I		Strength II	
	Max (kip-ft)	Min (kip-ft)	Max (kip-ft)	Min (kip-ft)	Max (kip-ft)	Min (kip-ft)	Max (kip-ft)	Min (kip-ft)	Max (kip-ft)	Min (kip-ft)
Span 2 Girder E, (PGXFR) 106.085	-107.87	-229.70	-108.03	-205.49	-53.51	-185.15	-94.78	-349.27	-95.36	-271.66
Span 2 Girder E, (Fo8) 107.502	-111.28	-234.72	-111.32	-210.07	-55.52	-188.97	-96.30	-356.68	-98.45	-277.77
Span 2 Girder E, (1.0L <sub>u</sub> ) 108.043	-112.57	-236.64	-112.57	-211.82	-56.29	-190.44	-99.63	-369.51	-99.63	-280.10

Total Girderline Reactions at Abutments and Piers

	DC		DW		ΣDC		ΣDW	
	Max (kip)	Min (kip)	Max (kip)	Min (kip)	Max (kip)	Min (kip)	Max (kip)	Min (kip)
Abutment 1	0.00	0.00	7.14	7.14	99.67	99.67	7.14	7.14
Pier 2	0.00	0.00	13.65	13.65	206.44	206.44	13.65	13.65
Abutment 3	0.00	0.00	6.81	6.81	106.98	106.98	6.81	6.81

Total Girderline Reactions at Abutments and Piers - Design Vehicles (Including Impact)

	Total Live Load					
	* LL+IM Design		* LL+IM Fatigue		* LL+IM Permit	
	Max (kip)	Min (kip)	Max (kip)	Min (kip)	Max (kip)	Min (kip)
Abutment 1	145.58	0.00	109.34	0.00	119.23	0.00
Pier 2	158.73	0.00	122.06	0.00	136.26	0.00
Abutment 3	124.59	0.00	93.75	0.00	102.43	0.00

\* Live Load values are per girder and include impact.

Total Girderline Reactions at Abutments and Piers (Including Impact)

	Design									
	Service I		Service III		Fatigue I		Strength I		Strength II	
	Max (kip)	Min (kip)	Max (kip)	Min (kip)	Max (kip)	Min (kip)	Max (kip)	Min (kip)	Max (kip)	Min (kip)
Abutment 1	252.39	106.81	223.27	106.81	217.41	53.41	390.06	94.34	296.26	94.34
Pier 2	378.83	220.10	347.08	220.10	293.14	110.05	556.31	194.67	462.48	194.67
Abutment 3	238.38	113.80	213.47	113.80	197.53	55.90	361.94	100.71	282.23	100.71

Live Load Reactions without Impact

Total Girderline Reactions at Abutments and Piers - Design Vehicles (Without Impact)

	Total Live Load					
	* LL Design		* LL Fatigue		* LL Permit	
	Max (kip)	Min (kip)	Max (kip)	Min (kip)	Max (kip)	Min (kip)
Abutment 1	119.23	0.00	99.36	0.00	119.23	0.00
Pier 2	136.26	0.00	113.55	0.00	136.26	0.00
Abutment 3	102.43	0.00	85.36	0.00	102.43	0.00

\* Live Load values are per girder and do not include impact.

Total Girderline Reactions at Abutments and Piers - Rating Vehicles (Without Impact)

	* LL Design		* LL Legal Routine		* LL Legal Special	
	Max (kip)	Min (kip)	Max (kip)	Min (kip)	Max (kip)	Min (kip)
	Max (kip)	Min (kip)	Max (kip)	Min (kip)	Max (kip)	Min (kip)
Abutment 1	119.23	0.00	74.57	0.00	84.37	0.00
Pier 2	136.26	0.00	68.81	0.00	76.50	0.00
Abutment 3	102.43	0.00	63.59	0.00	71.23	0.00

\* Live Load values are per girder and do not include impact.

Maximum Reaction  
for Girder Line E

Appendix C  
Prestress Loss Calculations

## **PRESTRESS LOSSES**

### **Tendons properties**

Grade 270 low relaxation steel					
Ultimate stress on prestressing steel	$f_{pu}$	270.000	ksi	1,861.650	Mpa
Yielding stress on prestressing steel	$f_{py}$	243.000	ksi	1,675.485	Mpa
Area of prestressing steel per tendon	$A_{psi}$	6.727	in <sup>2</sup>	43.403	cm <sup>2</sup>
Number of tendons	N	6.000			
Total area of prestressing steel	$A_{ps}$	40.362	in <sup>2</sup>	260.416	cm <sup>2</sup>
Length of tendons	L	81.000	ft		
Forcer per tendon at jacking	P	1,362.000	kips		
Stress in tendon at jacking	$f_{pj}$	202.468	ksi	1,396.015	Mpa
Prestressing steel Young modulus	$E_p$	28,500.000	ksi	196,507.500	Mpa
Gross area of section	$A_g$	7,752.000	in <sup>2</sup>	50,015.904	cm <sup>2</sup>
Concrete strenght at release	$f_{ci}$	5.000	ksi	34.475	Mpa
Modulus of elasticity of concrete at transfer	$E_{ci}$	4,069.644	ksi	28,060.193	Mpa
Average eccentricity at low point	$e_m$	1.417	in	3.598	cm
Stress in prestressing steel immediately prior to transfer	$f_{pbt}$	202.500	ksi	1,396.238	Mpa
Moment of inertia of gross section	$I_g$	6,720,984.000	in <sup>4</sup>	2.797	m <sup>4</sup>
Moment at midspan due to member self-weight	$M_g$	64,986.490	Kip-in	7,343.473	kNm
Volume of member	V	4,438.913	cf	124.290	m <sup>3</sup>
Surface exposed to drying	S	1,223.723	sf	113.806	m <sup>2</sup>

Table 5.9.3-1  
(AASHTO 2012)

### **Friction loss**

Wobble friction coefficient	k	0.000			
Coefficient of friction	$\mu$	0.230			
Distance from jacking end (lowest point)	x	38.250	ft	11.475	m
Angular change from jacking end	$\alpha_A$	0.194	rad	for tendons A	
	$\alpha_B$	0.139	rad	for tendons B	
	$\alpha_C$	0.083	rad	for tendons C	
	$\alpha_{aver}$	0.138	rad	Average	
Friction loss per tendon	$\Delta f_{pF}$	7.842	ksi	54.070	Mpa

### **Anchorage set loss**

Anchorage set	$\Delta L$	0.375	in	0.953	cm
Length of tendons	L	972.000	in	24.689	m
Anchorage set loss per tendon	$\Delta f_{pA}$	10.995	ksi	75.813	Mpa

### **Elastic shortening loss**

Total elastic shortening loss per tendon	$\Delta f_{pES}$	2.936	ksi	20.246	Mpa
--	------------------	-------	-----	--------	-----

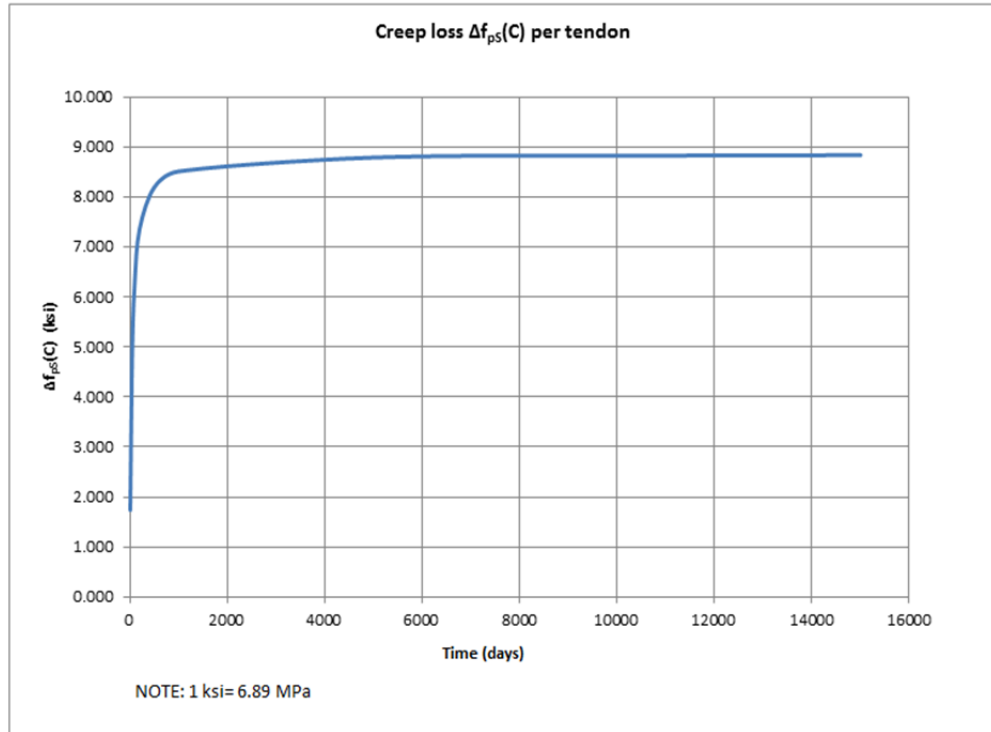


### Creep loss

Volume-to-surface ratio	V/S	3.627	in	9.214	cm
Volume-to-surface coefficient	$k_s$	1.000			
Relative humidity	H	60.000	%		
Humidity factor for creep	$k_{ho}$	1.080			
Factor for the effect of concrete strength	$k_f$	0.833			
Time of loading at load application	$t_i$	20.000	days		
Instantaneous strain due to loading	$\epsilon_{ci}$	2.591E-04			

The following table summarizes the values for creep loss at different times  $t$  from loading application

t (days)	Time development factor $k_{td}$	Creep coefficient $\Psi(t, t_i)$	Deformation due to creep $\epsilon_c$	Creep loss $\Delta f_{ps}(C)$ per tendon	
				ksi	Mpa
10	0.196	0.235	6.100E-05	1.739	11.987
50	0.549	0.660	1.709E-04	4.872	33.590
100	0.709	0.852	2.206E-04	6.288	43.357
200	0.830	0.997	2.582E-04	7.358	50.733
500	0.924	1.110	2.875E-04	8.194	56.501
1000	0.961	1.154	2.988E-04	8.517	58.726
5000	0.992	1.191	3.086E-04	8.794	60.637
10000	0.996	1.196	3.098E-04	8.830	60.884
15000	0.997	1.198	3.103E-04	8.842	60.967

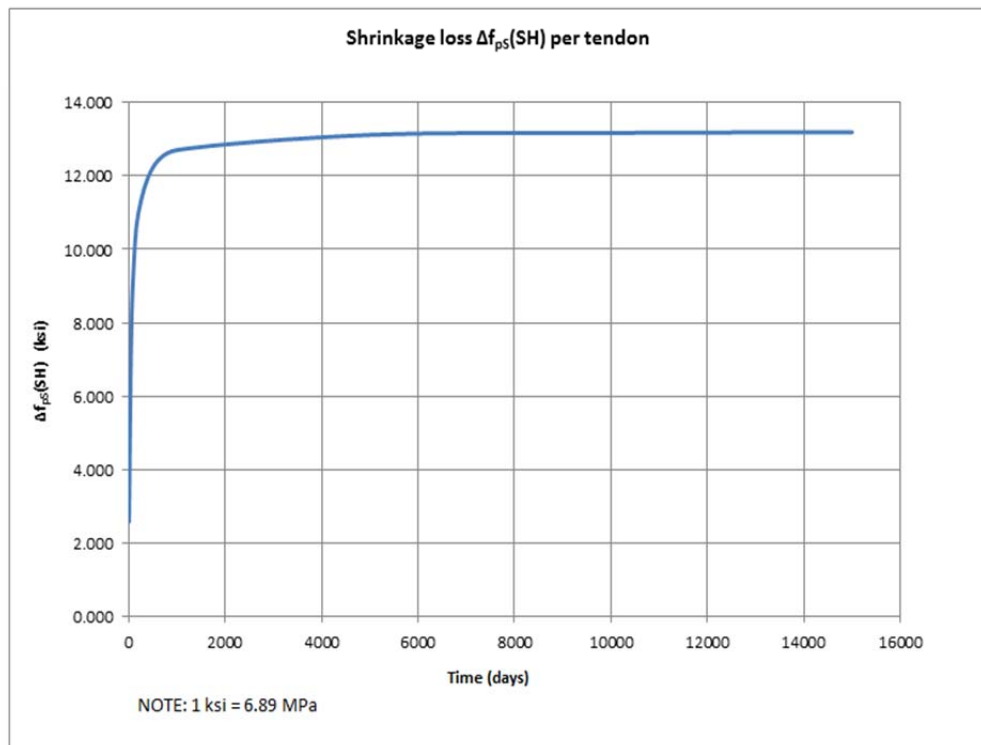


### Shrinkage loss

Volume-to-surface ratio	V/S	3.627	in	9.214	cm
Volume-to-surface coefficient	$k_s$	1.000			
Relative humidity	H	60.000	%		
Humidity factor for shrinkage	$k_{hs}$	1.160			
Factor for the effect of concrete strenght	$k_f$	0.833			

The following table summarizes the values for shrinkage loss at different times  $t$  from loading

t (days)	Time development factor $k_{td}$	Deformation due to shrinkage $\epsilon_{sh}$	Shrinkage loss $\Delta f_{ps}(SH)$ per tendon	
			ksi	Mpa
10	0.196	9.098E-05	2.593	17.878
50	0.549	2.549E-04	7.266	50.099
100	0.709	3.291E-04	9.379	64.666
200	0.830	3.851E-04	10.974	75.668
500	0.924	4.288E-04	12.222	84.269
1000	0.961	4.457E-04	12.703	87.588
5000	0.992	4.602E-04	13.116	90.438
10000	0.996	4.621E-04	13.170	90.807
15000	0.997	4.627E-04	13.188	90.931

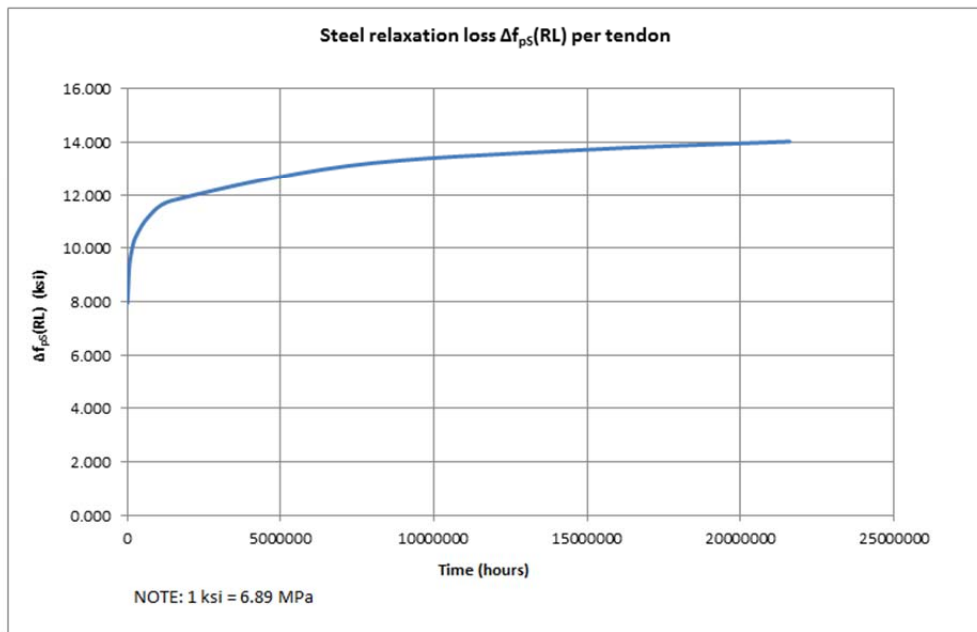


### Steel relaxation loss

Steel relaxation factor  $k = 30.000$

The following table summarizes the values for steel relaxation loss at different times  $t$  from loading application

t (hours)	Stress at prestressing steel at time t		Steel relaxation loss $\Delta f_{ps}(RL)$	
	ksi	MPa	ksi	Mpa
14400	194.547	1,341.402	7.953	54.835
72000	193.210	1,332.185	9.290	64.052
144000	192.635	1,328.216	9.865	68.022
288000	192.059	1,324.246	10.441	71.991
720000	191.298	1,318.999	11.202	77.239
1440000	190.722	1,315.029	11.778	81.208
7200000	189.385	1,305.812	13.115	90.426
14400000	188.810	1,301.842	13.690	94.395
21600000	188.473	1,299.520	14.027	96.717



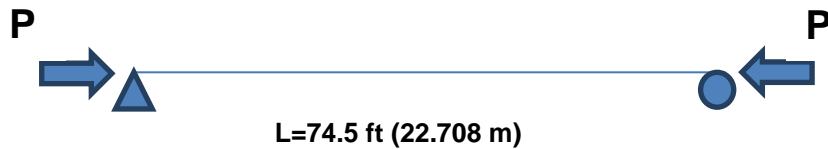
TOTAL PRESTRESS LOSS	$\Delta f_{pT}$	57.831	ksi	398.744	MPa
STRESS AT JACKING	$f_{pj}$	202.468	ksi	1,396.015	MPa
EFFECTIVE PRESTRESS STRESS	$f_{pe}$	144.637	ksi	997.270	MPa
LONG TERM PRESTRESS FORCE PER TENDON	P	972.971	kips	4,327.776	kN

Appendix D  
Post-Tensioned Concrete Cap Model.  
Validation Calculations

Since the section behaves elastically, the superposition principle is applicable. The calculations will be performed for three different loading cases:

- Case 1. Simply supported beam subjected to a uniform compressive force equal to the total effective prestress force (after losses).
- Case 2. Simply supported beam subjected to the concentrated loads applied by the beams.
- Case 3. Simply supported beam subjected to a constant distributed load result of the summation of the load-balancing force caused by the prestressing tendons and the concrete cap self-weight.

#### CASE 1



The compressive force applied to the member is equal to the total effective prestressing force, so:

$$P = 6 \times 972,971 = 5,837,826 \text{ p (25,523.12 kN)}$$

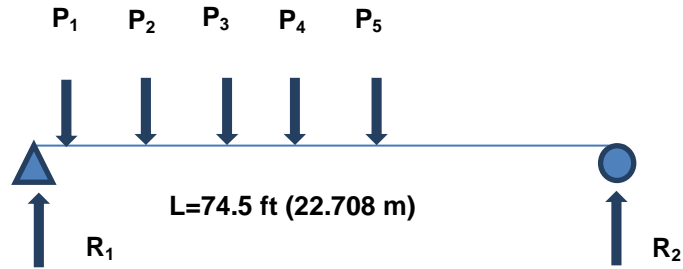
Under that load, the stress in the member is constant and with a value of (negative for compressive stress):

$$A = 76 \times 102 = 7,752 \text{ in}^2 (5.001 \text{ m}^2)$$

$$\sigma_{1top} = \frac{P}{A} = -753.07 \text{ psi } (-5.192 \text{ MPa}) \text{ (compression)}$$

$$\sigma_{1bot} = \frac{P}{A} = -753.07 \text{ psi } (5.192 \text{ MPa}) \text{ (compression)}$$

## CASE 2



The forces  $P_1$  to  $P_5$  are the result of the summation of the loads transferred by the backwards and forwards span beams 1 to 5, so:

$$P_1 = 285,690 \text{ p } (1,270.812 \text{ kN})$$

$$P_2 = 336,870 \text{ p } (1,489.472 \text{ kN})$$

$$P_3 = 433,270 \text{ p } (1,927.281 \text{ kN})$$

$$P_4 = 531,150 \text{ p } (2,362.673 \text{ kN})$$

$$P_5 = 556,310 \text{ p } (2,474.59 \text{ kN})$$

And the distances between the points of application of the loads and the left support are:

$$x_1 = 1.19 \text{ ft } (0.363 \text{ m})$$

$$x_2 = 6.84 \text{ ft } (2.085 \text{ m})$$

$$x_3 = 13.51 \text{ ft } (4.118 \text{ m})$$

$$x_4 = 24.38 \text{ ft } (7.431 \text{ m})$$

$$x_5 = 35.26 \text{ ft } (10.747 \text{ m})$$

By equilibrium of moments with respect to the left support:

$$\sum M = 0 = P_1 * x_1 + P_2 * x_2 + P_3 * x_3 + P_4 * x_4 + P_5 * x_5 - R_2 * L$$

$$R_2 = 551,175.40 \text{ p } (2,451.75 \text{ kN})$$

The maximum moment section is located at the point of application of the force  $P_5$ . The moment at that section is:

$$M = R_2 * (L - x_5)$$

$$M = 259,537,471.70 \text{ p-in } (29,323.783 \text{ kN-m})$$

So the stresses caused by the bending action are:

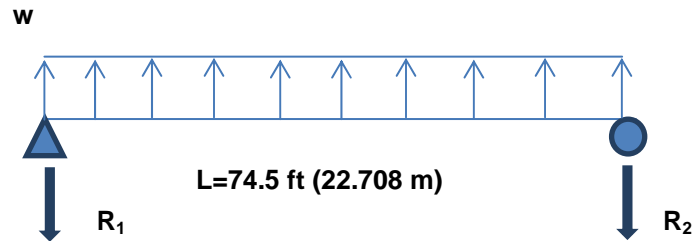
$$I = \frac{bh^3}{12} = \frac{76 * 102^3}{12} = 6,720,984 \text{ in}^4 (2.796 \text{ m}^4)$$

$$y = \frac{h}{2} = 51 \text{ in } (1.295 \text{ m})$$

$$\sigma_{2top} = -\frac{M * y}{I} = -1,969.42 \text{ psi } (-13.579 \text{ MPa}) \text{ (compression)}$$

$$\sigma_{2bot} = \frac{M * y}{I} = 1,969.42 \text{ psi } (13.579 \text{ MPa}) \text{ (tension)}$$

### CASE 3



The force  $w$  is the result of the summation of the factored self-weight of the cap and the load-balancing force caused by the prestressing tendons:

$$w = w_{sw} + w_{lb}$$

$$w_{sw} = 1.25 * \gamma_c * A = -813.11 \text{ p/in } (142.294 \text{ kN/m}) \text{ (downwards)}$$

$$w_{lb} = 1,680.69 \text{ p/in } (294.121 \text{ kN/m}) \text{ (upwards)}$$

$$w = 867.58 \text{ p/in } (151.827 \text{ kN/m}) \text{ (upwards)}$$

$$\sum M = 0 = w * \frac{L^2}{2} - R_1 * L$$

$$R_1 = 387,808.26 \text{ p (1,725.057 kN)}$$

So the moment at a section located 35.26 ft (10.747 m) from the left support is:

$$M = \left( w * \frac{(35.26 * 12)^2}{2} - R_1 * (35.26 * 12) \right)$$

$$M = -86,427,775.45 \text{ p-in (-9,765.023 kN/m)}$$

And the bending stresses are:

$$\sigma_{3top} = \frac{M * y}{I} = 655.83 \text{ psi (4.522 MPa) (tension)}$$

$$\sigma_{3bot} = -\frac{M * y}{I} = -655.83 \text{ psi (-4.522 MPa) (compression)}$$

#### TOTAL STRESSES:

Applying the superposition principle, the total compressive and tensile stresses due to bending and prestressing are:

$$\sigma_{top} = \sigma_{1top} + \sigma_{2top} + \sigma_{3top} = -2,066.66 \text{ psi (14.249 MPa) (compression)}$$

$$\sigma_{bot} = \sigma_{1bot} + \sigma_{2bot} + \sigma_{3bot} = 560.52 \text{ psi (3.865 MPa) (tension)}$$



Appendix E  
Steel-Concrete Composite Cap Model.  
Validation Calculations

Since the section behaves elastically, the superposition principle is applicable. The calculations will be performed for two different loading cases:

- Case 1. Simply supported beam subjected to the concentrated loads applied by the beams.
- Case 2. Simply supported beam subjected to a constant distributed load result of the summation of the load-balancing force caused by the prestressing tendons and the concrete cap self-weight.

To analyze the composite section, it will be first converted into a homogeneous section by obtaining an equivalent section conformed only by one type of material. The conversion factor,  $n$ , is defined as follows:

$$n = \frac{E_c}{E_s} = \frac{4,458,071.332}{29,000,000} = 0,154$$

And the 10 inches thick concrete slab is converted into a steel slab with its center of gravity coincident with the original one and a thickness of:

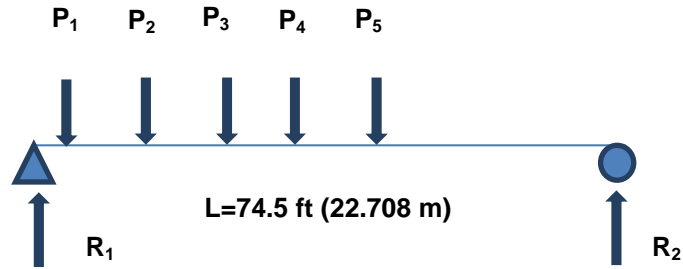
$$d' = 10 * 0.154 = 1.54 \text{ in } (0.039 \text{ m})$$

With that into consideration, the converted section has the following properties:

$$y_{cg} = 46.89 \text{ in } (1.191 \text{ m})$$

$$I_{tr} = 257,737 \text{ in}^4 (0.107 \text{ m}^4)$$

### CASE 1



The forces  $P_1$  to  $P_5$  are the result of the summation of the loads transferred by the backwards and forwards span beams 1 to 5, so:

$$P_1 = 285,690 \text{ p } (1,270.812 \text{ kN})$$

$$P_2 = 336,870 \text{ p } (1,489.472 \text{ kN})$$

$$P_3 = 433,270 \text{ p } (1,927.281 \text{ kN})$$

$$P_4 = 531,150 \text{ p } (2,362.673 \text{ kN})$$

$$P_5 = 556,310 \text{ p } (2,474.59 \text{ kN})$$

And the distances between the points of application of the loads and the left support are:

$$x_1 = 1.19 \text{ ft } (0.363 \text{ m})$$

$$x_2 = 6.84 \text{ ft } (2.085 \text{ m})$$

$$x_3 = 13.51 \text{ ft } (4.118 \text{ m})$$

$$x_4 = 24.38 \text{ ft } (7.431 \text{ m})$$

$$x_5 = 35.26 \text{ ft } (10.747 \text{ m})$$

By equilibrium of moments with respect to the left support:

$$\sum M = 0 = P_1 * x_1 + P_2 * x_2 + P_3 * x_3 + P_4 * x_4 + P_5 * x_5 - R_2 * L$$

$$R_2 = 551,175.40 \text{ p } (2,451.75 \text{ kN})$$

The maximum moment section is located at the point of application of the force  $P_5$ . The moment at that section is:

$$M = R_2 * (L - x_5)$$

$$M = 259,537,471.70 \text{ p-in } (29,323.783 \text{ kN/m})$$

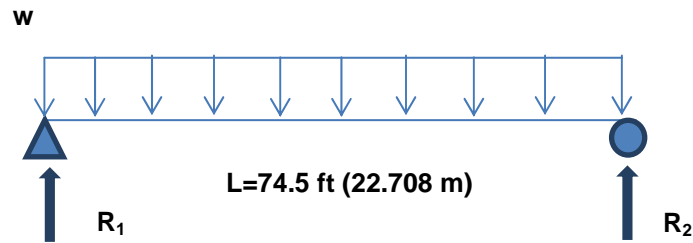
So the stresses caused by the bending action are:

$$\sigma_{1toptr} = -\frac{M * y_{top}}{I} = -31,327.30 \text{ psi } (215.994 \text{ MPa}) \text{ (compression)}$$

$$\sigma_{1top} = \sigma_{1toptr} * n = -4,824.41 \text{ psi } (33.263 \text{ MPa}) \text{ (compression)}$$

$$\sigma_{1bot} = \frac{M * y_{bot}}{I} = 47,217.56 \text{ psi } (325.554 \text{ MPa}) \text{ (tension)}$$

## CASE 2



The force  $w$  is the result of the summation of the factored self-weight of the steel cap and the top concrete slab:

$$w = w_{steel} + w_{concrete}$$

$$w_{steel} = 1.25 * \gamma_s * A_{steel}$$

$$A_{steel} = 72 * \frac{3}{4} + 2 * 68 * \frac{3}{4} + 76 * \frac{1}{2} = 194 \text{ in}^2 \text{ (0.125 m}^2\text{)}$$

$$w_{steel} = 1.25 * 0.490 * \frac{1000}{12^3} * 194 = 68.76 \text{ p/in } (12.033 \text{ kN/m})$$

$$w_{concrete} = 1.25 * \gamma_c * A_{concrete}$$

$$w_{concrete} = 1.25 * 0.145 * \frac{1000}{12^3} * 76 * 10 = 79.72 \text{ p/in } (13.951 \text{ kN/m})$$

$$w = 68.76 + 79.72 = 148.48 \text{ p/in } (25.984 \text{ kN/m})$$

Because of the symmetry of the loading case, the reactions at supports are equal with a value of

$$R_1 = R_2 = \frac{wL}{2} = 66,370.56 \text{ p (295.231 kN)}$$

So the moment at a section located 35.26 ft from the left support is:

$$M = \left( w * \frac{(35.26 * 12)^2}{2} - R_1 * (35.26 * 12) \right)$$

$$M = 14,791,484.47 \text{ p-in (1,671.213 kN-m)}$$

And the bending stresses are:

$$\sigma_{2toptr} = \frac{M * y}{I} = -1,785.40 \text{ psi (compression)}$$

$$\sigma_{2top} = \sigma_{2toptr} * n = -274,95 \text{ psi (compression)}$$

$$\sigma_{2bot} = -\frac{M * y}{I} = 2,590.50 \text{ psi (tension)}$$

#### TOTAL STRESSES:

Applying the superposition principle, the total compressive and tensile stresses are:

$$\sigma_{top} = \sigma_{1top} + \sigma_{2top} = -5,099.36 \text{ psi (-35.159 MPa) (compression)}$$

$$\sigma_{bot} = \sigma_{1bot} + \sigma_{2bot} = 49,908.56 \text{ psi (344.107 MPa) (tension)}$$

Appendix F  
Cost Estimation

POST-TENSIONED BENT CAP ESTIMATE									
ITEM	DESCRIPTION	QUANTITY						COST	
Concrete f'c 6,000 psi (material)	Only material	UNIT	QUANTITY	LENGTH (ft)	WIDTH (ft)	HEIGHT (ft)	TOTAL QUANTITY	UNIT PRICE	TOTAL COST (\$)
		CY	1.00	82.50	6.33	8.50	164.40		
		CY	1.00	82.50	3.17	0.04	0.40		
						<b>SUBTOTAL</b>	<b>164.81</b>	<b>86.35</b>	<b>14,231.14</b>
Concrete f'c 6,000 psi (placement)	Includes form work and shoring tower placement and removal, and concrete pouring	UNIT	QUANTITY	LENGTH (ft)	WIDTH (ft)	HEIGHT (ft)	TOTAL QUANTITY	UNIT PRICE	TOTAL COST (\$)
		CY	1.00	82.50	6.33	8.50	164.40		
		CY	1.00	82.50	3.17	0.04	0.40		
						<b>SUBTOTAL</b>	<b>164.81</b>	<b>806.17</b>	<b>132,862.98</b>
Grade 60 Reinforcing Steel	Includes material and labor	UNIT	QUANTITY	LENGTH (ft)	DIAMETER (ft)	UNIT WEIGHT (LB/FT3)	TOTAL QUANTITY	UNIT PRICE	TOTAL COST (\$)
	Bars A (#11)	LB	8.00	95.00	0.12	490.00	4,038.08		
	Bars B (#11)	LB	8.00	91.50	0.12	490.00	3,889.31		
	Bars T (#8)	LB	18.00	87.50	0.12	490.00	8,368.40		
	Bars K1 (#4)	LB	44.00	3.75	0.04	490.00	110.24		
	Bars K2 (#4)	LB	16.00	5.00	0.04	490.00	53.45		
	Bars K3 (#4)	LB	16.00	2.58	0.04	490.00	27.62		
	Bars K4 (#4)	LB	22.00	6.00	0.04	490.00	88.19		
	Bars K5 (#4)	LB	15.00	6.79	0.04	490.00	68.07		
	Bars M1 (#5)	LB	28.00	9.46	0.05	490.00	276.48		
	Bars M2 (#5)	LB	26.00	11.54	0.05	490.00	313.27		
	Bars S1 (#6)	LB	108.00	29.79	0.06	490.00	4,836.87		
	Bars S2 (#5)	LB	78.00	23.58	0.05	490.00	1,920.36		
	Bars S3 (#6)	LB	60.00	22.25	0.06	490.00	2,006.91		
	Bars U (#6)	LB	271.00	7.94	0.06	490.00	3,233.69		
	Bars V2 (#10)	LB	32.00	10.00	0.11	490.00	1,379.37		
	Bars Z2 (#3)	LB	4.00	104.72	0.03	490.00	157.43		
						<b>SUBTOTAL</b>	<b>30,767.74</b>	<b>0.47</b>	<b>14,460.84</b>
Grade 270 Low-Lax Prestressing Steel	31-0.6 in dia. tendon, including all additional elements, grout and tendon tensioning	UNIT	QUANTITY	LENGTH (ft)	WIDTH (ft)	HEIGHT (ft)	TOTAL QUANTITY	UNIT PRICE	TOTAL COST (\$)
	Tendons A	LFT	2.00	85.00	1.00	1.00	170.00		
	Tendons B	LFT	2.00	85.00	1.00	1.00	170.00		
	Tendons C	LFT	2.00	85.00	1.00	1.00	170.00		
						<b>SUBTOTAL</b>	<b>510.00</b>	<b>89.84</b>	<b>45,818.40</b>
<b>TOTAL</b>								<b>207,373.36</b>	

COMPOSITE BENT CAP ESTIMATE									
ITEM	DESCRIPTION	QUANTITY						COST	
Concrete f'c 6,000 psi (material)	Only material	UNIT	QUANTITY	LENGTH (ft)	WIDTH (ft)	HEIGHT (ft)	TOTAL QUANTITY	UNIT PRICE	TOTAL COST (\$)
		CY	1.00	83.50	6.33	0.83	16.32		
						<b>SUBTOTAL</b>	<b>16.32</b>	<b>86.35</b>	<b>1,409.41</b>
Concrete f'c 6,000 psi (placement)	Includes form work and shoring tower placement and removal	UNIT	QUANTITY	LENGTH (ft)	WIDTH (ft)	HEIGHT (ft)	TOTAL QUANTITY	UNIT PRICE	TOTAL COST (\$)
		CY	1.00	83.50	6.33	0.83	16.32		
						<b>SUBTOTAL</b>	<b>16.32</b>	<b>567.78</b>	<b>9,267.31</b>
Grade 60 Reinforcing Steel	Includes material and labor	UNIT	QUANTITY	LENGTH (ft)	DIAMETER (ft)	UNIT WEIGHT (LB/FT3)	TOTAL QUANTITY	UNIT PRICE	TOTAL COST (\$)
	Bars A (#4)	LB	13.00	84.58	0.12	490.00	5,842.38		
	Bars B (#4)	LB	13.00	84.58	0.12	490.00	5,842.38		
	Bars S (#4)	LB	168.00	13.83	0.12	490.00	12,348.03		
						<b>SUBTOTAL</b>	<b>24,032.80</b>	<b>0.47</b>	<b>11,295.41</b>
A709 Grade 50 Steel	A709 Grade 50 Steel in finished steel cap section including lifting	UNIT	QUANTITY	LENGTH (ft)	WIDTH (ft)	THICKNESS (ft)	TOTAL QUANTITY	UNIT PRICE	TOTAL COST (\$)
	Bottom flange	LB	1.00	46.25	6.00	0.06	8,498.44		
		LB	1.00	14.75	6.00	0.05	2,258.59		
		LB	1.00	22.50	6.00	0.05	3,445.31		
	Top flange	LB	2.00	3.33	1.67	0.04	226.83		
		LB	1.00	3.33	6.33	0.05	538.72		
		LB	2.00	71.17	1.67	0.04	4,843.38		
		LB	1.00	2.33	6.33	0.05	377.09		
		LB	2.00	3.33	1.67	0.04	226.83		
		LB	5.00	3.25	3.00	0.04	995.31		
		LB	7.00	1.00	3.00	0.04	428.75		
	Webs	LB	4.00	12.00	5.75	0.06	8,452.50		
		LB	2.00	59.50	5.75	0.04	13,970.10		
	Diagonals	LB	2.00	83.50	1.42	0.04	4,830.24		
	Diaphragm Column 1	LB	4.00	5.67	1.17	0.05	674.88		
		LB	8.00	5.67	0.58	0.05	674.88		
		LB	1.00	6.00	5.67	0.10	1,735.42		
		LB	1.00	6.00	5.67	0.04	694.17		
	Diaphragm Column 2	LB	4.00	5.67	1.17	0.05	674.88		
		LB	8.00	5.67	0.58	0.05	674.88		
		LB	1.00	6.00	5.67	0.06	1,041.25		
	Girder Stiffener	LB	5.00	6.00	5.67	0.06	5,206.25		
		LB	40.00	5.67	0.67	0.04	3,085.19		
	Interior Stiffener	LB	7.00	6.00	5.67	0.04	4,859.17		
		LB	28.00	5.67	0.42	0.04	1,349.77		
						<b>SUBTOTAL</b>	<b>69,762.84</b>	<b>2.55</b>	<b>177,895.23</b>
								<b>TOTAL</b>	<b>199,867.37</b>



## References

- AASHTO. (2012). *AASHTO LRFD Bridge Design Specifications*. American Association of State Highway and Transportation Officials.
- Alenius, M. (2003). *Finite Element Modelling of Composite Bridge Stability*. Stockholm: Royal Institute of Technology.
- Ales, J. M. (1994). *The Connection Between an Integral Steel Cap Girder and a Concrete Pier*. University of Texas at Austin.
- Al-Mashta, S. (2010). *Integrated Cost Budgeting and Cost Estimation Model for Building Projects*. Concordia University.
- AZDOT. (ND). *LRFD Substructure Example 3. Hammerhead Pier on Spread Footing*. Arizona Department of Transportation.
- Barker, R. M., & Puckett, J. A. (2013). *Design of Highway Bridges. An LRFD Approach*. Wiley.
- Barr, P. J., Halling, M. W., Huffaker, C., & Boyle, H. (2013). *Behavior and Analysis of an Integral Abutment Bridge*. Utah State University.
- Bhargava, A. (2009). *A Probabilistic Evaluation of Highway Project Costs*. Purdue University.
- Billington, S. L. (1994). *Behavior of Two-Span Continuous Pier Caps With Varying Levels of Prestress*. The University of Texas at Austin.
- Billington, S., Barnes, R., & Breen, J. (1998). *A Precast Substructure Design for Standard Bridge Systems*. Center for Transportation Research. The University of Texas at Austin.
- Birtel, V., & Mark, P. (2006). *Parameteised Finite Element Modeling of RC Beam Shear Failure*. Ruhr-University Bochum.

- Bracci, J. M., Keating, P. B., & Hueste, M. B. (2000). *Cracking in RC Bent Caps*. Texas Department of Transportation.
- Chen, W.-F., & Duan, L. (2014). *Bridge Engineering Handbook: Substructure Design*. CRC Press.
- Clifford J. Youngberg, R. J., & Bergson, P. M. (2003). *Fatigue Evaluation of Steel Box-Girder Pier Caps*. Minnesota Department of Transportation.
- Coletti, D., & Puckett, J. (2012). *Steel Bridge Design Handbook: Structural Analysis*. Federal Highway Administration.
- Colleti, D., & Sheahan, J. (2012). *Steel Bridge Design Handbook: Substructure Design*. Federal Highway Administration.
- Collins, M. P., Mitchell, D., & MacGregor, J. G. (1993). *Structural Design Considerations for High-Strength Concrete*. American Concrete Institute.
- Construction, A. I. (2012). *Steel Construction Manual*. American Institute of Steel Construction.
- Dassault Systemes Simulia Corp. (n.d.). *Abaqus 6.9 Abaqus/CAE User's Guide*. Dassault Systemes Simulia Corp.
- Dassault Systemes Simulia Corp. (n.d.). *Abaqus 6.9 Analysis User's Manual*. Dassault Systemes Simulia Corp.
- Dassault Systemes Simulia Corp. (n.d.). *Abaqus 6.9 Example Problems Manual*. Dassault Systemes Simulia Corp.
- Dassault Systemes Simulia Corp. (n.d.). *Abaqus 6.9 Theory Manual*. Dassault Systemes Simulia Corp.
- De, S. (n.d.). *Abaqus Handout*. Rensselaer Polytechnic Institute.
- Denio, R. J., Yura, J. A., & Kreger, M. E. (1995). *Behaviour of Reinforced Concrete Pier Caps Under Concentrated Bearing Loads*. Texas Department of Transportation.

- Estimation, A. T. (2006). *A Guide for Cost Estimation*. AASHTO.
- Ferley, R. F. (2013). *Finite Element Analysis of Reinforced Concrete Pile Caps To Cast-In-Shell Steel Piles*. Tennessee Technological University.
- FHWA. (2003). *LRFD Design Example for Steel Girder Superstructure Bridge*. Federal Highway Administration.
- Furlong, R. W., Ferguson, P. M., & Ma, J. S. (1971). *Shear and Anchorage Study of Reinforcement in Inverted T-Beam Bent Cap Girders*. Center for Highway Research. The University of Texas at Austin.
- Gandiaga, L. (2009). *Serviceability Limits and Economical Bridge Design*. University of Wyoming.
- Hueste, M. B., Adil, M. S., & Keating, P. B. (2006). *Impact of LRFD Specifications on Design of Texas Bridges*. Texas Transportation Institute.
- Hutchings, J. F. (2004). *Project Scheduling Handbook*. Marcel Dekker, Inc.
- Johansoon, B., & Reitzel, P. (2011). *Numerical Analysis of a Reinforced Concrete Beam in Abaqus 6.10*. Aalborg University.
- Kim, S., Bai, Y., & Yang-Ki Jung, D. Y. (2014). *Highway Construction Productivity Measurement With A Wireless Real-Time Productivity Measurement System*. Journal of the Transportation Research Board.
- King, S., & Richards, T. (2013). *Solving Contact Problems with Abaqus*. Simulia.
- Kmiecik, P., & Kaminski, M. (2011). *Modelling of Reinforced Concrete Structures and Composite Structures with Concrete Strength Degradation Taken Into Consideration*. Wroclaw University of Technology.
- Lebet, J.-P., & Hirt, M. A. (2013). *Steel Bridges. Conceptual And Structural Design of Steel and Steel-Concrete Composite Bridges*. EPFL Press.

- Lee, G. C., & Sternberg, E. (2015). *Bridges. Their Engineering and Planning*. State University of New York Press.
- Logan, D. L. (2012). *A First Course in the Finite Element Method*. CENGAGE Learning.
- Matsumoto, E. E., Waggoner, M. C., Sumen, G., Kreger, M. E., Wood, S. L., & Been, J. E. (2001). *Development of a Precast Bent Cap System*. Center for Transportation Research. The University of Texas at Austin.
- Menesi, W. (2010). *Construction Scheduling Using Critical Path Analysis with Separate Time Segments*. University of Waterloo.
- Mertz, D. (2012). *Steel Bridge Design Handbook: Limit States*. Federal Highway Administration.
- Mertz, D. (2012). *Steel Bridge Design Handbook: Loads and Load Combination*. Federal Highway Administration.
- Mubarak, S. (2010). *Construction Project Scheduling and Control*. Wiley.
- Naaman, A. E. (2012). *Prestressed Concrete Analysis and Design*. Techno Press 3000.
- Nawy, E. G. (2010). *Prestressed Concrete. A Fundamental Approach*. Prentice Hall.
- Newitt, J. S. (2009). *Construction Scheduling. Principles and Practices*. Pearson.
- Nicholas, T., Barth, K. E., & Boyajian, D. M. (2011). A Simplified Approach to Bridge Substructure Design. *Geotechnical and Geological Engineering*.
- Nikravan, N. (2013). *Structural Design Issues for Integral Abutment Bridges*. Ryerson University.
- Nilson, A. H., Darwin, D., & Dolan, C. W. (2004). *Design of Concrete Structures*. McGraw hill.
- Owens, J. A. (2010). *Project Management for Complex Transportation Projects*. Iowa State University.

- Patel, K. N. (1990). *Construction Cost Estimating in Project Management*. New Jersey Institute of Technology.
- Patel, P. (2009). *LRFD Design of Double Composite Box Girder Bridges*. University of South Florida.
- Pawar, R. (2007). *Predicting Bid Prices in Construction Projects Using Non-Parametric Statistical Models*. Texas A&M University.
- Pereira, R. M. (1994). *Behavior of Structural Concrete Cantilever Piers Using T-Headed Reinforcing Bars and Varied Prestressing Design Criteria*. The University of Texas at Austin.
- Pratt, D. (2011). *Fundamentals of Construction Estimating*. DELMAR CENGAGE Learning.
- Rombach, G. A. (2004). *Finite Element Design Of Concrete Structures*. Thomas Telford.
- Saiedi, R. (2007). *Load-deflection response of a prestressed concrete T-beam*. Queen's Univsity, Canada.
- Salmon, C. G., Johnson, J. E., & Malhas, F. A. (2009). *Steel Structures. Design and Behavior*. PEARSON Prentice Hall.
- Samphaongoen, P. (2009). *A Visual Approach To Construction Cost Estimating*. Marquette University.
- Shepherd, J. F. (2006). *Hexahedral Mesh Generation Constraints*. University of Utah.
- Thiagarajan, G. (2005). *Finite Element Modeling of Reinforced Concrete Bridge Decks with Abaqus*. U.S. Department of Transportation.
- Till, R. (2002). *Investigation of Steel Box Girder Pier Caps on S05 of 63103*. Michigan Department of Transportation.
- TxDOT. (2010). *Inverted Tee Bent Cap Design Example*. Texas Department of Transportation.

- TxDOT. (2010). *Rectangular Bent Cap Design Example*. Texas Department of Transportation.
- TxDOT. (2013). *Bridge Design Manual - LRFD*. Texas Department of Transportation.
- TxDOT. (2015). *Preferred Practices for Steel Bridge Design, Fabrication, and Erection*. Texas Department of Transportation.
- Only, D. (2010). *Rapid Bridge Construction Technology: Precast Elements for Substructures*. University of Wisconsin-Madison.
- Wahalathantri, B. L., Thambiratnam, D. P., Chan, T. H., & Fawzia, S. (2011). *A Material Model for Flexural Crack Simulation in Reinforced Concrete Elements Using Abaqus*. Queensland University of Technology.
- Wassef, W. G., & Davis, D. (2004). *NCHRP REPORT 527. Integral Steel Box-Beam Pier Caps*. Transportation Research Board of the National Academies.
- Wassef, W. G., Smith, C., Clancy, C. M., & Smith, M. J. (2003). *Comprehensive Design Example for Prestressed Concrete (PSC) Girder Superstructure Bridge with Commentary*. Federal Highway Administration.
- Wekezer, J., Li, H., Kwasniewski, L., & Malachowski, J. (2004). *Analytical and Experimental Evaluation of Existing Florida Dot Bridges*. Florida Department of Transportation.
- White, D. (2012). *Steel Bridge Design Handbook: Structural Behaviour of Steel*. Federal Highway Administration.
- Wight, J. K., & MacGregor, J. G. (2012). *Reinforced Concrete. Mechanics & Design*. Pearson.
- Zhao, J. Z., & Tonnias, D. E. (2012). *Bridge Engineering: Design, Rehabilitation, and Maintenance of Modern Highway Bridges*. McGraw-Hill.

### Biographical Information

Francisco David Berrocal Ruiz was born in Estepona (Malaga, Spain) on the 27<sup>th</sup> of November of 1980. He obtained his Civil Engineering degree from the University of Granada (Spain) in 2007. He started his professional career as an intern in the Spanish company IDOM Servicios Integrales de Ingenieria S.L. in July 2006. After finishing his degree, he was hired as an engineer by this company. In September 2007, he was offered a position in the technical department of a complex highway project in the south of Spain developed by Ferrovial-Agroman. In 2012 he was transferred to the US to collaborate in the development of the LBJ project in Dallas. Supported by his company, the author was admitted to the graduate program in Structural and Applied Mechanics at the University of Texas at Arlington in spring 2013.